



HAL
open science

An integrative approach to characterize and predict cell death and escape to beta-lactam antibiotic treatments

Viktoriiia Gross

► **To cite this version:**

Viktoriiia Gross. An integrative approach to characterize and predict cell death and escape to beta-lactam antibiotic treatments. Médecine humaine et pathologie. Université Paris-Saclay, 2024. Français. NNT : 2024UPASB035 . tel-04778378

HAL Id: tel-04778378

<https://theses.hal.science/tel-04778378v1>

Submitted on 12 Nov 2024

HAL is a multi-disciplinary open access archive for the deposit and dissemination of scientific research documents, whether they are published or not. The documents may come from teaching and research institutions in France or abroad, or from public or private research centers.

L'archive ouverte pluridisciplinaire **HAL**, est destinée au dépôt et à la diffusion de documents scientifiques de niveau recherche, publiés ou non, émanant des établissements d'enseignement et de recherche français ou étrangers, des laboratoires publics ou privés.

An integrative approach to characterize and predict cell death and escape to beta-lactam antibiotic treatments

Une approche intégrative pour caractériser et prédire la mort cellulaire et l'échappement aux traitements antibiotiques par beta-lactamines

Thèse de doctorat de l'Université Paris-Saclay

École doctorale n°581 : agriculture, alimentation, biologie, environnement, santé
(ABIES)

Spécialité de doctorat: Biotechnologies

Graduate School: Biosphera. Référent : AgroParisTech

Thèse préparée dans les unités de recherche **InBio** (Inria, Institut Pasteur) et **IAME** (Inserm, UPC, USPN), sous la direction de **Gregory BATT**, Directeur de recherche, et le co-encadrement de **Imane EL MEOUCHE**, Chargée de recherche et de **Erick DENAMUR**, Professeur.

Thèse soutenue à l'Institut Pasteur, le 3 octobre 2024 par

Viktoriia GROSS

Composition du Jury

Membres du jury avec voix délibérative

Lulla OPATOWSKI Professeure, Université de Versailles Saint-Quentin-en-Yvelines	Présidente
Kevin WOOD Associate Professor, University of Michigan (USA)	Rapporteur
Olivier TENAILLON Directeur de recherche, Inserm (Université Paris-Cité)	Rapporteur & Examineur
Helen ALEXANDER Principal Investigator, University of Edinburgh (UK)	Examinatrice
Claude LOVERDO Directrice de recherche, CNRS (Sorbonne Université)	Examinatrice

Titre : Une approche intégrative pour caractériser et prédire la mort cellulaire et l'échappement aux traitements antibiotiques par bêta-lactamines

Mots clés : résistance aux antibiotiques, beta-lactamases, traitements répétés, effets environnementaux, modélisation, optimisation de protocoles expérimentaux

Résumé : La résistance aux antibiotiques est de plus en plus courante. En particulier, la fraction croissante d' *Escherichia coli* commensaux et pathogènes exprimant des bêta-lactamases à spectre étendu et/ou des carbapénémases est alarmante. *E. coli* est une cause majeure d'infections courantes, telles que les infections urinaires, qui touchent plus de 150 millions de personnes dans le monde. Il est important de noter que de nombreuses infections récidivent. Il est donc essentiel de comprendre en profondeur la sensibilité des isolats cliniques d'*E. coli* aux bêta-lactamines pour proposer des traitements efficaces.

Les bactéries peuvent échapper aux traitements de différentes manières. Les bactéries résistantes se développent et se divisent normalement en présence d'antibiotiques. Leur caractérisation est facile à l'aide de tests de diagnostic standard. Les bactéries tolérantes se contentent de survivre en présence d'antibiotiques et repoussent lorsque l'antibiotique est retiré ou dégradé. Ce comportement biphasique complique la prédiction des résultats du traitement. La résilience au traitement est notamment observée dans la tolérance collective aux antibiotiques, où les cellules mortes libèrent des bêta-lactamases qui dégradent l'antibiotique dans l'environnement. Les approches standard ne sont pas adaptées pour quantifier et comprendre le rôle de la résistance et/ou de la résilience.

Nos principaux objectifs sont de quantifier la dynamique de la mort cellulaire au cours de traitements répétés et d'évaluer l'impact des différentes conditions environnementales sur la mort cellulaire. Tout d'abord, nous avons développé de nouveaux protocoles pour résoudre les problèmes de variabilité dans les mesures de densité optique et pour effectuer des tests

d'unités formant colonies de manière efficace. Grâce à ces techniques, nous avons généré un vaste ensemble de données décrivant l'impact de traitements répétés sur différents isolats cliniques. Nous avons calibré un modèle, précédemment développé par l'équipe, de la réponse de la population aux antibiotiques et de l'évolution de l'environnement dans le contexte de tolérance collective aux antibiotiques. Nous avons calibré le modèle sur l'ensemble des données et avons montré qu'il peut capturer l'évolution temporelle de la biomasse et du nombre de cellules vivantes. En outre, nous avons démontré qu'en utilisant ce modèle, nous pouvons prédire le nombre de cellules vivantes à partir des mesures de la biomasse. Dans ce travail, nous avons mis en évidence l'écart entre l'*in vitro* et l'*in vivo* en évaluant l'effet de différentes conditions de croissance sur la survie des cellules. Pour relever ce défi, nous avons étudié la réponse bactérienne dans l'urine humaine et dans le milieu de Mueller-Hinton (milieu utilisé pour les antibiogrammes standard), ainsi que dans un milieu défini avec différentes sources de carbone. Tout d'abord, nous avons observé une meilleure survie dans l'urine par rapport au milieu Mueller-Hinton, mais ce résultat variait en fonction de la souche et de la concentration d'antibiotique. Il est intéressant de noter que les données expérimentales ont montré que la concentration en nutriments n'avait pas d'effet sur le taux de croissance, mais un effet important sur la capacité de charge et la réponse aux antibiotiques. Grâce à l'étalonnage du modèle et à l'analyse des valeurs des paramètres du modèle, nous avons identifié des processus biologiques qui pourraient expliquer les différences entre le comportement des bactéries dans différents milieux.

Title: An integrative approach to characterize and predict cell death and escape to beta-lactam antibiotic treatments

Keywords: antibiotic resistance, beta-lactamase, repeated treatments, environmental factors, modelling, optimisation of experimental protocols

Abstract: Resistance to first-line antimicrobial drugs is now commonly encountered. In particular, the increasing fraction of commensal and pathogenic *Escherichia coli* expressing extended-spectrum beta-lactamases and/or carbapenemases is alarming. *E. coli* is a major cause of common infections such as urinary tract infections, affecting over 150 million people worldwide. Importantly, many infections relapse. Therefore, an in-depth understanding of the susceptibility of *E. coli* clinical isolates to beta-lactams is essential for proposing effective treatments.

Bacteria might escape treatments in many different ways. Resistant bacteria grow and divide normally in the presence of antibiotics. Their characterization is easy using standard diagnostic tests. Resilient bacteria merely survive in the presence of antibiotics and regrow when the antibiotic is removed or degraded. This biphasic behavior complicates the prediction of treatment outcomes. Resilience to treatment is notably observed in collective antibiotic tolerance, where dead cells release beta-lactamases degrading the antibiotic in the environment. Standard approaches are not adapted for quantifying and understanding the role of resistance and/or resilience.

Our main objectives are to quantify the dynamics of cell death during repeated treatments and to quantify the impact of different growth conditions on cell death. First, we developed novel protocols to address variability issues in optical density measurements, and to perform colony

forming unit assays in an efficient manner. Using these techniques, we generated an extensive dataset describing the impact of repeated treatments on different clinical isolates. We calibrated a previously developed in the team model of population response to antibiotic and evolution of the environment in the context of collective antibiotic tolerance. We calibrated the model to our dataset, and we showed that the model accounts for the temporal evolution of both biomass and live cell counts. Further, we demonstrated that using this model we can predict live cell number from biomass measurements.

In addition, in this work we highlighted the *in vitro* - *in vivo* gap by assessing the effect of different growth conditions on cell survival. To address this challenge, we studied the bacterial response in human urine and in Mueller-Hinton media (media used for standard antibiotic susceptibility tests), as well as a defined media with different carbon sources. First, we observed better survival in urine compared to Mueller-Hinton media, but this result varied depending on the strain and the antibiotic concentration. Interestingly, the experimental data showed that nutrient concentration had no effect on growth rate, but a strong effect on carrying capacity and antibiotic response. Through model calibration and analysis of identified model parameter values, we identified biological processes that could explain the differences between bacterial behavior in different media.

An integrative approach to characterize and
predict cell death and escape to β -lactam
antibiotic treatments

Viktoriia Gross

October 21, 2024

Acknowledgements

I would like to thank here all the people who helped me or were close to me during these four years.

Firstly, I would like to thank my supervisors: Gregory Batt, Imane El Meouche and Erick Denamur. It was a great pleasure and honor to work with them and to learn from them. Coming from different backgrounds, they helped me discover the field of antibiotic resistance from different perspectives. Gregory and Imane taught me a lot not only scientifically, but also on many other aspects of a research project.

I would also like to thank the thesis advisory committee and the jury members: Mary Dunlop, Marie Doumic, Olivier Tenaillon, Kevin Wood, Helen Alexander, Lulla Opatowski and Claude Loverdo, whose works have been sources of inspiration for me.

I would also like to thank my parents for their love and support and all my friends, especially Anna, Sofia, Mariia(s), Lisa.

I would like to thank all the people that I worked and / or spent time with at Institut Pasteur throughout these years. Special thanks goes to Agnes for all the coffee breaks, all the Friday night (and not only) afterwork drinks, for the wonderful trips, birthday celebrations and many other moments we spent together. I would also like to thank Sara for the support, scientific discussions and especially late night dinner in the lab. I would also like to warmly thank Esteban, Alicia, Lea, Henri, Nassim, Francesco and Lorenzo for everything that they have done for me, for their support, their help to make this thesis happen and for all the fun time we spent together. I would also like to thank previous member of InBio : Francois Bertaux, Sebastian Sosa Corrillo, Helen Phillipe. I would also like to StaPa and especially Valerio, Francesca and Remi. I would like to thank the theater group, the Pasteurussian tea club, the dance teacher and the running

team of Institut Pasteur that allowed me to disconnect from work and do something fun with other Pasteurians.

I would like to thank Virgile Andreani for scientific discussion and fruitful collaboration. I would also like to thank Vincent Aranzana-Climent for collaboration and sharing his software. I would also like to thank the Maestro team of Institut Pasteur for giving me access and helping me to obtain the enormous amount of model calibrations that was needed for this PhD. I would also like to thank IT department and especially Nicolas for rescuing my PhD after an unfortunate accident with my laptop.

Résumé en français

La résistance aux antibiotiques est un problème de santé mondiale, identifié comme prioritaire par l'Organisation Mondiale de la Santé. De nombreuses infections récidivent. *Escherichia coli* est une cause majeure d'infections courantes, telles que les infections urinaires, qui touchent plus de 150 millions de personnes dans le monde. Pour traiter ces infections, il existe plusieurs classes d'antibiotiques, définies en fonction de leur mécanisme d'action. La classe la plus prescrite actuellement est celle des bêtalactamines. Ces petites molécules inactivent des protéines liées aux pénicillines, qui jouent un rôle crucial dans la formation et le maintien de la paroi cellulaire. Cette inactivation peut entraîner la filamentation (élongation sans division), la perte de la forme habituelle, voire la mort des bactéries.

Les bactéries peuvent échapper aux traitements de différentes manières. Les bactéries résistantes se développent et se divisent normalement en présence d'antibiotiques. Leur caractérisation est relativement facile à réaliser à l'aide de tests de diagnostic standard. Les bactéries tolérantes, en revanche, survivent difficilement en présence d'antibiotiques, mais lorsqu'on retire ou dégrade l'antibiotique, elles repoussent. Ce comportement biphasique complique la prédiction des résultats du traitement. La résilience au traitement se manifeste notamment dans la tolérance collective aux antibiotiques, où les cellules mortes libèrent des bêta-lactamases qui dégradent l'antibiotique dans l'environnement. Les approches standards ne sont pas adaptées pour quantifier et comprendre le rôle de la résistance et/ou de la résilience.

De plus en plus d'*E. coli* commensaux et pathogènes expriment des bêta-lactamases à spectre étendu. Ces bactéries provoquent des échecs de traitement et des infections récurrentes. Il est donc essentiel de comprendre en profondeur la sensibilité des isolats

cliniques d'*E. coli* aux bêtalactamines pour proposer des traitements efficaces.

Dans cette thèse, je me suis intéressée aux infections récurrentes. Plusieurs facteurs pourraient impacter l'efficacité du traitement. Premièrement, il est crucial de comprendre les mécanismes de survie de la population bactérienne au traitement par bêtalactamines. Deuxièmement, la réponse d'une population bactérienne aux antibiotiques est multifactorielle et peut dépendre de son environnement. Comprendre l'influence de l'environnement peut être un bon point de départ pour appréhender la différence entre les conditions *in vitro* et *in vivo*. Pour cette raison, un autre objectif de ce travail est de quantifier l'impact des différentes conditions environnementales sur la mort cellulaire.

Notre approche combine différentes méthodes de caractérisation *in vitro* permettant de générer des données de haute qualité sur la densité optique (DO, 600 nm) ainsi que des comptages respectifs des cellules vivantes (UFC) de manière efficace. Grâce à cette approche, j'ai généré un ensemble de données riche décrivant la réponse d'une variété d'isolats cliniques aux différents traitements antibiotiques dans diverses conditions expérimentales. Afin d'améliorer l'analyse et la compréhension des mécanismes sous-jacents, nous avons utilisé un modèle mathématique qui synthétise les connaissances sur la réponse bactérienne aux traitements par bêtalactamines à plusieurs échelles. Nous avons calibré ce modèle avec nos données pour obtenir les résultats intéressants, décrits ci-dessous.

Cette thèse est divisée en sept chapitres et quatre annexes. Le premier chapitre présente le contexte général de l'étude : il définit ce qu'est la résistance aux antibiotiques et décrit les principaux défis associés aux échecs de traitement. Il aborde également l'écart entre les expériences *in vitro* et *in vivo* et les approches quantitatives de caractérisation de la résistance aux antibiotiques. Dans ce chapitre, je détaille également mon approche et les principales contributions de ce travail.

Le chapitre 2 décrit les développements expérimentaux que j'ai réalisés afin d'améliorer la quantité et la qualité des données. Comme mentionné précédemment, nous nous sommes intéressés à caractériser la réponse de divers isolats cliniques dans plusieurs conditions environnementales et face à différents traitements. Notre approche inclut la calibration d'un modèle mécanistique sur les données expérimentales, ce qui nécessite une grande quantité de données de bonne qualité.

Le premier problème que j'ai rencontré est la forte variabilité des mesures de densité optique (DO). Cela inclut non seulement la variabilité entre les expériences, mais aussi celle entre les répliquas techniques d'une même expérience. Le comportement typique que nous observons consiste en une phase de croissance exponentielle, suivie d'un arrêt de croissance, puis parfois d'une reprise de croissance. Au cours de certaines expériences, nous avons observé des différences de plusieurs heures dans le temps de repousse ou même, parfois, l'absence de repousse pour un répliqua tandis qu'elle était présente pour l'autre. Pour étudier la cause de ces observations, nous avons effectué un scan complet du fond de chaque puits de la plaque expérimentale à la fin de l'expérience et découvert des motifs inhomogènes.

L'un des mécanismes connus d'adaptation des bactéries à un environnement défavorable est la formation de biofilms, qui sont des agrégats de bactéries formant des couches de protection contre les antibiotiques. J'ai utilisé le cristal violet, un marqueur des biofilms, et j'ai confirmé la présence de ces structures. La solution que nous avons trouvée a été d'ajouter du Tween 20 au milieu, une technique déjà utilisée pour lutter contre les biofilms dans les bioréacteurs.

La deuxième partie du protocole expérimental qui a dû être améliorée concerne l'estimation du nombre de cellules vivantes. Dans cette thèse, je propose une approche où l'échantillonnage, les dilutions en série et les dépôts sur les boîtes de Petri sont réalisés pour les 96 conditions simultanément à l'aide d'une pipette à 96 canaux. Pour pouvoir compter les colonies sur ces boîtes, j'ai utilisé un logiciel développé par une autre équipe, que j'ai re-entraîné avec mes données et adapté à mon setup expérimental.

Le chapitre 3 décrit les travaux réalisés pour caractériser en détail la réponse de la population bactérienne aux traitements antibiotiques. Je présente ici le modèle utilisé tout au long de cette thèse. Il s'agit d'un modèle mécanistique précédemment développé au sein de l'équipe, qui capture les différents aspects de la réponse bactérienne : la filamentation induite par les bêtalactamines, la mort cellulaire lorsque les bactéries atteignent une longueur critique, la dépendance de cette longueur critique à la concentration d'antibiotique, et enfin la dégradation de l'antibiotique par les bêta-lactamases libérées par les cellules mortes dans le milieu.

En utilisant l'approche détaillée décrite précédemment, j'ai caractérisé phénotyp-

iquement la réponse à la cefotaxime pour une collection de 11 isolats cliniques. J'ai ensuite réussi à calibrer le modèle sur les données de densité optique (DO) et de unités formant colonies (UFC) ensemble, ce qui nous a permis de réconcilier les différences entre l'évolution temporelle de la biomasse et le nombre de cellules vivantes, et de mieux comprendre les mécanismes d'échec des traitements pour ces bactéries. L'analyse des valeurs des paramètres du modèle a également permis de relier la réponse phénotypique au contexte génétique de certaines souches.

Le chapitre 4 décrit les travaux réalisés pour tester la capacité prédictive du modèle. L'objectif principal était de pouvoir prédire le nombre de cellules vivantes en utilisant uniquement les données de DO. J'ai tenté d'utiliser les données de DO des expériences décrites dans le chapitre précédent, mais cette approche n'a pas fourni de bonnes prédictions de manière robuste. J'ai donc réalisé des expériences supplémentaires où j'ai ajouté une deuxième dose d'antibiotique quelques heures après le début de l'expérience.

En utilisant l'évolution temporelle de la DO pour quatre expériences (une expérience de traitement simple où tous les antibiotiques sont administrés au début et trois expériences de traitement répétées avec une deuxième administration), j'ai réussi à obtenir de bonnes prédictions du nombre de cellules vivantes pour les traitements simples de manière robuste. Dans ce chapitre, je décris également les analyses que j'ai effectuées pour enquêter sur la valeur ajoutée des expériences avec traitements répétés. Pour aller plus loin, nous avons testé la capacité du modèle à prédire le nombre de cellules vivantes associé à l'effet de l'inoculum et à identifier un traitement optimal.

C'est déjà connu que les conditions dans lesquelles la susceptibilité aux antibiotiques est normalement testée sont très éloignées de celles des infections réelles. Plusieurs facteurs peuvent influencer l'efficacité des traitements : l'identité de la souche, des facteurs pharmacologiques, des facteurs humains (l'immunité locale, l'exposition antérieure aux antibiotiques, les infections passées) et des facteurs environnementaux. Dans le chapitre 5, j'ai utilisé la même approche que dans le chapitre 3 pour caractériser la réponse de la population bactérienne aux traitements de cefotaxime dans différents milieux. Pour cette caractérisation, nous avons choisi le milieu Mueller-Hinton (MH), le milieu standard pour les tests de susceptibilité en clinique, et l'urine humaine, milieu choisi pour mimer les conditions des infections urinaires.

Nous avons observé que les souches survivent mieux dans l'urine par rapport au MH lorsqu'elles sont soumises à de faibles concentrations d'antibiotique, alors que l'inverse est vrai : elles repoussent plus rapidement dans le MH par rapport à l'urine quand elles sont soumises à de fortes concentrations d'antibiotique. Étant donné que les nutriments principaux dans l'urine et dans le MH sont les acides aminés, mais qu'il existe une quantité différente disponible, j'ai également testé certaines souches dans un milieu défini (M9) avec différentes concentrations de casamino acids.

À partir de ces expériences, nous avons observé que le taux de croissance ne varie pas entre les différentes concentrations de nutriments, mais qu'il y a une grande différence dans le temps de repousse. Afin de mieux comprendre les différences entre les milieux, j'ai calibré le modèle et analysé les valeurs des paramètres. L'utilisation d'un algorithme de réduction de dimensionnalité (PCA) a permis d'identifier une explication possible pour les différences observées : il pourrait y avoir une différence dans le niveau de production et/ou d'activité des bêta-lactamases entre l'urine et le MH. Le PCA a également montré que le milieu a un impact plus important sur les valeurs des paramètres que l'identité de la souche.

Il existe plusieurs extensions possibles pour ce travail. La première serait de tester expérimentalement l'hypothèse identifiée par l'analyse en composantes principales (PCA). De manière plus globale, il serait très intéressant de quantifier l'impact d'autres facteurs environnementaux, tels que le pH ou la concentration de fer. Une autre extension consisterait à combiner les approches des chapitres 4 et 5 afin d'étudier la réponse aux traitements multiples dans différents milieux. Par ailleurs, il serait fascinant de tenter de distinguer les effets individuels des bêta-lactamases et des mutations variées. Notre modèle pourrait également servir de base solide pour un modèle pharmacodynamique et pharmacocinétique (PK/PD), qui pourrait un jour aider les cliniciens à améliorer leurs méthodes de diagnostic.

Contents

1	Introduction	17
1.1	Context and motivation	17
1.2	Problem statement and approach	28
1.3	Contributions	29
1.4	Outline	31
2	Experimental developments	33
2.1	Introduction	33
2.2	Addressing the issue of OD measurement variability	34
2.3	Protocol for efficient plate-based CFU assays	38
2.4	Conclusions	42
3	In-depth characterization of bacterial population response to β-lactam treatments	43
3.1	Introduction	43
3.2	Characterization of antibiotic response of clinical isolates	45
3.3	The impact of genetic background on response to antibiotic	53
3.4	Can the model capture the temporal evolution of OD for other β -lactam antibiotics?	55
3.5	Conclusions	57
4	Quantifying the impact of multiple antibiotic applications on cell death	59
4.1	Introduction	59

4.2	Prediction of the temporal evolution of CFU based on the temporal evolution of OD	60
4.3	Effect of repeated treatment experiments on parameter search efficiency	66
4.4	Prediction of complex temporal evolution of CFU for delayed treatments	69
4.5	Optimal treatment	71
4.6	Conclusions	75
5	Quantifying the impact of growing conditions on cell death	77
5.1	Introduction	77
5.2	Characterization of bacterial population's response to β -lactam treatment in different growing conditions	79
5.3	Model-based approach to identify potential differences between the media	84
5.4	Conclusions	89
6	Discussions	91
6.1	Thesis summary	91
6.2	Discussions and Perspectives	93
7	Materials & Methods	97
7.1	Strains and antibiotics	97
7.2	Growth conditions	97
7.3	Growth curves acquisition	100
7.4	Live cell number estimation.	101
7.5	Data analysis	101
7.6	Model	101
7.7	Model fitting	104
7.8	Crystal violet staining	106
7.9	eVOLVER experiment	106
7.10	Microscopy experiment using CellASIC ONIX plate	106
A	Alternatives to CFU assays: auto-fluorescence and propidium iodide staining	109

B	The automated platform for repeated antibiotic applications	113
C	Application of bioreactor platform to study antibiotic resistance	117
D	Study of filamentation and critical length using microscopy and image segmentation pipelines	123

Abbreviations

AF Autofluorescence. 109

BF Bright-Field. 124

CFU Colony Forming Unit. 28

MH Mueller Hinton broth. 78

MIC Minimal Inhibitory Concentration. 25

ML Machine Learning. 24

OD Optical Density at 600nm. 28

PI Propidium Iodide. 110

Chapter 1

Introduction

1.1 Context and motivation

Antimicrobial resistance is recognised by the World Health Organization (WHO) as one of today's major health problems [1]. An increasing incidence of hospital-acquired infections, such as bacteremia, pneumonia and urinary tract infections (UTIs) is caused by antibiotic resistant pathogens. These infections can be associated with an increased morbidity and mortality (15% in bacteremia) and their burden is thought to be substantial compared to other infectious diseases [2]. Carbapenem-resistant and third-generation cephalosporin-resistant Enterobacterales continue to be in the critical priority category of the WHO bacterial priority pathogen list 2024 in terms of the need for new antibiotic development [3]. This includes *Escherichia coli*, *Klebsiella pneumoniae*, and *Enterobacter* spp.

E. coli is a commensal member of the vertebrate gut microbiota and a major opportunistic pathogen [4, 5]. *E. coli* strains can cause intestinal and extra-intestinal infections such as UTIs, bacteremia, meningitis and diverse intra-abdominal, pulmonary and skin infections. *E. coli* genome is highly plastic comprising between 3900 and 5800 genes. These genes are found in the chromosome or carried on plasmids. Phenomena like mutations, genetic recombination and horizontal gene transfer contribute largely to the diversity of the species. While *E. coli* has a high genetic diversity, it has a clonal population structure represented by eight phylogroups: B2, G, F, D, A, B1, C and E.

No strict phylogenetic differences separate commensal or extra-intestinal pathogenic strains. However, while strains from the phylogroups A, B1 and E are mostly commensal, strains of the phylogroups B2 and D are associated with extra-intestinal infections. While *E. coli* is an intrinsically sensitive species, it has a large capacity to accumulate genetic resistance via mutations and horizontal gene transfer.

The most commonly prescribed class of antibiotics today (about 50% of all antibiotic prescriptions worldwide [6]) is the β -lactam class. Based on the chemical structure of their core scaffold, they are divided into penicillins, cephalosporins, monobactams and carbapenems. Cephalosporins are the most widely used β -lactams and are commonly prescribed for both mild and severe infections, including UTIs and skin and soft tissue infections. They are divided into four generations, the most commonly used being second generation, narrow-spectrum antibiotics and third generation, broad-spectrum antibiotics [7]. Combining a beta-lactam with a beta-lactamase inhibitor increases the antibacterial action and spectrum of beta-lactams especially against beta-lactamase producers *E. coli*. Lastly, carbapenems are the newest and most effective antibiotics in this class. They are the antibiotics of last resort, reserved for serious and complicated infections.

The mechanism of action of these penicillin-derived antibiotics is to inactivate penicillin-binding proteins (PBPs), named after their affinity for the famous antibiotic. These proteins play an important role in the formation and maintenance of the cell wall and cell shape. During their normal life cycle, bacteria undergo several morphological transformations, each of which depends on different PBPs. For example, in *E. coli*, PBP3 acts during septation and PBP2 controls cell elongation. Class A PBPs (including PBP1) affect general morphological development. Inhibition of PBP3 can lead to inhibition of cell division. Deletion of PBP2 can result in loss of rod shape and formation of spherical cells. Inhibition of PBP1 disrupts the peptidoglycan synthesis machinery, resulting in loss of coordination between elongation and septation, "breaks" in the peptidoglycan surface, or changes in cell diameter [8].

At one time, these broad-spectrum antibiotics were highly effective against gram-negative bacilli and most enterobacteriaceae [9]. However, the extensive use of these antibiotics in both medicine and agriculture exerted selective pressure on bacteria, leading

to the acquisition of resistance to all known β -lactams [6]. Resistance to beta-lactams mainly through beta-lactam hydrolysis is nowadays one of the main problematic mechanisms of antibiotic resistance in *E. coli*.

There are many ways for bacteria to evade antibiotic treatment. The best-studied phenomena is individual resistance, which allows cells to grow and divide normally in the presence of supposedly inhibitory concentrations of antibiotics. Antibiotic resistance is often mediated by acquisition of resistance genes and can emerge due to selective pressure from the antibiotic.

In terms of resistance to β -lactam treatments, we can identify three main groups of mechanisms: (i) modification of the antibiotic target, (ii) regulation of influx or efflux pumps, or other membrane permeability modifications, or (iii) enzymatic degradation of antibiotics [10]. The most prominent of the three is the expression of β -lactamases, which are able to hydrolyse β -lactam antibiotics inside and outside the cell. Based on peptide sequence and their active site, the β -lactamases were classified in 1980 and divided into groups [11, 12]. For instance, the CTX-M enzyme is a class β -lactamase (Ambler definition), that hydrolyse the antibiotic after the formation of an acyl-enzyme intermediate. Interestingly, multiple β -lactamases encoding genes can be found together in one bacterial strain [13].

Another form of antibiotic escape is tolerance, which allows bacteria to merely survive during treatment without necessarily being genetically resistant. This can occur through individual adaptations such as changes in growth rate, length of lag phase or changes in cell shape, or through population effects which can also affect bacterial response to β -lactams [14, 15].

As well as having individual survival means, bacteria as a population can survive antibiotic concentrations that are lethal to individual cells. This can be due to a variety of different mechanisms, such as inter-population communication or growth inhibition. One of the most common strategies is called Collective Antibiotic Tolerance (CAT) and consists of the release into the environment of β -lactamases capable of degrading antibiotics following the death of a fraction of the population. The growth of the population depends on its initial density: if the antibiotic is degraded to sub-lethal levels before the entire population is eradicated, the survivors are able to rebuild the population [16].

Nowadays, an increasing proportion of commensal and pathogenic *E. coli* expresses extended spectrum β -lactamases (ESBL) and/or carbapenemases. The emergence of ESBL-producing bacteria causing urinary tract and bloodstream infections worldwide is one of the major epidemiological challenges [17]. Infections caused by these bacteria are associated with delays in appropriate treatment, resulting in longer hospital stays, increased hospital costs and even higher patient mortality [18].

Urinary tract infections (UTIs) are among the most common infections today [19]. In 2019, there were more than 400 million cases of UTI worldwide. These infections also caused more than 200,000 deaths in the same year. About half of all women will experience a UTI at least once in their lifetime [20]. Although more common in women, UTIs can also affect men [21]. If left untreated, UTIs can progress to renal failure or sepsis. *E. coli* is one of the major pathogens in both complicated and uncomplicated urinary tract infections [22].

The recommended treatment is a short course of a commonly used empirical antibiotic, which in the majority of cases is prescribed before bacteriological testing is available [23]. Urinary tract infections represent a significant global health burden due to a high rate of recurrence as a result of increasing antimicrobial resistance, which compromises the effectiveness of treatment [22]. There is evidence of an association between advancing age and an increased risk of bacterial resistance, but even among young women, one in seven people treated with antibiotics is expected to return for a repeat prescription within a month. In addition, a patient's previous exposure to antibiotics is known to increase the risk of treatment failure. Pregnancy and diabetes have also been associated with an increased risk of treatment failure [23]. Despite their prevalence, UTIs are still under active investigation and the underlying mechanisms are not fully understood [24]. Therefore, understanding the molecular mechanisms and developing alternative treatments are essential to address this global health issue [22].

Previous studies [25] have identified some of the risk factors for acquiring infection with ESBL-producing bacteria, such as previous hospitalisation or antibiotic treatment in the 3 months prior to infection, especially if the antibiotic belonged to the cephalosporin or quinolone classes. Older age, diabetes and male sex also contribute to the acquisition of ESBL-producing bacteria. We find similar observations in another

study [26], which shows that UTIs are more common and cause more serious complications in patients with diabetes. Previous studies [27] have also shown that in trauma patients (those requiring intensive care unit admission and indwelling urethral catheters) there are several significant changes in urine composition, such as increases in urinary glucose, some amino acids, iron and norepinephrine concentration. Decreases in urea concentration and osmotic pressure have also been reported in these patients. Changes in the concentrations of amino acids and glucose are known to influence bacterial growth in the urine. A decrease in urea concentration is also beneficial for bacterial proliferation because of its antibacterial effect and its effect on osmotic pressure. All these effects were observed until at least the fifth day after the trauma and could be one of the factors facilitating the acquisition of UTI in these patients.

Another often relapsing infection is a bloodstream infection (BSI). It can be a complication of a previous infection or a primary infection. BSIs account for 40% of community and hospital-acquired sepsis and 20% of intensive care unit (ICU)-acquired sepsis. Standard treatment is 5-8 days of antibiotic therapy. Once again, *E. coli* is the most common cause of community-acquired infections. In addition, there is a massive spread of ESBL-producing pathogens at the origin of these infections; especially those secondary to urinary tract infections or intra-abdominal infections [28]. BSIs are also known to relapse, particularly those caused by *E. coli*. It has been found that resistant strains are often associated with an increased risk of additional infection shortly after the original infection and an earlier occurrence of recurrent infection. Uropathogenic *E. coli* is known to be predominant in recurrent UTI BSI episodes. Other established risk factors for BSI recurrence include age, previous illnesses and their severity, structural abnormalities of the biliary or urinary tracts [29]. It has also been shown that previous infections caused by ESBL producers and the use of multiple antibiotics prior to infection increase the risk of ESBL producer infections. Early identification of such infections allows early and effective treatment and minimises overuse of carbapenems, the antibiotics of last resort [30].

With the global and rapid spread of antibiotic resistance, there is an urgent need for new treatments. However, there has been a noticeable decline in antibiotic discovery over the last 20 years: only 17% of clinical trial projects reach market approval after

12 years of development, and the median approval time is over 9 years for proposals submitted in the 2000s. Due to the high costs of development, preclinical and clinical studies, large pharmaceutical companies are leaving the field and most proposals come from small companies [31, 32].

In summary, the two main challenges of treatment failure are that the mechanisms of antibiotic resistance are not fully understood and need to be studied in more detail, and that there is a strong dependence of infection severity and incidence on the environmental conditions in which bacteria grow. Therefore, in-depth phenotypic characterisation of the antibiotic susceptibility of *E. coli* clinical isolates to β -lactams is essential to propose effective treatments.

1.1.1 *In vitro* / *in vivo* prediction gap

Most *in vitro* susceptibility tests are performed in Mueller-Hinton medium [33]. It is very rich and allows good bacterial growth, but is quite far from the conditions under which infections usually occur. Many studies have shown significant discrepancies between *in vitro* and *in vivo* conditions in terms of antibiotic susceptibility. For example, a study [34] showed that imipenem and ertapenem were unexpectedly effective *in vivo* against isogenic carbapenemase-producing *E. coli* despite *in vitro* resistance. The reasons for these paradoxical results are not fully understood. There have also been studies on the importance of the inoculum effect for peritonitis, one of which (Godron A.-S. et al, in preparation) has shown that there is a significant effect of initial population size on the efficacy of cefiderocol against NDM-producing *E. coli* *in vitro*, but this phenomenon is not observed *in vivo*. This may be related to the micro-environment of *in vivo* conditions.

Murine models are valuable for understanding UTI treatments but are costly, labour intensive and ethically problematic, which limits their systematic use. In addition, animal models may not fully replicate the human environment for disease physiology and treatment prediction, especially since mice do not naturally suffer from UTI. Therefore, the debate among UTI researchers about the use and accuracy of animal models continues [21].

Bridging the gap between classical *in vitro* assays, which are limited in their ability

to comprehensively elucidate bacterial activity within the host environment, and the *in vivo* already interested scientific community. There are several studies aimed at developing new *in vitro* experimental setups. Good *in vitro* alternatives to animal infection models are human cell-based models such as cell mono-layers, tissue cultures or organoids, but all these techniques are not easily accessible [21]. Another commonly used technique is the hollow fiber infection model: a two-compartment model where bacteria are trapped in the hollow fiber cartridge while nutrients and drugs can circulate inside [35]. This setup allows systematic sampling without affecting the bacterial population, it also allows observations of drug-drug interactions and the efficacy of combination therapies in a closed environment. This system has proven to be very useful for pharmacokinetic and pharmacodynamic evaluations [36, 37]. The disadvantage of this system is that the cartridges cannot be reused after one experiment and the hollow fibre membranes are very fragile and quite expensive.

Another *in vitro* experimental system is a MiniBioReactor Array [38] contained in an anaerobic chamber, which allowed the authors to reliably mimic the gut microbiota and study the effect of antibiotics on its diversity and on β -lactamase activity [39]. This setup has the capacity to run up to 24 separate conditions simultaneously, and the duration of an experiment was about 2 weeks. Several other similar but simpler experimental platforms using low volume bioreactors have been developed [40, 41]. The experimental workflow combines evolution in a continuous culture device with sequencing of population samples. The main application is to study the acquisition of resistance in the context of antibiotic selective pressure created by alternating between media with and without antibiotics for regular culture dilutions. the use of bioreactors allows manipulation of the chemical environment and systematic sampling over time.

All of these novel experimental platforms aim to mimic *in vivo* conditions in order to elucidate the environmental factors influencing treatment failure, and have proven to be very useful in their own way. However, they all remain quite low throughput and do not allow a wide variety of conditions to be tested. Therefore, the state of the art consists either of high-throughput tests, that are very far from real infection conditions, or low-throughput and experimentally demanding systems that aim to bridge the gap between *in vitro* and *in vivo*. Our approach aims at the middle ground: using a simple

set-up supplemented by additional systematic measurements to characterise a significant number of conditions. We combine this method with model-based approaches for quantitative characterisation. This combination of experiment and model would provide a detailed view and compensate for the reduced amount of data.

1.1.2 State of the art in antibiotic resistance models

As nicely argued by Lopatkin and Collins [42], in the current era of big data and technological development, the field of predictive analytics has significantly changed the way we experience our daily lives. In this context, it seems that we can greatly benefit from the ability to predict biological outcomes from a set of known inputs. Today, there are two major approaches in predictive biology: mathematical models that aim to interrogate, explain and identify relevant parameter values for biological systems, and machine learning (ML) techniques that focus on exploiting the huge amount of data collected over all these years of fighting antibiotic resistance to identify trends and predict outcomes.

In the era of big data and up-scaling, there is a tendency to collect as much generated data as possible and use machine learning approaches to detect trends that can be used to predict antibiotic resistance. There are several different strategies for this approach. Some studies, such as [43], use deep learning to distinguish cells with a susceptible phenotype from cells with a resistant phenotype in images based on single-cell microscopy data. Their approach was to first use deep learning to segment images of treated and untreated cells, and then to classify segmented cells as resistant and susceptible. The authors argue that their approach enables the assessment of susceptibility to a specific antibiotic in a much shorter time than traditional assays based on growth analysis. The limitation of this approach is that it requires a large number of images of cells with the same phenotype, which is homogeneous across cells and isolates of the same phenotypic class, which can be complicated given the variability of bacterial behaviour and the rapid evolution of resistance mechanisms.

Most studies using big data approaches to antimicrobial resistance focus on genomes, trying to predict bacterial response to treatment. As sequencing, and in particular whole genome sequencing (WGS), has become possible and widely available, more and more

data is available on different pathogens. Pataki B. and colleagues used the genomes of 704 *E. coli* combined with their respective minimal inhibitory concentration (MIC) measurements to develop a machine learning approach to predict the MIC for a given antibiotic based on genome-wide mutation profiles and information on acquired resistance genes [44]. In this study, the authors have identified a number of biologically understandable features, such as specific mutations in DNA gyrase subunit *gyrA* or topoisomerase *parC* or presence of *qnrS1* gene (quinolone resistance gene), that strongly influence susceptibility and MIC level, which is consistent with previous experimental studies. Interestingly, this approach works better for strains with high MICs (32 mg/L and higher), but is less accurate for lower MICs. The authors also mentioned that as sequencing becomes more widespread and available, it may one day be easier to sequence pathogens than to perform MIC tests. This is not the only study interested in data-driven approaches to linking genotype and phenotype resistance. The authors of another study analysed 234 isolates and the MIC of 11 clinically relevant antibiotics [45]. Again, most discrepancies occurred for isolates with MICs close to the EUCAST breakpoint. Some have developed a tool that uses WGS to predict outer membrane porin defects, which play an important role in carbapenem resistance in *Pseudomonas aeruginosa*, however, this tool covers only some of the known mutations, additional data and effort are needed to include other variants [46].

Much effort is now being put into homogenising available datasets and linking genomes to infection information, as well as tracking the origin of infections and their spread [47, 48]. This has allowed some studies to find clinical application. Several studies have presented a new ML approach for algorithmic antibiotic prescription [49, 50]. This approach consists of using combinations of pathogen genome and electronic health record to prescribe antibiotic treatment for a new patient. The motivation for these studies is that in many cases the prescription is made before the susceptibility of the pathogen has been tested, leading to empirical treatments that are either ineffective in eradicating the infection and lead to relapse, or consist of broad-spectrum antibiotics, exposure to which promotes antibiotic selection pressure and increases the risk of a new infection being resistant to that antibiotic. Interestingly, many UTIs originate from the patient's own microbiota, making the patient's medical history valuable for person-

alised treatment recommendations. Deep neural networks have also proved useful for drug discovery [51].

The success and popularity of predictive biology is largely due to the rise of the field of synthetic biology. Over the last two decades since the first publication of Toggle Switch, more and more applications of synthetic biology have been developed, and antibiotic resistance is no exception. The design of genetic elements and genetic modifications has made it possible to independently study different mechanisms that contribute to antibiotic resistance. For example, Chung and colleagues [52] have studied the mechanisms of cell lysis during β -lactam treatments that inhibit penicillin-binding proteins (PBPs). These proteins are involved in peptidoglycan synthesis and processes such as cell division and cell wall maintenance. It is well known that some β -lactams target division-specific PBPs, thereby inducing filamentation (growth without division). By measuring population dynamics and performing time-lapse microscopy on genetically engineered cells, the authors sought to address the lack of understanding of the lysis mechanism of these filaments. Another team carried out a detailed study of correlations between bacterial behaviour in different culture media and heterogeneity in β -lactamase production, using a microfluidic chip for single-cell analysis of bacteria with fluorescently tagged β -lactamases [53]. They observed that under poor nutritional conditions, bacteria tend to reduce their growth rate and protein expression levels in the presence of antibiotic stress. If conditions deteriorate further, the cells may eventually enter a dormant state, reducing the rate of cell wall synthesis and thus escaping antibiotic treatment. These and other similar studies have provided a better understanding of the subtle mechanisms of antibiotic resistance, but they require the construction of mutant libraries, which is an experimentally demanding task and difficult to scale up to study a wide range of mechanisms and build up a complete picture.

Kim and colleagues went further, combining single-cell microscopy analysis with population dynamics measurements and mathematical modelling [54]. This study provided insights into antibiotic-induced filamentation and cell lysis: they showed that the probability of cell lysis increases as the size of filamentous bacteria increases, and that the critical length that bacteria can reach before dying decreases with increasing antibiotic concentration. The authors also observed a correlation between the population

growth rate and its lysis rate. Most importantly, this study used mathematical modelling to link single-cell and population-level responses to antibiotic treatments and to predict the population-level response from the single-cell level. This work required significant experimental effort and single cell analysis, but allowed to capture and characterise subtle mechanisms of lysis of filamentous cells, which is an important and poorly understood problem. This work demonstrates the importance of combining experimental and modelling techniques in the study of antibiotic resistance.

In short, there are two main approaches to the study of antibiotic resistance today: on the one hand, a very detailed, low-scale approach that requires a great deal of experimental and analytical effort and allows elucidation of specific responses or resistance mechanisms; on the other hand, a data-driven, high-throughput approach that requires large amounts of genotype and phenotype data and allows phenotype and genotype to be linked in a limited way without providing much information about the cellular mechanisms of resistance and without considering population effects. Our approach aims at the middle ground between the two: it consists of using a mathematical model [55] together with measures of population dynamics in response to antibiotic treatment. The idea to use combination of simple experiments and a mathematical model was already exploited in several studies, but did not lead to the same precision of phenomenon understanding. The utility of models in complementing experimental efforts to gain insight into antibiotic treatment response has previously been argued by Tandar and colleagues [56]. There are several studies that have already used similar approaches and proposed models of population response to β -lactam treatments. Lee and colleagues, in their study of correlations between growth rates and β -lactam-mediated lysis rate, measured growth and killing curves for a range of bacterium-antibiotic combinations under different experimental conditions. In addition, they used stochastic modelling to provide a deeper mechanistic interpretation of the observed population-level responses and link them to single-cell dynamics. In general, biological processes are complex and diverse, and the presence of collective antibiotic tolerance makes it even more difficult to capture the whole picture [57]. As argued by the authors of this study and also the one of [15], a quantitative understanding of population effects and their correspondence to single-cell dynamics is essential for the design and evaluation of future treatments, such

as combinations of β -lactam antibiotics with β -lactamase inhibitors.

1.2 Problem statement and approach

Understanding the underlying mechanisms and overcoming the diagnostic challenges are essential in the current fight against recurrent infections. The mechanisms of treatment failure are not fully understood and can be influenced by the environment, in particular the composition of the media. Furthermore, there is a known gap between *in vitro* and *in vivo* conditions. Therefore, a detailed phenotypic characterisation of the antibiotic response of *E. coli* clinical isolates to β -lactams is essential to propose effective treatments.

In this work, I focused on β -lactamase-producing (mostly ESBL) *E. coli* clinical isolates and their response to β -lactam treatments (mostly exclusively cefotaxime, a third-generation cephalosporin). We selected 11 clinical isolates with different origins, different genetic backgrounds and different levels of antibiotic susceptibility [58, 59]. These strains express a panel of different families of β -lactamases, including carbapenemases, and some express several of them simultaneously. Some of these strains also contain gene mutations that contribute to their antibiotic susceptibility. This selection includes strains from both human and animal infections, represents several sequence types and ranges from highly susceptible to highly resistant to β -lactam treatments.

Our experimental approach combines different methods of *in vitro* characterisation and allows us to generate high quality optical density (OD, 600 nm) data together with the corresponding number of live cells through colony forming unit (CFU) assays performed in a high throughput manner. Using this approach, I generated a rich dataset describing the response of a variety of clinical isolates to a range of antibiotic concentrations under different experimental conditions. To improve analysis and understanding of the underlying effects, we used a mathematical model that synthesises the field's knowledge of bacterial response to β -lactam antibiotics across multiple scales. We calibrated the model to experimental data and used the resulting parameter value sets to: 1/ provide a consolidated view that captures the temporal evolution of both total biomass and live cell counts; 2/ analyse the impact of the genetic background of clinical isolates on their

response to cefotaxime treatments; 3/ study the effect of multiple antibiotic applications on population response and predict live cell counts based on OD measurements; and last but not least, 4/ investigate the role of environmental conditions on bacterial response to antibiotic treatments.

1.3 Contributions

This thesis presents several methodological and theoretical contributions to the field of antibiotic resistance.

On the methodological side, in chapter 2, section 2.2, I present variability issues of OD measurements that I encountered while characterising clinical isolates' response to antibiotics, as well as experimental diagnostics of the underlying problem (biofilm detection), and a simple solution to address this problem and significantly improve the reproducibility of observations (addition of Tween 20 to growth media). As a result, the proposed approach allows the generation of high quality OD data with minimal adjustments and no significant impact on growth rate. This approach already existed for higher volume experiments (bioreactor platforms) but had been overlooked for microplate experiments.

Another methodological contribution was the development of a new experimental protocol for up-scaling the CFU assay, which is presented in chapter 2, section 2.3. Given the number of experimental conditions we wanted to test, the standard protocol was too slow and too experimentally demanding, so I started a droplet-based protocol using a 96-channel pipette to prepare dilutions and spot the entire 96-well plate at once. In order to limit the use of plastic and the cost of consumables, I developed a protocol that included washing steps and therefore allowed the reuse of tips for all dilutions within one time point, limiting the risk of contamination. This protocol has been experimentally validated. I also adapted for this project a counting software developed by Vincent Aranzana-Climent and the Pharmacology of Antimicrobial Agents and Antibioresistance team at INSERM: I retrained the machine learning part on my images and adapted the R code to my experimental conditions, plate types, coordinates, dilutions and file naming system.

There are some other methodological advances described in the appendices. I have tested possible alternatives for CFU assays that would be less experimentally demanding. I also contributed to the development of automated platforms in the team. This platform combined a pipetting robot and a plate reader controlled by a computer. I tested two applications for this platform: automated antibiotic administration based on OD measurements and a turbidostat in a microplate with antibiotic pressure in the media. I also set up a bioreactor platform and carried out two applications of this setup: studying the lag time and maximum growth rate in different media and observing the inoculum effect in a bioreactor.

This work focuses on characterising the response of bacterial populations to different antibiotic treatments in different environmental conditions. There are several important results from this project. First, using a model-based approach, we were able to propose a very detailed understanding of the population response to β -lactam treatment and, in the meantime, reconcile differences between the temporal evolution of OD and CFU. Second, we studied the population response to multiple doses of antibiotics. These conceptually simple experiments gave us a lot of valuable information about cell death and β -lactamase activity. They also allowed us for the first time to predict live cell counts (very informative, but very experimentally demanding) from OD data (easy to generate, hard to exploit). These results improve our understanding of collective antibiotic tolerance.

Another important result was obtained by comparing the bacterial response to antibiotic treatment in different growth conditions, specifically urine and Mueller-Hinton media (standard media for antibiotic susceptibility testing). We were able to identify interesting trends in parameter values, suggesting that β -lactamase production and activity may differ between these two media. In addition, further analysis of the model parameter values revealed a clear distinction between sets of parameter values corresponding to different media. Interestingly, among our selected set of strains, strain identity had less influence than growth conditions on the results of clustering in dimensionality reduction.

To obtain these results, I generated a large dataset using the methodological adjustments presented in chapter 2. Further adjustments were necessary for efficient data anal-

ysis and model calibration (more than 7500 individual calibrations on different datasets). This required parallelizing the search for parameter values and the use of computational clusters. Additional efforts were made to adapt the calibration protocol to different types of datasets: 1/ to fit the model to both OD and CFU data, we developed a two-step procedure that first calibrated a subset of parameters to growth without antibiotics, and then fixed this subset to optimal values and restarted the search for the rest of the parameters; 2/ we investigated the effect of the composition of the experimental dataset on the predictive capabilities of the model calibrated to that dataset; 3/ to test different media in relevant manner, we had to adjust bacterial growth models.

1.4 Outline

This document is divided into 7 chapters and 4 appendices. This chapter is an introductory overview of the general threat and challenges of treatment failures, the existing gap between *in vitro* and *in vivo* experiments and the main quantitative approaches for antibiotic resistance characterisation. It presents the approach I used for my PhD and the contributions I made.

Chapter 2 presents the experimental developments that have been made to generate high quality data in an optimised way: improving OD quality by addressing the biofilm issue and scaling up the CFU assay protocol. In this chapter I describe in detail the experimental protocol used for data generation in the following chapters.

Chapter 3 presents our in-depth characterisation of the response of clinical isolates to β -lactam treatments. It first introduces a model previously developed in the team and the challenges of standard experimental methods for characterising antibiotic resistance. We demonstrate that the model captures the temporal evolution of both OD and CFU, despite large decorrelations between the two measures.

Chapter 4 describes how the bacterial population responds to two antibiotic applications instead of just one. We found that repeated antibiotic application experiments reveal additional aspects of antibiotic escape to treatments and allow to better predict the temporal evolution of live cell numbers.

Chapter 5 is dedicated to the study of the effect of growth conditions on the bacterial

population response to antibiotic treatments. It presents experimental results together with model calibration results and further analysis of parameter value sets.

Chapter 6 summarises the main conclusions and discusses the potential and limitations of this work.

Chapter 7 is dedicated to the description of the strains and methods used in this project.

Annexes present work that was carried out during this thesis but was not developed further due to specific limitations. Annex A describes attempts to replace CFU assays as a measure of live cell number by measuring auto-fluorescence to estimate live cells and by staining with propidium iodide to estimate the size of dead biomass. Annex B presents an automation project linking a plate reader and a pipetting robot for automated antibiotic administration. Annex C presents our work with the bioreactor platform. Finally, annex D describes microscopy experiments together with image segmentation.

Chapter 2

Experimental developments

2.1 Introduction

As mentioned in chapter 1, we are interested in characterising the population response of ESBL-producing bacteria to β -lactam antibiotics in different media. A typical behaviour observed under these conditions consists of an initial growth phase, followed by a growth arrest or crash, sometimes followed by regrowth (Figure 2.1a). This behaviour will be discussed in much more detail in the next chapter. Our approach includes calibration of a mechanistic model to experimental data. To do this we need a large amount of high quality data. One of the problems we encountered was the high variability of optical density measurements. This includes not only day-to-day variability, but also variability between technical replicates during the same experiment. We are not talking about measurement noise here, we are talking about a difference of several hours in the time of regrowth, or even the presence of regrowth in some replicates and the absence of regrowth in the others. Section 2.2 presents how we have addressed this issue in order to obtain reliable data to be used for model calibration.

The second experimental challenge I faced was generating CFU data in an efficient manner. This protocol involves making up to 6 serial dilutions of a sample and then plating these dilutions onto agar-filled Petri dishes. My standard experiment contained 2 technical replicates of 48 different experimental conditions. Doing CFU assays in the standard way would take a very long time and result in $6 * 6 * 96 = 3456$ Petri dishes to

plate and analyse by colony counting. Section 2.3 presents the protocol I have set up to make this assay more efficient.

2.2 Addressing the issue of OD measurement variability

When performing our experiments in a 96-well microplate in M9 media with 1 g/L glucose, we observed a lot of well-to-well variability: using the same media, the same antibiotic and the same bacterial inoculum in the same microplate, but in different wells, gave quite different results in terms of regrowth after antibiotic treatment. The top panel of Figure 2.1a shows an example of such variability: lines of the same colour correspond to the same experimental conditions. From this data, we can observe that higher antibiotic concentration, greater difference in regrowth time between lines of the same colour. To investigate the cause of this variability, at the end of the experiment we performed a complete scan of the bottom of each well of the experimental plate and discovered inhomogeneous patterns (top right panel of Figure 2.1a).

One of the known mechanisms of bacterial adaptation to an unfavourable environment is the formation of biofilms, which are aggregations of bacteria that form layers of protection against antibiotics. Biofilm formation is a known virulence factor that contributes to the severity and chronicity of infections. Many clinical isolates known to cause recurrent infections are prone to form biofilms [60]. In urinary tract infections, bacterial biofilms are responsible for approximately 60% of nosocomial and 80% of all microbial infections [61]. Studies [62] have shown that uropathogenic *E. coli* can form intracellular bacterial communities (IBCs) during the early stages of infection, shielding bacteria from antibiotics. The ability of clinical isolates to form biofilms varies significantly with their clonal types and the site of collection [60]. In addition, biofilm formation of the same strain can be influenced by growth, nutrient and environmental conditions [63, 64].

With this in mind, we decided to test whether biofilms were present in our setup and whether the dynamics we were trying to model were caused by planktonic bacteria, as we had assumed. To answer the first question, I used crystal violet staining (detailed protocol in the Materials & Methods chapter 7.8), which showed that the patterns we

saw on the well bottom scans were caused by biofilms (second panel of Figure 2.1a). We tested the same strain (IB302) in three different media: M9 with either glucose, fructose or casamino acids. We observed different levels of biofilm presence in the different media. Interestingly, the highest amount of aggregates was observed in media with fructose as the main nutrient. One would have expected to see more biofilms in media with casamino acids because the population density at the end of the experiment was higher. This suggests that there is some effect of this specific nutrient on the expression of genes relevant to biofilm formation.

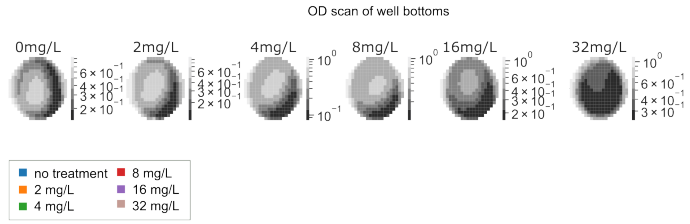
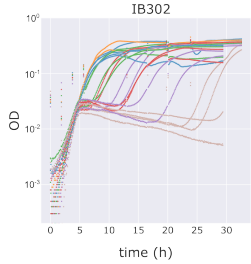
To answer the second question, we conducted an experiment in which we experimented as usual for the first four hours, then mixed the cultures and transferred half of the liquid to a new microplate. The experiments in this new plate and in the original plate, both containing half of the original bacterial culture, continued in parallel. The resulting growth dynamics are shown on the left in the second panel of Figure 2.1b. Interestingly, we observed regrowth at all tested concentrations in the new plate, in contrast to the initial plate. There were also fewer patterns on the well bottom scans. This suggests that regrowth is due to collective antibiotic tolerance of free-swimming bacteria rather than to bacteria escaping treatment in biofilms.

This problem caused a lot of variability, failed model calibrations and also forced me to repeat each experiment many times. It was therefore crucial to find a solution to the variability problem. The simplest idea was to use ultra-low adhesion plates instead of our standard plates. However, for some strains (NILS64) in some media (M9 with fructose), crystal violet staining revealed the presence of biofilms even on these coated plates (top left panel of Figure 2.1b).

A known method to prevent biofilms is to add Tween 20 to the media [64]. We tested different concentrations of Tween20: 0.2%, 0.1% and 0.01%. The highest concentration tested seemed to interfere too much with growth and regrowth to the antibiotic. However, 0.1% Tween20 was sufficient to remove all aggregates from the bottom of the plate, significantly improve the reproducibility of the results and at the same time did not affect growth or regrowth. Our choice was confirmed by the literature: this concentration is commonly used in bioreactor platforms [65] and has been shown to prevent biofilm formation without affecting growth rate [64]. We repeated the same experiments as be-

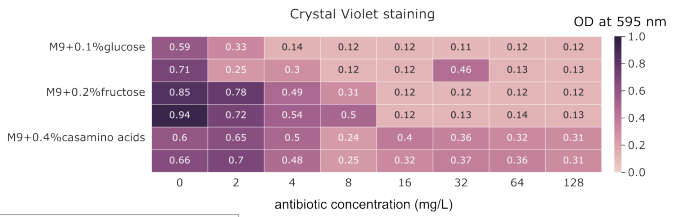
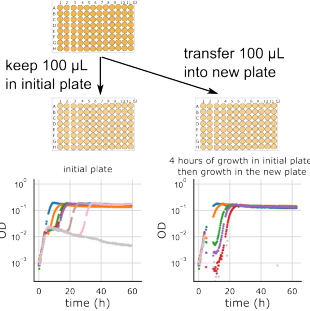
a Variability of optical density readouts issue

Variability of OD measurements



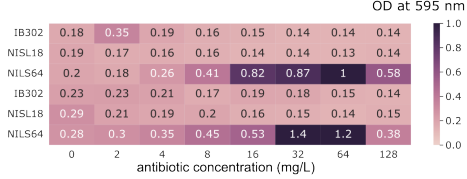
Investigating underlying cause

after 4 hours split initial plate into two

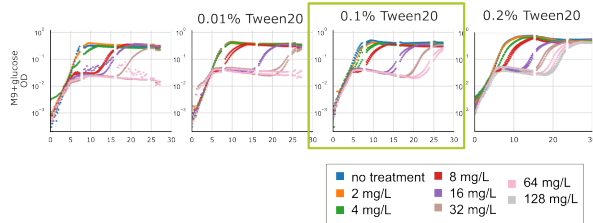


b Addressing the variability issue through preventing biofilm formation

Testing ultra-low adhesion plates



Testing different concentrations of Tween 20



Final solution: adding 0.1% of Tween20 prevents biofilm formation

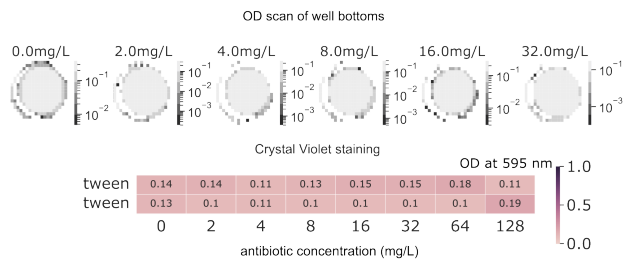
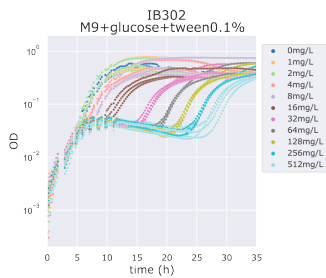


Figure 2.1: **Addressing the issue of OD measurement variability.** **a.** Top left: *Well-to-well variability of OD measurements.* Characterisation of bacterial response to cefotaxime treatments, different colours correspond to different antibiotic concentrations, same colours correspond to same experimental conditions. Top right: *OD scans of well bottoms.* For each well, OD was measured at 308 different positions; the darker the colour, the less dense the bacterial population at that position. Bottom left: *Testing the collective antibiotic tolerance of free-swimming bacteria.* After 4 hours of the standard experiment, half of the liquid volume was transferred to a new plate. Experiments in both new and original plates continued in parallel. Here the OD dynamics of the first hours are shown, followed by observation for each plate. Bottom right: *Crystal violet staining for biofilm detection.* Different columns correspond to different antibiotic concentrations. Different rows correspond to different media. Values correspond to the OD at 595 nm of the final step of the crystal violet staining. **b.** Top left: Crystal violet staining at the end of the experiment in M9 with fructose in ultra low adhesion plates. Top right: OD dynamics of bacterial response to antibiotic in original media without Tween20 (first plot), in media with 0.01% (second plot), 0.1% (third plot) or 0.2% Tween20 (fourth plot). The green square indicates the chosen solution. Bottom left: Same experiment as top left of panel a, but with 0.1% Tween20 added to the media. Bottom right: OD scans of well bottoms and results of crystal violet staining for the 0.1% Tween20 experiment.

fore (top panel of Figure 2.1a), but this time with 0.1% Tween 20 in the media (bottom panel of Figure 2.1b). Well-to-well variability was significantly reduced, OD scans of well bottoms at the end of the experiment showed no patterns, and finally, crystal violet staining confirmed the absence of biofilms.

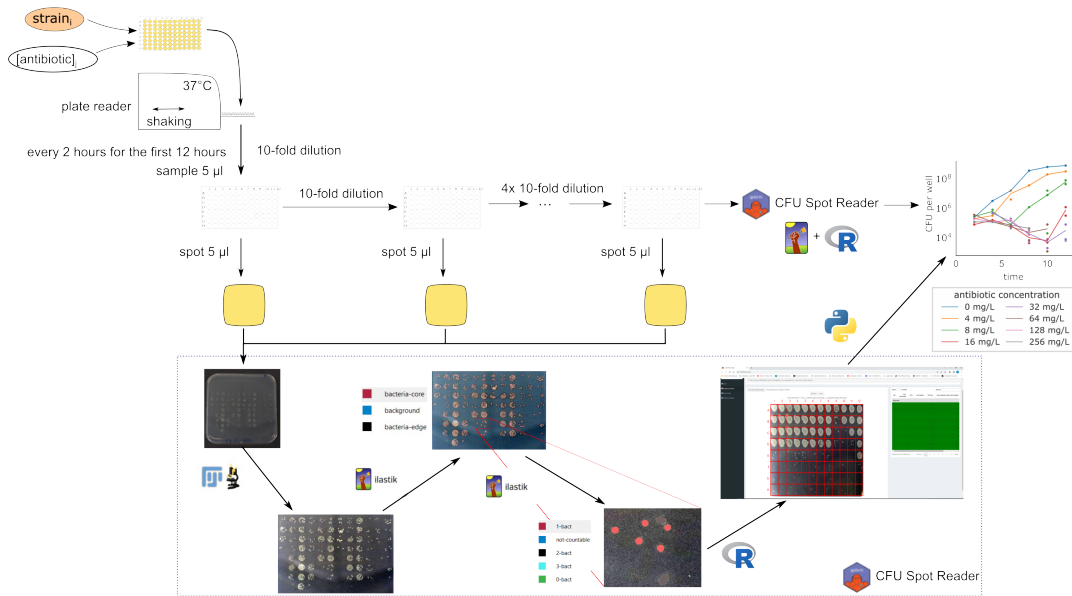
This easy to implement solution helped to solve a long standing and very common problem. All experiments in chapters 3 and 4 were performed in media containing Tween20 to ensure high quality and reproducibility of OD readings.

2.3 Protocol for efficient plate-based CFU assays

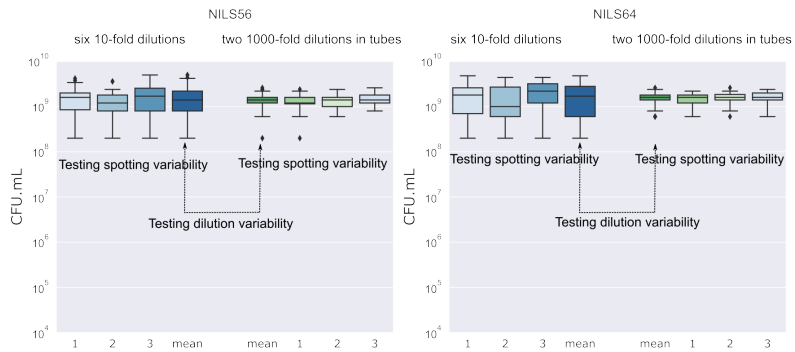
Another aspect of the experimental protocol that needed improvement was the way we performed CFU assays. As mentioned in the introduction to this chapter, my typical experimental plate contained 2 technical replicates of 48 different conditions (for example, 6 different strains exposed to 8 concentrations of antibiotic). To see the evolution of the live cell count over time, we need to perform CFU assays at different times. In the same plate, depending on the concentration, we can have a biomass close to full grown stationary phase (10^9 CFU/mL) and an almost completely lysed population (10^3 CFU/mL), forcing us to do up to 6 serial dilutions to capture the dynamics for all antibiotic concentrations. Therefore, using standard methods and using 1 agar-filled Petri dish per dilution per condition to track dynamics for 12 hours with a 2-hour resolution for an experiment, we would get 96 conditions x 6 time points x 6 dilutions = 3456 Petri dishes to plate and count. This motivated me to move to a droplet-based protocol.

The new experimental protocol that I have set up (the scheme of the protocol is shown in Figure 2.2a) consists in using a 96-channel electronic pipette (Integra Biosciences MINI96) for sampling, serial dilution and spotting on agar plates. Each step is plate-based, meaning that I take a sample from the whole plate, transfer it to a new plate, and then dilute that plate in another plate. Spotting is also done in the same way for the whole plate, resulting in 96 drops of bacterial culture per agar-filled plate. To reduce plastic consumption and the cost of each experiment, I have added a washing step between dilutions. Before starting a new dilution, the tips are washed with ethanol and PBS (ethanol, then air-dry, then PBS). Using this protocol, it usually took me 30-45

a Protocol



b Validation experiment



strain	dilution type	CFU, mean	number of 10-fold dilutions	ratio	precision per dilution
NILS56	six 10-fold dilutions	1.68e+09	6	1.19	0.97
NILS56	two 1000-fold dilutions in tubes	1.41e+09	0		
NILS64	six 10-fold dilutions	1.88e+09	6	1.17	0.97
NILS64	two 1000-fold dilutions in tubes	1.60e+09	0		

Figure 2.2: **Presentation and validation of droplet-based CFU assay protocol.** a. *Graphical representation of the protocol.* An experimental plate containing bacterial culture subjected to a series of antibiotic treatments is placed in a Tecan Spark plate reader where periodic OD measurements are taken and the plate is shaken and incubated at 37°C. Every two hours the plate is removed from the plate reader for sampling and then returned to incubation and OD measurement. This sample is diluted six times tenfold. 5 μL of each dilution is spotted onto an agar-filled square Petri dish. The agar plates are kept at room temperature and then all incubated at 37° for 10 hours, and then photographed. Images are analysed using the CFU Spot Reader application. b. *Test of spotting and dilution variability.* For two strains (NILS56 and NILS64), two different dilution protocols were performed: one as described above (in blue), the other consisting of two thousand-fold dilutions in tubes (in green). In all four cases, the last dilution was spotted three times on agar plates (light colours) to test spotting variability. To assess dilution variability, we compared the mean values of all results obtained using each dilution protocol (dark blue vs. dark green). In the table, we presented the mean value of CFU/mL for each case, the ratio between the two means corresponding to the different dilution protocols and estimate of the precision per dilution.

minutes to run a time point with 96 conditions, which would be unthinkable otherwise.

The next step is to count the colonies for each of the droplets produced. For this step, I adapted image-analysis based software to my project, which I will present below. To simplify image analysis and colony segmentation, all prepared agar plates are kept at room temperature until the last time point and then placed in an incubator at 37° for overnight incubation. This step was added to limit the variability between colony sizes from different time points due to differences in incubation time.

To count the grown colonies and thus estimate CFU, I adapted my project "CFU Spot Reader", a Shiny-based application [66] developed by Vincent Aranzana-Climent and the "Pharmacology of Antimicrobial Agents and Antibioresistance" team. This software allows to obtain the CFU/mL value for each experimental condition from raw images of agar plates corresponding to different dilutions and different time points, and a table specifying the experimental conditions for each position on the plate.

The pipeline consists of several steps. First, each image passes through ImageJ Fiji [67] macros to be cropped, resized, and converted to the right format. Second,

the image passes through pixel classification in ilastik [68], a user-friendly GUI for machine learning algorithms, which classifies pixels into 3 classes: background, core or edge of the bacterial colony. Next, the raw image, together with the probability map from the pixel classification, undergoes object classification, also using ilastik. Here, objects formed by pixels classified as core of a colony are labelled as 1 bacterial colony, 2 or 3 colonies grown together, an uncountable number of colonies stuck together or an unknown object that is not a colony. From this step we obtain a list of detected objects for each image, together with information about their label, position and size. We then use R to divide the images into 96 sectors, each of which is assigned a unique coordinate. The colonies corresponding to the objects detected in that sector are counted, taking into account the information on dilution and experimental conditions from the filename and the descriptive table provided at the input. The results of this step are displayed through a graphical interface, allowing the user to manually verify all counted results.

For this project, I retrained both ilastik projects on my images by manually labelling several images and adding a not-a-colony object. This step required 10 typical images and several manual annotations in different segments of different images. Annotations were added until the live classification predictions reached the proper performance. I also adapted the R script to my project (my filename format, my type of experimental conditions and corresponding data, my number of sectors and my way of referencing them). In doing so, I encountered a problem of image size decorrelation between the image in ilastik format and the image used to display the results, but this was easy to resolve once it was finally identified.

To test the variability of spotting and dilution, I carried out the following experiment: I took a bacterial culture on stationary phase, vortexed it and made two types of dilutions. On one hand, I put 100 μL of this culture per well in a microplate and then did six tenfold dilutions in PBS buffer using the new protocol. On the other hand, I made two thousand fold dilutions in tubes and filled a microplate with this diluted culture, 100 μL per well. To estimate dilution variability, I compared the results of these two different dilution protocols, taking the second as the ground truth. To test spotting variability, the last dilution from both protocols was spotted 3 times on separate plates. The results of this experiment are shown in figure 2.2b. By comparing the results of the

plate replicates (results of the same colour but different colour shade) we can conclude that the spotting variability is quite low. Comparing the mean results of the two different dilution protocols, we can see that on average both methods give the same result (97% accuracy when calculated per dilution), however, as expected, doing 6 dilutions with the 96-channel pipette introduces more well-to-well variability.

2.4 Conclusions

In this chapter I have presented the two modifications to the standard protocol that allowed me to generate all the data presented in subsequent chapters. Although the solution to the OD variability problem was finally very simple, it caused a lot of failed experiments, unanswered questions and many hours of experimentation. Many laboratories around the world use plate readers to measure growth dynamics, but surprisingly not many studies mention this problem in this setup, and even fewer use Tween to address this issue [64]. This issue might not be encountered when working exclusively with laboratory strains, and therefore, represents one of the challenges associated with use of clinical biological material.

By using a 96-channel pipette and switching to a plate-based CFU protocol, I was able to generate a lot of data that would otherwise have been impossible. However, it is worth noting that this protocol is still demanding in terms of time and effort. A typical experiment involving characterisation of the bacterial response by both OD and CFU readings takes me 16 hours of experimental work and at least half a day to photograph the plates and analyse the results.

Chapter 3

In-depth characterization of bacterial population response to β -lactam treatments

3.1 Introduction

There are several ways for bacterial populations to escape antibiotic treatment [10]. This can be done by altering the molecular targets resulting in a lack of antibiotic binding, or by regulating β -lactam influx and efflux through mutations or expression changes in porins. In this project, we are focusing on another important mechanism of resistance to β -lactams, the degradation of antibiotics by enzymes called β -lactamases, which are efficient both inside and outside the cell.

As well as having individual survival methods, bacteria as a population can survive antibiotic concentrations that are lethal to individual cells. This can be due to a variety of different mechanisms, such as communication between populations or growth inhibition. One of the most common strategies is called Collective Antibiotic Tolerance (CAT) and consists of the altruistic death of part of the population accompanied by the release into the environment of β -lactamases capable of degrading the antibiotic. The growth of the population depends on its initial density (also known as the inoculum effect): if the antibiotic is degraded to sub-lethal levels before the entire population is eradicated,

the survivors are able to rebuild the population [16]. Nowadays, the increasing proportion of commensal and pathogenic *E. coli* express extended-spectrum β -lactamases and/or carbapenemases and exhibit an inoculum effect. Therefore, a detailed phenotypic characterisation of the antibiotic susceptibility of clinical *E. coli* isolates to β -lactams is essential to propose effective treatments.

One of the standard methods for detailed susceptibility characterisation is the CFU assay, which allows quantification of antibiotic killing capacity. This method consists of measuring the number of living cells after a certain time in the presence of a certain concentration of antibiotic by plating serial dilutions of a sample on agar-filled Petri dishes and counting the colony-forming units (CFUs) after the incubation period. Although very informative, this method is time consuming and tedious. Another popular method of characterising antibiotic response is the growth kinetics assay, which consists of measuring the optical density (OD) of a bacterial culture subjected to antibiotic treatment. This method is experimentally much simpler, but it is much less informative because it only measures the total biomass, both living and dead, masking cell death and filamentation, among other things. This leads to the question of whether there is a way to reconcile the two different views of cell death.

Our experimental approach combines the two characterisation methods mentioned above and allows us to generate high quality OD data together with the corresponding CFUs measured in a high throughput manner. Using this approach, I generated a rich dataset describing the response of a variety of clinical isolates to a range of antibiotic concentrations. For better analysis and a deeper understanding of the underlying effects, I used a mathematical model [69] that synthesises the field's knowledge of bacterial response to β -lactam antibiotics and encompasses multiple scales. This model allowed us to correctly capture the temporal evolution of OD and CFU for a range of antibiotic treatments.

3.2 Characterization of antibiotic response of clinical isolates

For this study, we selected 11 clinical isolates with different origins, different genetic backgrounds and different levels of antibiotic susceptibility. These strains express a panel of different families of β -lactamases, including carbapenemases, and some express several of them simultaneously. Some of these strains also contain gene mutations that contribute to antibiotic susceptibility, such as mutations in genes encoding porins (*ompC*, *ompF*), genes encoding the PBP3 protein responsible for cell division (*ftsI*) or genes encoding DNA gyrase and topoisomerase subunits (*gyrA* and *parC* respectively).

This selection includes strains from both human and animal infections, represents several sequence types and ranges from highly susceptible to highly resistant to β -lactam treatments. A full description of the collection can be found in the Materials and methods section (7.1). As antibiotic we chose cefotaxime, a broad-spectrum third-generation cephalosporin.

When choosing the experimental protocol, it is important to consider the decorrelations between OD and CFU data. In Figure 3.1a we have shown a typical example of the two types of data we obtained for our strains with (red line) or without (blue line) cefotaxime present in the media, together with typical challenges of these data. We can see that in the presence of the antibiotic, the OD increases exponentially during the first few hours, similar to normal growth, but the number of live cells does not increase, suggesting that the cells are filamenting. We also have a period where OD remains stable. The same period in the CFU data corresponds to an initial decrease in the number of live cells, i.e. cell lysis, and then an increase corresponding to population regrowth due to degradation of the antibiotic in the media by β -lactamases released by the lysed cells. After a while, the regrowth starts to be detectable by OD data and we can observe an increase in both OD and CFU. In the case of a high concentration of antibiotic (light pink line), degradation of the antibiotic may not be efficient enough to restart population growth. To fully characterise the antibiotic response of our 11 clinical isolates, we exposed them to 8 different concentrations of cefotaxime and measured the time course of both OD and CFU.

Our experimental characterisation protocol consists of measuring the OD dynamics of the population response to a range of antibiotic concentrations in a Tecan Spark plate reader. The OD readings are complemented by systematic CFU assays performed in a droplet-based manner as previously described in the 2.3 section.

As mentioned earlier, the relationship between OD and live cell counts during β -lactam treatment is a notoriously difficult problem due to cell filamentation and collective effects. As a result, there is a need for models that not only capture the complex dynamics, but are also able to incorporate data from multiple observations: optical density readings and viable cell counts.

This challenge was addressed in a previous study [69] by Virgile Andreani, a former PhD student in the team. He developed a mathematical model of the bacterial population's response to β -lactam treatments targeting cell segregation and cell wall maintenance, incorporating all relevant processes at multiple scales. This model uses available readouts such as temporal evolution of OD with or without temporal evolution of CFU to reconstruct hidden dynamics. As this model is essential for the results presented in this and subsequent chapters, a brief presentation of the model is given below. A full description is available in the Materials & Methods chapter (7.6).

3.2.1 Filamentation-based model of bacterial population response to β -lactam treatment

Modelling cell length and filamentation is needed in order to explain tolerance β -lactam treatments [70]. However, simply considering that all the cells have the same length, which evolves with time because of filamentation, cannot explain the complex dynamics of cell lysis. Indeed, only the longest cells die, which creates a non-trivial feedback on the average length of surviving cells. Hence, accounting for the heterogeneity in cell lengths in the surviving cell population is required. Therefore, we developed a partial differential equation (PDE) model of the temporal evolution of the distribution of cell lengths within the population, and described with ordinary differential equations (ODEs) other processes such as the active degradation of the antibiotic by β -lactamases released in the medium upon cell lysis. The evolution of the cell length distribution is

represented by a process of growth-fragmentation that relies on the assumption that cells elongate exponentially and divide with a rate depending on their length, into possibly more than two fragments, which is notably the case for filamented cells after removal of the antibiotic [71]. Because some β -lactams like cefotaxime can inhibit PBP3, involved in the septum formation [72, 73], the division rate is assumed to be a decreasing function

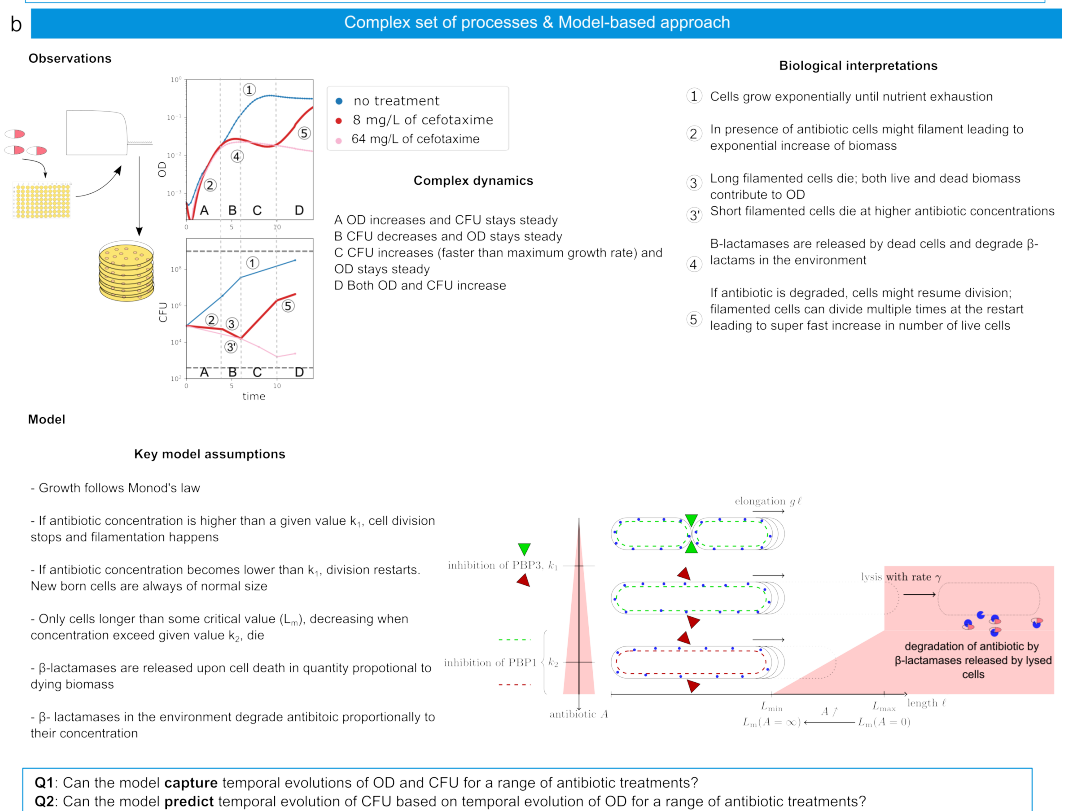
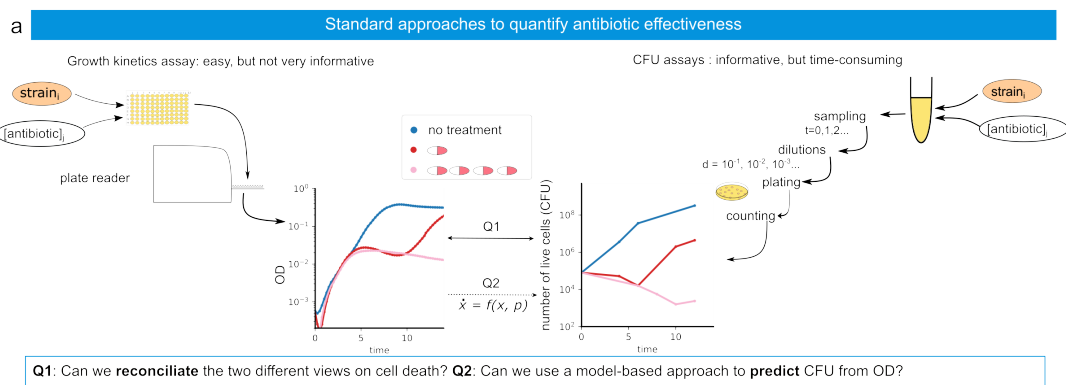


Figure 3.1: **Characterization of bacterial population's response to β -lactam treatment.** **a.** Standard approach to quantify antibiotic effectiveness. *Growth kinetics assay:* this approach consists in following optical density (OD) of liquid cultures inoculated with an isolate to be tested and containing a certain antibiotic concentration. *CFU assay:* This approach consists in following the dynamics of live cell counts through systematically taking samples, making serial dilutions of them, plating them on agar-filled Petri dishes and after hours of incubation counting the colonies of the Petri dishes. Resulting dynamics are drastically different. **b.** Description of observed discrepancies between OD and CFU data. *Bacterial response to β -lactam treatment:* For one clinical isolate (NLS56), growth kinetics assays together with CFU assays were measured without antibiotic and in the presence of one medium and one high concentrations of cefotaxime. The population response to the medium concentration (red line) can be divided in several periods: A) OD increases and CFU stays steady; B) CFU decreases and OD stays steady; C) CFU increases (faster than maximum growth rate) and OD stays steady; D) both OD and CFU increase. These observations can be interpreted as following: 1) in the absence of antibiotic (blue line) cells grow exponentially until nutrient exhaustion; 2) in the presence of antibiotic (red line, A) cells might filament leading to exponential increase of biomass (OD) without increase in number (CFU); 3) long filamented cells die (B); both live and dead biomass contribute to OD; 3') short filamented cells die at higher antibiotic concentrations (pink line); 4) β -lactamases are released by the lysed cells and degrade β -lactams in the environment; 5) if the antibiotic has been cleared, cells might resume division (C&D); filamented cells can divide multiple times at the restart leading to super-fast increase in live cell number. Graphical representation of the model. *Cell response:* Cells elongate exponentially at a rate g that depends on nutrients but is not affected by the antibiotic. Above a concentration k_1 , the antibiotic inhibits PBP3, which deprives the cells of their capacity to divide. Cells that cannot divide filament until they reach a critical length L_{max} from where they experience a cell death with rate γ . Higher concentrations of antibiotics, around k_2 , inhibit the PBP1s which fragilizes the cells and reduces the critical length, such that cells die earlier. Population response: When the cell population is attacked by the β -lactam treatment, cells elongate and eventually lyse, releasing β -lactamase in the environment (blue circles) that degrade the antibiotic thus protecting the surviving cells.

of the antibiotic concentration in the medium. However, the elongation rate is only a function of the nutrient concentration, and remains unchanged by the antibiotic, as is

the case for most β -lactams [74]. It is known that for a given β -lactam concentration, the time to cell lysis is inversely proportional to the growth rate [75]. This suggests that the death mechanism can be easily modelled with a critical cell length, reachable when cell division is blocked. Cell filaments longer than this threshold experience a significant death rate (Figure 3.1b). This makes cell lysis a direct function not of the antibiotic itself but of cell length, that drastically increases because of antibiotic. The antibiotic can however, at high doses, reduce this critical length, through the inhibition of other PBPs such as the PBP1s which have a fundamental role in the repair of wall defects [76]. All the bacteria in this study express β -lactamases, enzymes released in the culture medium upon cell lysis, with the ability to cleave the antibiotic molecules [77]. Although strains can express several β -lactamases with different efficiencies, the model aggregates them into a single average one. The concentration of antibiotics as well as of β -lactamases, are tracked by means of ODEs. The model also accounts for the excess OD contributed by fragments of lysed cells (the dead biomass). The equations of the corresponding PDE model are given in the methods section 7.6. To make the model computationally tractable, we eliminated the explicit representation of the cell length distribution $n(l, t)$ to keep only its first moments: number of cells N and average length L . The ODEs for these quantities involve partial moments of the cell length distribution, which we managed to express only in terms of N and L through careful approximations.

This leads us to our first question: can the model capture the temporal evolution of OD and CFU for a range of antibiotic treatments?

3.2.2 Can the model capture the temporal evolution of OD and CFU for a range of antibiotic treatments?

To answer this question, I had to calibrate the model to the experimental data. Due to the complexity of the data set, the calibration was done in two steps. First, from the full set of model parameters, I selected a subset responsible for normal growth of a bacterial population in the absence of antibiotics (maximum growth rate μ , maximum division rate β , half-velocity constant of nutrients K_s , conversion factor of nutrients λ and conversion rate between OD and CFU η). I fixed all other parameters to some initial

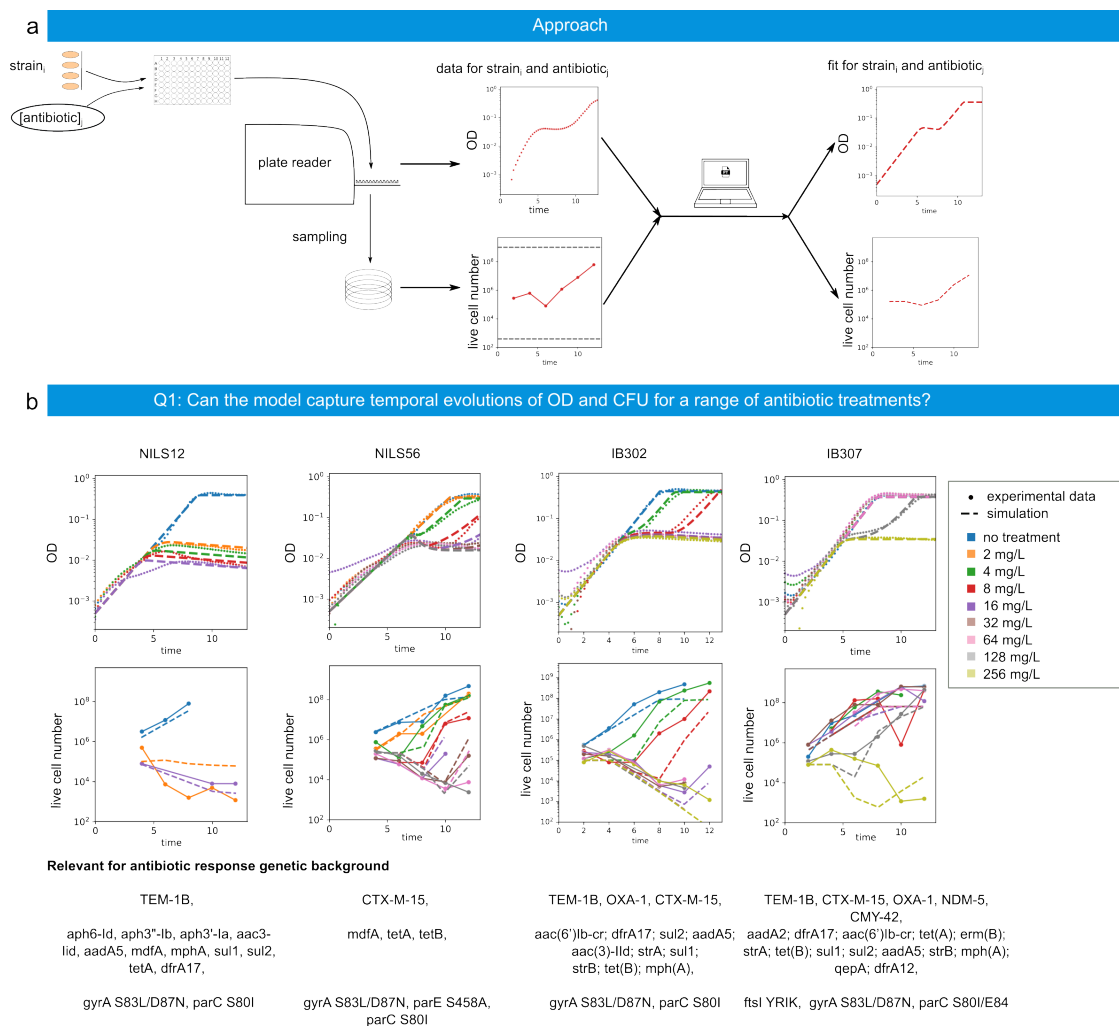


Figure 3.2: Characterization of the response of clinical isolates to a range of cefotaxime treatments. **a** Our approach. A 96-well plate is inoculated with the isolates to be tested, and a range of antibiotic concentrations is applied. The OD is read by a plate-reader, that also controls temperature and shaking. Every two hours a sample is taken for CFU assay. The data from both OD and CFU is then fed into the model, for which numerical parameters are estimated for each isolate. On the basis of these parameters, simulations corresponding to OD and CFU data are generated and compared to the experimental results. **b** Comparison of experimental data and the model fit. Four clinical isolates, representing a range of susceptibility to β -lactam treatment from very susceptible (NILS12), to highly resistant (IB307), are treated with different concentrations of cefotaxime, and optical density and live cell number are measured as described in the Methods section. We show in points with (CFU) or without (OD) solid lines the experimental data and in dashed lines the output of the model fitted on OD and CFU data simultaneously.

values and searched for optimal values for this selected subset of parameters using both OD and CFU data of a growth kinetics without cefotaxime present. Secondly, I restarted the search for optimal parameter values on OD and CFU data obtained for a range of cefotaxime concentrations, fixing the growth parameters to the optimal values found in the first step.

In summary, our approach to in-depth characterisation consists of exposing clinical isolates to a range of concentrations of cefotaxime, measuring the temporal evolution of OD using a plate-reader and the temporal evolution of CFU using a droplet-based method, and calibrating the model to OD and CFU data (Figure 3.2a). From the collection of strains mentioned above, I selected four strains that represent the collection well: one strain has a weak β -lactamase against cefotaxime (TEM-1) and is therefore susceptible to all tested treatments, one strain has several β -lactamases, a carbapenemase and a mutation in the gene encoding PBP3 and is highly resistant to cefotaxime, and two others are between these two extremes. A good representation of these four strains would suggest a good representation of the whole collection. On Figure 3.2b I present the results of the characterisation of the four strains mentioned together with the corresponding model simulations. Results for all eleven strains are shown on figure 3.3. From the OD data for the susceptible strain, we can observe that biomass growth stops earlier at higher antibiotic concentrations, which we do not observe for other strains. From intermediate strains (e.g. IB302, third column) we can observe that the number of live cells remains constant during the first hours while the biomass grows exponentially, indicating the presence of filamentation. Another interesting observation from the same data is that the death rate does not depend on the antibiotic concentration, but the size of the dead biomass does. These effects are well captured by the model and are consistent with the main assumptions of the model such as filamentation, lysis caused by reaching a critical length and finally the dependence of the critical length on antibiotic concentration. In the case of low antibiotic concentration, given the granularity of our CFU data, the number of dead cells is not noticeable and is masked by the onset of regrowth. This is the case for NILS56 at 4 mg/L, IB302 at 4 or 8 mg/L and IB307 at 128 mg/L. As these cases are prone to high variability, they are difficult to capture and the model sometimes tends to overestimate the degree of cell lysis. Other interesting and not trivial obser-

Q1: Can the model capture temporal evolutions of OD and CFU for a range of antibiotic treatments?

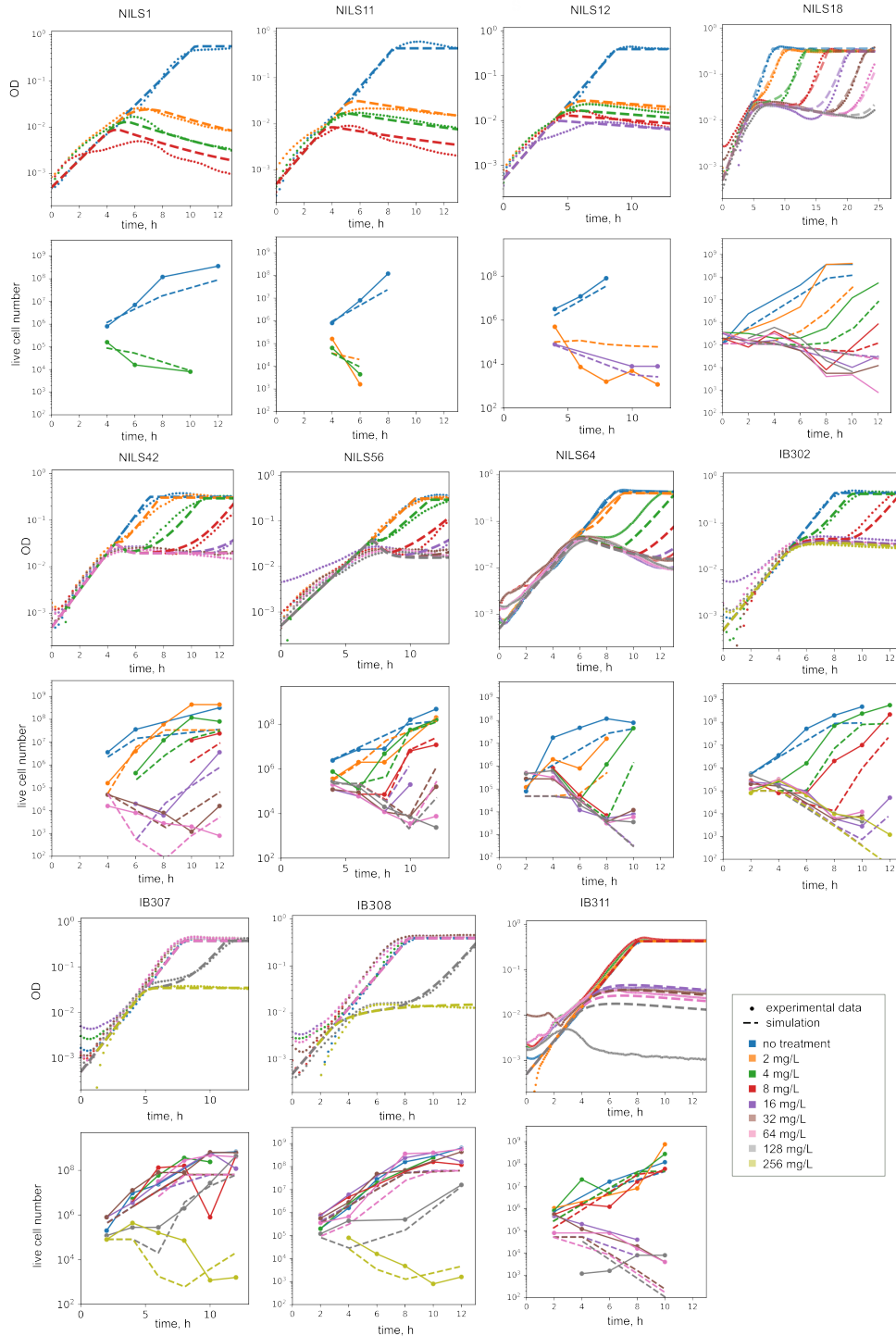


Figure 3.3: **Comparison of experimental data and model simulations.** Eleven clinical isolates, representing a range of susceptibility to β -lactam treatment from very susceptible (NILS1, 11, 12), to highly resistant (IB307, IB308), are treated with different concentrations of cefotaxime, and optical density and live cell number are measured as described in Methods section. We show in points with (CFU) or without (OD) solid lines the experimental data and in dashed lines the output of the model fitted on OD and CFU data simultaneously.

vations come from looking at the first hours of regrowth. Firstly, regrowth is initially masked by dead biomass and is therefore not detectable from the OD data, which can be observed for IB302 at 16 mg/L, NILS56 at 16, 32 or 64 mg/L. Secondly, in some cases (e.g. NILS56 at 8 mg/L) the number of live cells increases faster than the maximum growth rate, which can be explained by a filamentation effect, i.e. filaments dividing into more than 2 smaller cells. Despite their complexity and limited observability, both phenomena are well captured by the model.

Overall, the model provides good agreement with the data for all 4 strains, thus demonstrating its ability to quantitatively capture the temporal evolution of both OD and CFU, despite the decorrelations between these two modes of measurement, for a range of antibiotic treatments for a variety of clinical isolates with different levels of cefotaxime susceptibility. Other kinetic models in the field describe only OD or only CFUs, and often in a non-mechanistic way, for example with an artificial delay after the start of the experiment to provoke growth arrest. To our knowledge, this model is the first to reconcile these quantities with mechanistic arguments.

3.3 The impact of genetic background on response to antibiotic

The non-susceptible strains presented earlier express a variety of different β -lactamases. For each strain we selected 45 best on fitting score parameter value sets. Firstly, we looked into parameter, which is the minimal concentration at which cells stop growing and dividing normally and start filamenting. The higher this value, the more resistant the strain is. On the left boxplot, three strains stand out due to high value: IB307, IB308 and IB311. This high value means that these strains can grow and divide normally subjected to higher concentrations of antibiotic than the other strains. This is confirmed by the experimental data. The strain with the lowest value is NILS31, for which we observe growth arrest even at smaller concentration of antibiotic.

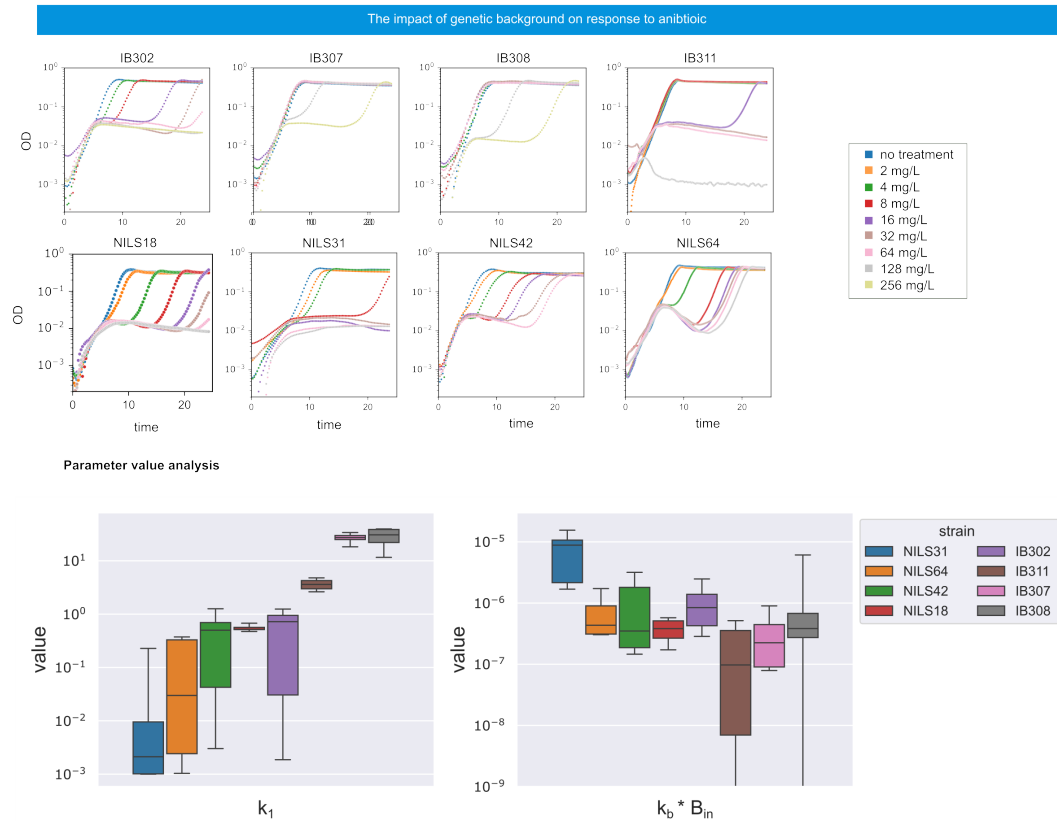


Figure 3.4: The impact of genetic background on bacterial population's response to antibiotic. *Top:* Overview of bacterial population response to 8 cefotaxime concentration for 8 non-susceptible strains from the collection. *Bottom:* Box-plot of parameter values for k_1 (minimal antibiotic concentration that stops cell division) on the left and $k_b * B_{in}$ (antibiotic degradation activity and production rate per cell length respectively) on the right for about 45 fits on OD and CFU for the 8 non-susceptible strains.

Secondly, we looked into , a production of two parameters and which correspond to β -lactamase degradation activity rate and number of enzymes produced by unit of cell respectively. These two parameters form a structurally unidentifiable pair, for this reason here we consider the product of the two parameters. Interestingly, the three strains with highest value have the lowest values, especially IB311. This means, that these cells can grow normally until some relatively high concentrations, however, when sub-

jected to even higher concentrations, the β -lactamases they express are not sufficiently efficient. In other words, these strains are individually resistant, but not very resilient as population. For IB311, this translates into a specific phenotype: at concentrations up to 8 mg/L there is no impact of antibiotic treatment on the growth dynamics, at one specific concentration from the tested range (16 mg/L) there is the phenomenon of crash, growth arrest and regrowth, at higher concentrations (starting from 32 mg/L) there is crash and growth arrest, but no regrowth. This also concurs with the fact that one common attribute of all strains but this one is that they express a β -lactamase of CTX-M class, contrary to IB311.

3.4 Can the model capture the temporal evolution of OD for other β -lactam antibiotics?

In all the experiments described so far, we have studied the bacterial population response to a specific β -lactam - cefotaxime. Here we were interested in characterising the population response to other β -lactams and testing the ability of the model to capture this. We chose two antibiotics: first, ceftriaxone, a broad-spectrum cephalosporin that inhibits cell wall synthesis and induces filamentation; second, mecillinam, an extended-spectrum penicillin that primarily targets PBP2 and induces the production of osmotically stable round cells [78]. Using growth parameters from previously generated parameter sets on cefotaxime data, I calibrated the model to new data. The simulations are in perfect agreement with the experimental data corresponding to ceftriaxone treatments (Figure 3.5), which is to be expected given that ceftriaxone is very similar to cefotaxime in its mode of action.

However, the agreement between simulations and experiments is less perfect in the case of mecillinam, which is understandable given that mecillinam is quite different from the other two antibiotics and does not induce filamentation. The growth kinetics assays show quite different responses to antibiotic treatment.

In the case of IB302, there is still a period of exponential growth followed by growth arrest. Biomass degradation is much more pronounced and the time to regrowth is less dependent on antibiotic concentration. Interestingly, the population treated with

mecillinam does not fully regrow to carrying capacity.

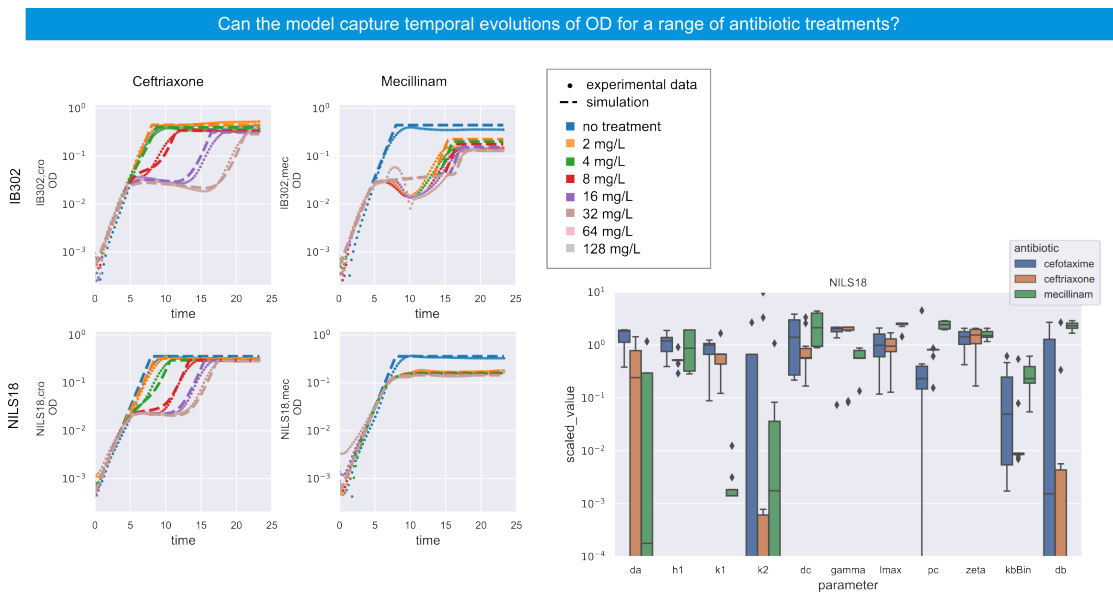


Figure 3.5: **Can the model capture the temporal evolution of OD for a range of antibiotic treatments?** *Left:* For two clinical isolates (IB302 – top row, Nils18 – bottom row), I measured temporal evolution of OD in response to two other β -lactams: ceftriaxone – left column, mecillinam – right column. Experimental data is in points, simulations of the model is in dashed lines. *Right:* β -lactams: (cefotaxime in blue, ceftriaxone in orange and mecillinam in green).

In the case of Nils18, the exponential growth period is much longer than for other antibiotics and is followed by growth arrest at an OD lower than carrying capacity and there is no regrowth. This behaviour of Nils18 was actually quite well captured by the model, so we decided to look at the parameter values for the three antibiotics to see if there was a possible explanation for these different dynamics.

In Figure 3.5 I have presented a box plot showing the distribution of parameter values for the best 5-10 fits for each antibiotic (cefotaxime in blue, ceftriaxone in orange and mecillinam in green). From the figure we can see that cefotaxime and ceftriaxone are quite close, but in the case of mecillinam I obtained a much lower value of k_1 , meaning that the effect of the antibiotic on cell wall integrity starts at low concentrations. Interestingly, the lysis rate γ is lower and L_{max} is higher, which in the model means that death starts later and is less important. In addition, p_c , the proportion of non-degradable

biomass, is higher, meaning that less dead biomass can be degraded.

3.5 Conclusions

In this chapter I presented the model previously developed in the team. I also presented the approach I adopted and results of characterising the population response to cefotaxime treatments for a number of clinical isolates. I also presented decorrelations between OD readings and CFU measurements. Using this model-based approach, we were able to reconcile the two types of measurements, fit the model to both OD and CFU data, and obtain good agreement between simulations and experimental data for a collection of clinical isolates with different levels of antibiotic susceptibility. This method provides us with valuable insights and a detailed picture of collective antibiotic resistance.

Further analysis of the model parameter values revealed differences between strains in terms of β -lactamase activity and/or production levels, which were confirmed by known genetic background. Finally, for two strains, I presented the results of a similar characterisation of the population response to two other antibiotics: ceftriaxone and mecillinam. From these results we can conclude that the model is able to capture the filamentous response to β -lactams, but struggles to capture the non-filamentous response.

Chapter 4

Quantifying the impact of multiple antibiotic applications on cell death

4.1 Introduction

Antibiotic resistance has been studied for decades. However, most *in vitro* studies characterise the response of bacterial populations only when exposed to a single dose of antibiotics. When faced with treatment failure, the most common alternative treatments are combinations of two different antibiotics [79] or combinations of an antibiotic with a β -lactamase inhibitor [22]. The two newest combination therapies against ESBL-producing bacteria are ceftazidime-avibactam [80] and ceftolozane-tazobactam [81]. There are also some trials where the authors looked at regular antibiotic use over a period of time. One study [82] has shown that optimised periodic treatment can reduce the dose of antibiotics needed to fight persistent biofilm-forming bacteria. Tan and colleagues [83] investigated the effect of periodic antibiotic administration on the inoculum effect. They have shown the non-linearity of bacterial response to periodic treatments.

In Chapter 3 I have shown that the model [69] is able to capture the temporal evolution of both OD and CFU for a range of clinical isolates exposed to a range of antibiotic concentrations, which was an important result considering significant de-correlations between the two modes of measurement during β -lactam treatments. To further challenge the model, I attempted to use only OD data, easily measurable but notoriously

difficult to exploit, for model calibration and to test its predictive capabilities on CFU data, requiring long and tedious experimental protocols, but the results were not fully satisfactory.

In the previous chapter, for characterisation experiments, the total antibiotic concentration was always added at the beginning (hereafter referred to as *single treatment*). In order to obtain more informative data for model calibration, a second dose of antibiotic was added several hours after the first dose at the beginning of the experiment (hereafter referred to as *repeated treatment*). Fitting the model to OD data from both single and repeated treatment experiments allowed us to obtain robustly better predictions of the temporal evolution of CFUs compared to previous attempts using single treatments only. Further analysis of parameter values and their uncertainties showed that the inclusion of repeated treatments in the calibration dataset provided additional constraints on some of the parameters.

4.2 Prediction of the temporal evolution of CFU based on the temporal evolution of OD

To further challenge the predictive power of the model, we tested its capacity to predict the temporal evolution of CFU based solely on OD data (Figure 4.1a). This was also motivated by the fact that even using plate-based protocol CFU assays (*cfu*) remains a time-consuming and complicated task, especially when compared to the generation of OD curves by an automated plate reader.

For one of the non-susceptible strains (IB302), the model was recalibrated using only OD data, and the simulated live cell number was compared to the experimental data (from the experiments generated for Figure 3.2). To assess the predictive quality of the model, the stochastic fit was repeated forty times, generating forty different parameter value sets on the same dataset. For each set, the CFU prediction score was calculated, defined as the mean square error of the logarithm of cell counts for all experimental points and all concentrations of antibiotic. Statistical analysis of these generated fits demonstrated that in all cases, it is possible to reach a parameter value set that predicts the live cell number accurately within 40 fitting attempts. However, the stochastic

fitting algorithms employed were unable to reach this global optimum with every initial random seed, and the average fitting score is disappointing (Figure 4.1b). Given the time-consuming nature of fitting a model of this size, we sought to determine whether it was possible to more consistently reach a fit that predicts cell numbers accurately without using any cell number while fitting.

In order to increase the power of our experimental dataset, I conducted additional experiments. Previously, the entire dose of antibiotic was administered at the start of the experiment, this type of experiment will be referred to as *single treatment*. In new experiments, I again administered a range of antibiotic concentrations at the start of the experiment (first dose), but added a second dose at a specified later time (usually 2, 4 or 6 hours after the start), experiments I will refer to as *repeated treatments*. These experiments were also performed in a 96-well plate, in M9 minimal media with glucose and Tween 20. The second treatment was performed simultaneously on an entire column using a multichannel electronic pipette to minimise the time spent outside the incubation conditions.

As a new calibration dataset, we selected OD data from a single treatment experiment along with 3 repeated treatment experiments. As before with single treatments, I fitted the model to the new dataset forty times, with forty different initial random seeds for the optimiser, and calculated CFU prediction scores. This method allowed the optimiser to reach the global optimum much more consistently, enabling robust and good predictions (Figure 3.2b). The average prediction score with this method is similar to the best prediction score with the previous method using only single treatment trials.

In Figure 4.2 I show CFU predictions simulated using four parameter value sets, with the best fit score calibrated to single treatment and another four calibrated to single treatment and three repeated treatment experiments. The fitting cost on the single treatment experiment alone is much (5-10 times) lower than on the more complex dataset, but the CFU prediction score is lower when repeated treatments are used for calibration. This leads us to believe that the parameter search on single treatment experiment only tends to overfit the OD data and overestimate the cell death and de-filamentation rate.

We observed the same for four other strains (two on Figure 4.1c, all four on Figure 4.3). Therefore, calibrating the model on only OD data for four slightly different experi-

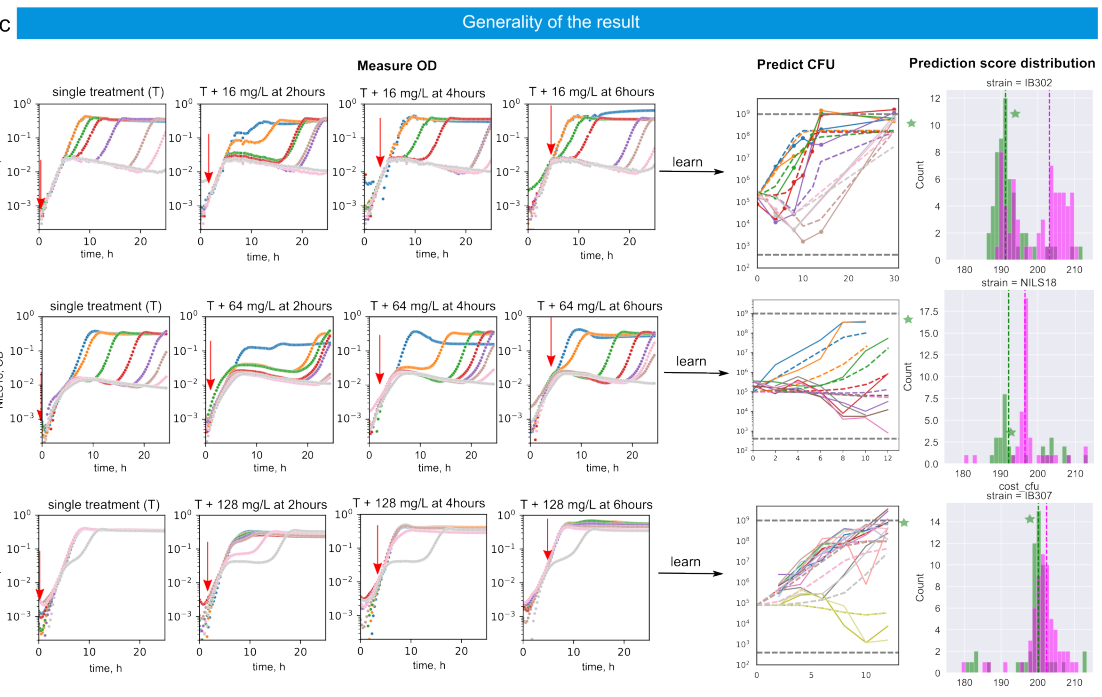
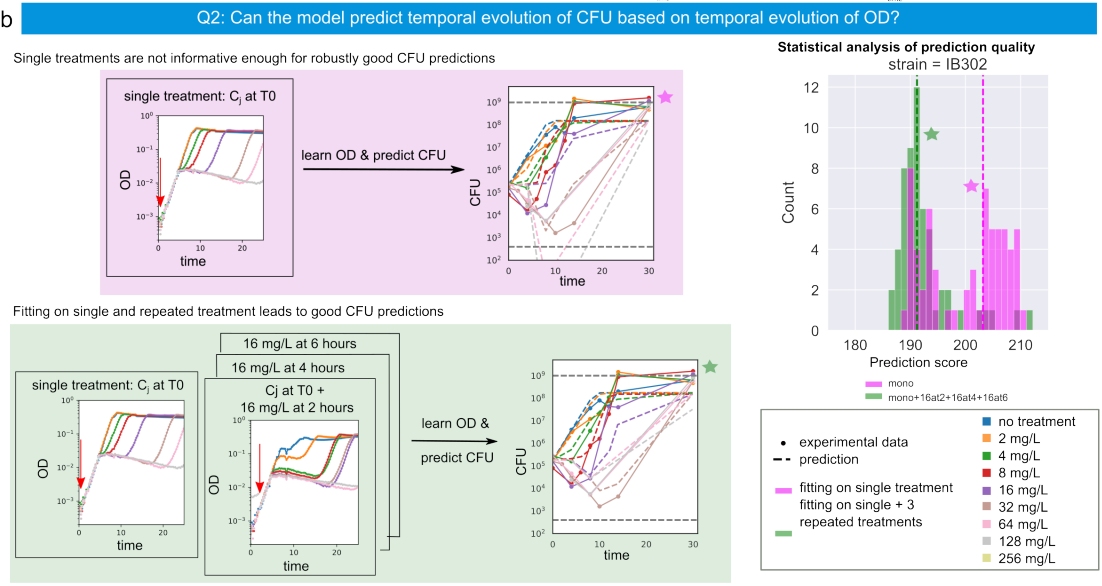
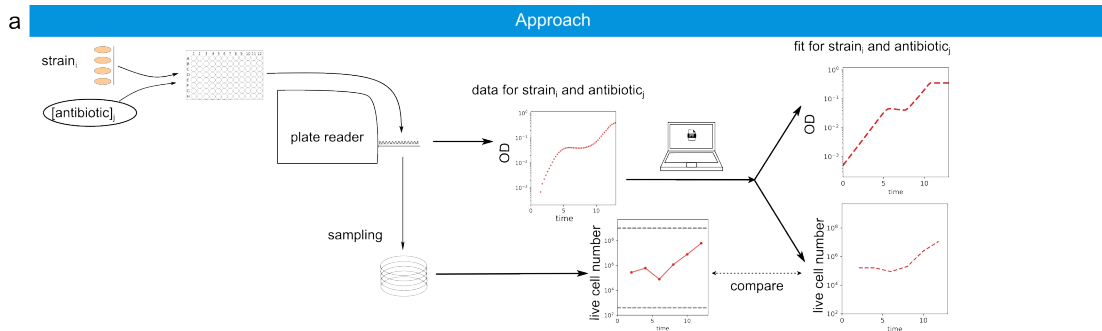


Figure 4.1: **Prediction of the temporal evolution of CFUs based on the temporal evolution of OD.** **a** Our approach. A 96-well plate is inoculated with the isolates to be tested, and a range of antibiotic concentrations is applied at the beginning (single treatment). For some experiments, a second antibiotic dose is applied several hours later (repeated treatment). The OD is read periodically by an automated plate reader. During single treatment experiments, every two hours a sample is taken for the CFU assay. Only the OD data is fed into the model, for which numerical parameters are estimated for each isolate. Based on these parameters, simulations corresponding to both OD and CFU data are generated and compared to the experimental results. **b** Can the model predict the temporal evolution of CFU based on the temporal evolution of OD for a range of treatments? *Fitting the model on single treatment experiments:* On the same calibration dataset containing only single treatment experiments, around 40 parameter value sets are generated (by repetitive fitting with a stochastic optimiser). For each of these, a CFU prediction score is calculated. The CFU predictions shown here were generated with the parameter set value that yielded the median CFU prediction score. The full distribution of the 40 prediction scores is shown on the histogram on the right in magenta. *Fitting the model on both single and repeated treatment experiments:* On the same calibration dataset containing both single treatment and three different repeated treatment experiments, around 40 parameter value sets were generated. For each of them, a CFU prediction score is calculated, with the distribution presented on the histogram on the right in green. The CFU predictions were simulated using the set with the median prediction score. The experimental data is shown in points and solid lines, while the model simulations are shown in dashed lines. The line colours correspond to different initial concentrations of cefotaxime. **c** Generality of the result: Each row of plots corresponds to one clinical isolate. The first plot in a row represents the bacterial response to different antibiotic concentrations applied at the beginning (single treatment). The next three plots correspond to repeated treatments: to the range of initial single treatments, a second antibiotic concentration is administered after several hours. The last plot in the row shows the distribution of CFU prediction scores of different parameter value sets that were calibrated either only on single treatment (in magenta) or on all four experiments (in green). The plot on the left of the histogram depicts the experimental CFU data for the single treatment (in points and solid lines) and the simulations (in dashed lines) using the parameter value set that corresponds to the median prediction score.

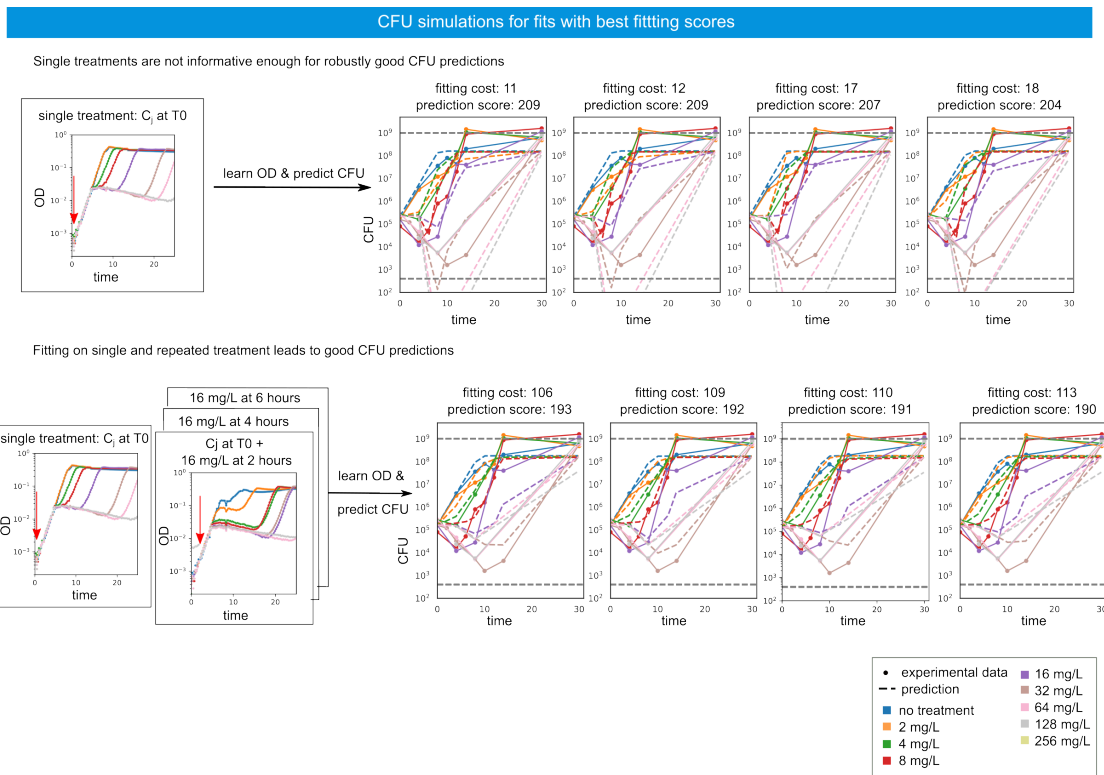


Figure 4.2: Prediction of temporal evolution of CFU using parameter values with lowest fit score. Top: Four parameter value sets, obtained by calibration on a single treatment experiment and giving the lowest fitting score on OD, were used to simulate the temporal evolution of CFU. Each plot on the right corresponds to simulations from one parameter value set. The title of each plot shows the OD fit score and the CFU prediction score. Bottom: Four parameter value sets, obtained by calibration on single and three repeated treatment experiments (shown on the left) and yielding the lowest OD fitting score, were used to simulate the temporal evolution of CFU. Each plot on the right corresponds to simulations from one parameter value set. The title of each plot shows the OD fit score and the CFU prediction score.

ments, we were able to predict the temporal evolution of the number of live cells during antibiotic treatment, a major result that has never been achieved before.

What makes repeated treatment experiments so informative that they allow the model to make good CFU predictions? One reason is that they provide information on β -lactamase efficiency: with a high initial dose of antibiotics, the second dose has little effect on the time to regrowth, showing that the proportion of the population that dies

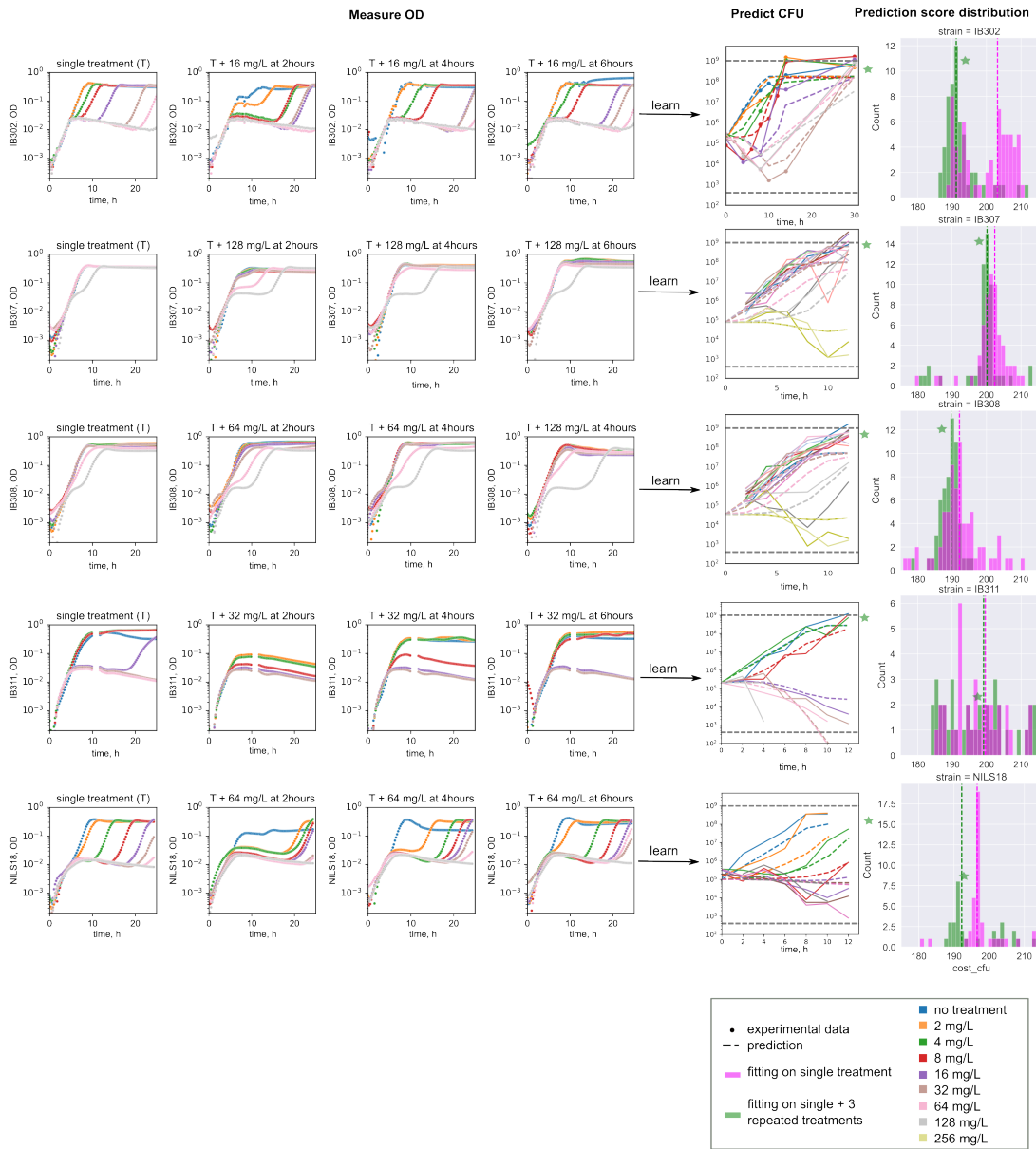


Figure 4.3: **Prediction of temporal evolution of CFU based on temporal evolution of OD.**

Each series of plots corresponds to a clinical isolate. The first plot in a series represents the bacterial response to different antibiotic concentrations applied at the beginning (single treatment). The next three plots correspond to repeated treatments: a second antibiotic concentration is added to the range of initial single treatments after several hours. The next plot shows the experimental CFU data for the single treatment (in points and solid lines) and the simulations (in dashed lines) using the parameter value set corresponding to the median prediction score. The last plot in a row shows the distribution of CFU prediction scores of different parameter value sets calibrated either on single treatment only (in magenta) or on all four experiments (in green).

depends mainly on the initial dose, and that the amount of β -lactamases released by the dead cells is sufficient to degrade the two doses of antibiotic. Another reason is that they provide information on the inoculum effect: if there is no (or small) initial dose, the second dose is the main treatment, and the later we apply it, the higher the population density at the time of treatment, the smaller the effect of the treatment. Last but not least, an observation that could shed some light on cell death is that no matter when the treatment is applied, if there is an effect of this treatment, the ratio between the OD at the moment of antibiotic administration and the OD at the moment of crash (end of exponential increase of biomass) remains the same, which is consistent with the model's assumption that death is caused by critical length.

In the next section, we examined the impact of the choice of calibration data set by comparing the results of calibration to different combinations of available repeated treatment experiments in terms of success rate, fitting cost and CFU prediction score, and optimal parameter value uncertainties.

4.3 Effect of repeated treatment experiments on parameter search efficiency

Previously we compared parameter value sets, resulting from model calibration on either a single treatment experiment alone or together with three repeated treatment experiments in terms of CFU predictivity. For Figure 4.1c and 4.3 I have chosen specific three repeated treatment experiments for the calibration dataset: in most cases it was the same antibiotic concentration applied at 2, 4 and 6 hours. However, for some strains (for example IB302 shown on Figure 4.1b) I have performed more than three different repeated treatment experiments. The logical question that arises is whether we need three repeated treatments for good predictions or whether one or two would be sufficient. Another question is what repeated treatment experiments bring to the calibration dataset in terms of parameter value constraints.

To answer these questions, I generated different variations of the calibration dataset containing zero, one, two or three (or more in the case of IB302) different repeated treatment experiments. The dataset type is defined based on the number of repeated

treatment experiments added to it. In Figure 4.4 I summarise the number of fits generated for each type of calibration dataset and the number of individual datasets of that type. For each fit, I calculated the fit score to the OD of the calibration dataset and the prediction score to the CFU of the individual treatment. Based on previous observations and analyses, I set a threshold of 200 for both scores to separate good fits from moderate or even poor fits. For a subset of strains (IB302, NILS18 and IB307) for each dataset type I calculated the percentage of fits with a good fit score out of the total number of fits of that type. I also calculated the percentage of fits with a good prediction score out of the fits with a good prediction score. This data is presented in a bar chart in the figure 4.4. From the plot we can see that adding repeated treatment trials decreases the probability of having a good fit, but increases the probability of a fit with a good fit score having a good prediction score. In other words, it is more difficult to fit a more complex dataset, but if we get a good fit, it is more likely to produce good CFU predictions. To consolidate this result, we looked at the evolution of fitting score and prediction score as a function of the number of experiments in the calibration dataset. We observe that the average fit score goes up when we add at least one repeated treatment experiment and, at the same time, when we compare fits to single treatment only and fits to single and three repeated treatment experiments, we observe that the average prediction score is lower and, importantly, there are many separate variations of this dataset that lead to very good prediction scores (below 190).

In order to study the influence of the calibration data set on the uncertainties of the parameter values, I calculated the standard deviation of the optimal parameter values for each specific dataset, further I grouped the datasets by type and calculated a mean of these standard deviations. On the Figure 4.4 I show individual dataset standard deviations in scores and means for each dataset type in the solid line for a small selection of parameters: growth rate μ , a parameter easily identifiable with a minimal amount of data; antibiotic concentration inducing filamentation k_1 , an antibiotic-related parameter important for good CFU predictions but still identifiable from a single treatment experiment; and finally the product of two parameters characterising β -lactamase production and efficiency $k_b * B_{in}$, difficult to identify but important for good CFU predictions. As expected, the growth rate is well identified on all calibration datasets. Especially

for IB302, but also for IB307, we observe that adding experiments tends to constrain the parameter values. For NILS18, it depends a lot on which three repeated treatment experiments we choose.

Overall, choosing a single treatment along with three repeated treatment experiments as a calibration dataset is a good compromise between the complexity of the training dataset and the constraints on cost and parameter variability.

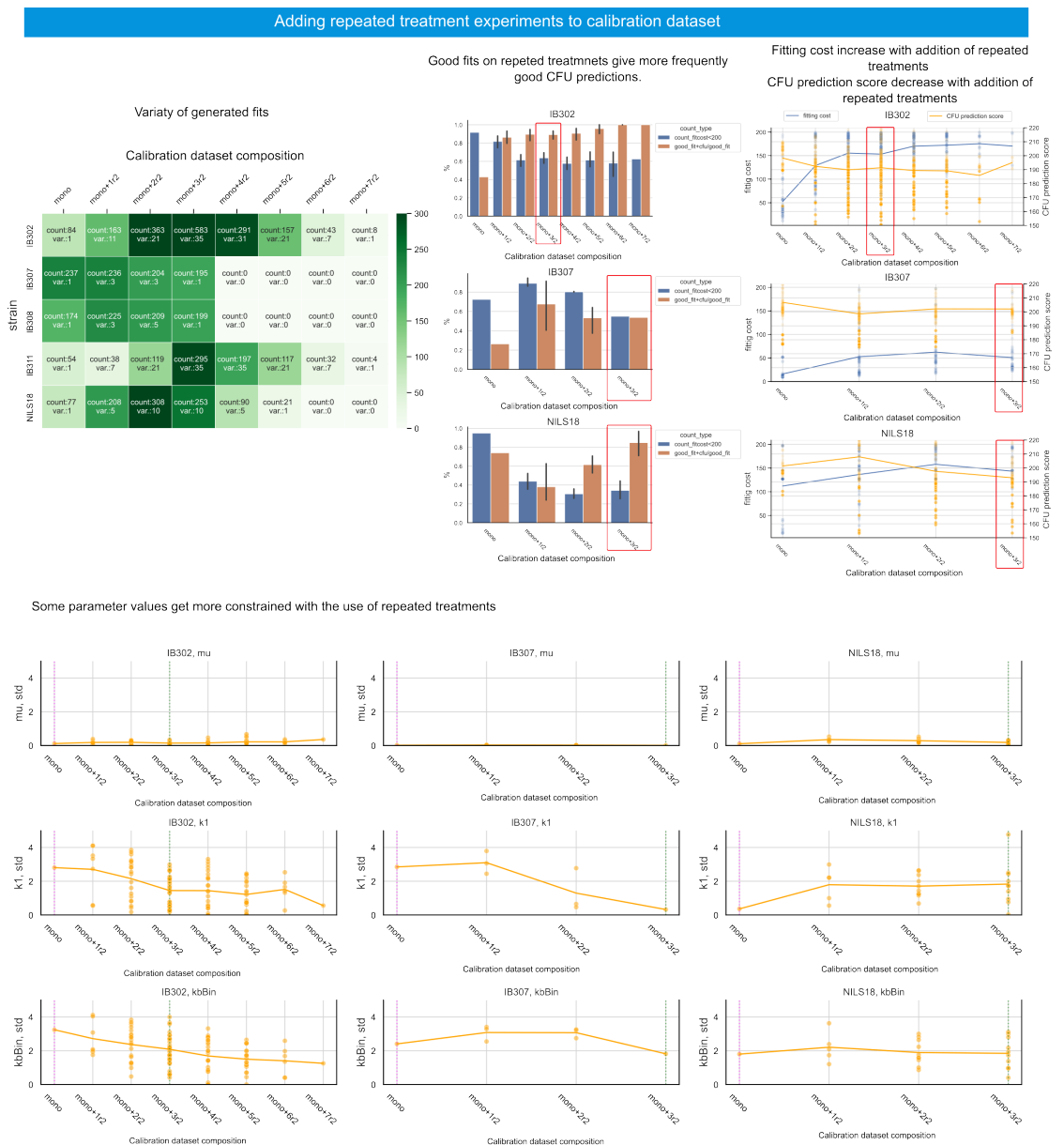


Figure 4.4: **Impact of addition of repeated treatments to calibration dataset on parameter identification.** *Top:* Analysis of fit quality depending on calibration dataset type. *Left:* This table represents a summary of number of generated fits for each strain and for each dataset type. “Count” and colour of the cell correspond to total number, “var.” corresponds to number of individual variants of this type with at least one fit. *Center:* For each individual dataset total number of fits, number of fits with fitting score less than 200 and number of fits with both prediction score and fitting score are less or equal to 200 were calculated. On this plot blue bars correspond to average per dataset type percentage of fits with good fitting score, orange bars correspond to average per dataset type percentage of fits with good prediction score among those with good fitting score. Error bars represent variability between different individual datasets of the same type. *Right:* This plot shows evolution of fitting and prediction scores as a function of calibration dataset type. Points represent individual parameter value sets; solid lines represent average per dataset type. Blue colour corresponds to fitting score, orange colour corresponds to CFU prediction score. *Bottom:* Analysis of parameter value constraints. For each individual dataset for each parameter a standard deviation of value distribution was calculated, represented here in dots. Solid lines correspond to average per dataset type. Different columns correspond to different clinical isolates. Different rows correspond to different parameters. Here we selected three parameters: growth rate μ (first row), a parameter easily identifiable with minimal amount of data; antibiotic concentration inducing filamentation k_1 (second row), a antibiotic-related parameter, important for good CFU predictions, but still identifiable from single treatment experiment; and, finally, product of two parameter characterizing production and efficiency of β -lactamase $k_b * B_{in}$ (third row), hard to identify, but important for good CFU predictions.

4.4 Prediction of complex temporal evolution of CFU for delayed treatments

In the previous sections, the temporal evolution of CFU that we attempted to predict from OD data corresponded only to single treatment experiments. As an additional challenge to the predictive power of the model, we attempted to predict the temporal evolution of CFU for delayed treatments, i.e. no antibiotic treatment at the start of the experiment and the entire antibiotic dose administered several hours later. This experiment is a version of the inoculum effect under nutrient-limited conditions, as the bacte-

rial population has time to grow to higher densities before antibiotics are administered. If the relationship between OD and CFU data was non-trivial for single treatments, this relationship becomes even more complex and puzzling when treatment is delayed. For example, there is no difference in the temporal evolution of OD between treatment at 4 hours, treatment at 6 hours or normal growth without treatment, but the evolution of live cell counts is drastically different in these cases (Figure 4.5).

When treated at the beginning, from the OD data we observe exponential growth for about four or five hours, then a steady period and then regrowth; from the CFU data we observe a decrease in live cell numbers followed by regrowth (Figures 3.2 and 4.1). If the treatment is delayed by two hours, the OD continues to grow exponentially for another five hours, then we observe a shorter steady period and then regrowth. From the CFU data, we observe a period of no increase in live cell numbers after treatment, followed by regrowth. This corresponds to antibiotic-induced filamentation, followed by a short period of cell death, compensated by de-filamentation, and finally regrowth of the population. When treated after four hours, the time course of OD shows no effect of antibiotic treatment, but the CFU data reflect a significant slowing of the growth rate. This could be explained by antibiotic-induced filamentation at the beginning, followed by regrowth under nutrient-limited conditions. Finally, the treatment after six hours of growth does not affect the temporal evolution of the OD, nor does the treatment after four hours. On the other hand, we observed fluctuations in the number of live cells without a significant increase after the treatment. This could be interpreted as cells starting to filament after antibiotic treatment (previously shown results), but due to glucose exhaustion there are not enough nutrients left for the population to regrow. The most difficult observations for the model to capture correspond to simultaneous cell lysis, antibiotic degradation and onset of regrowth, possibly accompanied by filamentation, the timing of these events being highly sensitive to initial and environmental conditions (Figure 3.2b).

We asked whether the parameter set fitted from OD data only (one single and three repeated treatment experiments, Figure 4.1b) could enable accurate model predictions for the CFUs of delayed treatment experiments.

I subjected similar bacterial populations to the same concentration of cefotaxime ad-

a

Predicting CFU of delayed treatments

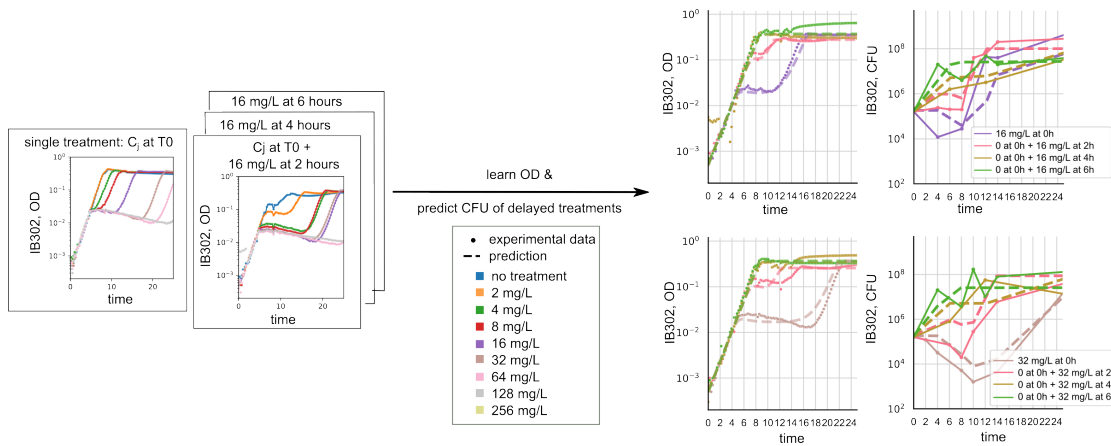


Figure 4.5: **Predicting complex temporal evolution of CFU for delayed treatments.** The calibration dataset is represented on the left side. Experiments corresponding to the data on the plots on the right side are delayed treatment experiments, where no antibiotics are added at the beginning of experiment, and the whole amount (the same for all presented plots) is administered several hours later. Experimental data is presented in points with solid lines and simulations are represented by dashed lines.

ministered at different times (2, 4 and 6 hours). We observed here too a good agreement between the model predictions and the experimental data (Figure 4.5), even though the model was only trained on OD curves.

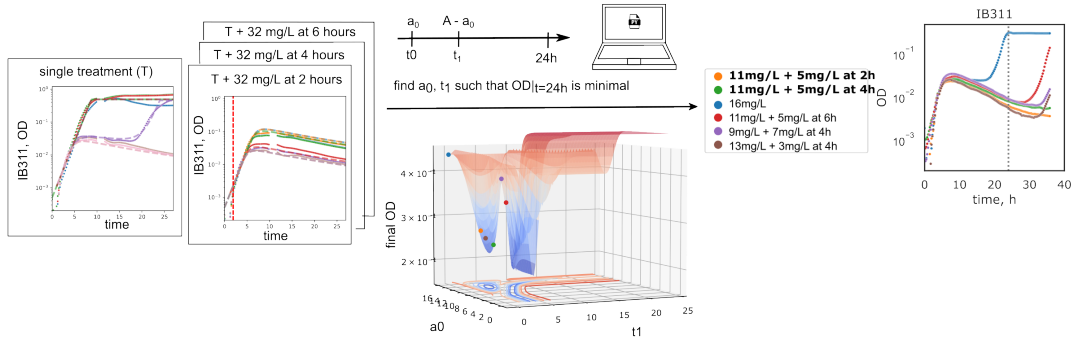
4.5 Optimal treatment

Another challenge we tried to tackle with the model was to find an optimal treatment: more precisely, given a total amount of antibiotic, split it into two doses: one (a_0) to be applied at the beginning, the rest to be applied later (at t_1 hours), in such a way as to minimise the OD at 24 hours. For one strain (IB311), using the same type of dataset as for Figure 4.1, containing one single and three repeated treatment experiments, I generated 40 different fits. From these generated parameter value sets, I selected one based on the sum of the OD fitting score and the CFU prediction score, the CFU prediction score itself, and the accuracy of the prediction of population behaviour during complex

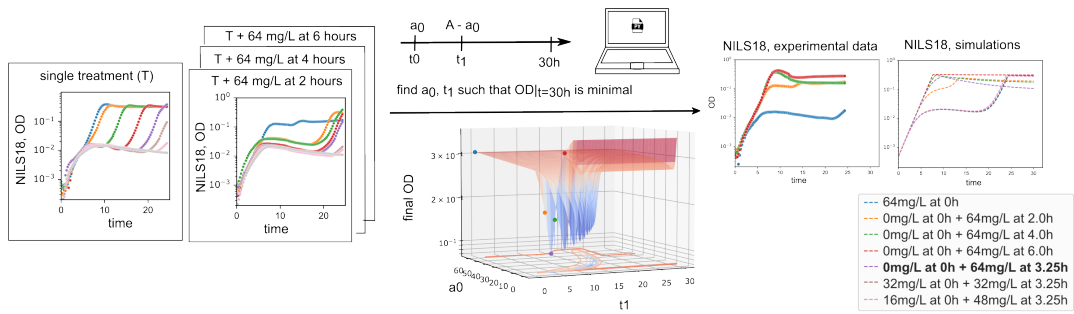
antibiotic treatments. Given this parameter set, a grid optimisation was performed on a_0 and t_1 to find the treatment plan that minimised the OD after 24 hours (Figure 4.6a). The predicted optimal solution was tested experimentally, as well as a number of different treatments selected in the neighbourhood of the predicted optimal one. We found that among these, the predicted optimal treatment was indeed the best performing of all the treatments tested, and that all of them performed according to the model predictions. Incidentally, this search for the treatment that gives the lowest OD at 24 hours seems to correlate with the treatment that prevents cell regrowth for the longest time: all the combinations tested prevented regrowth before 24 hours, while the optimal solutions prevented regrowth even after 30 hours. Given these promising results for IB311, I tried to do the same for another strain (NILS18). As before, using a single and three repeated treatment experiments as a calibration data set, I generated a number of fits, from which I selected one based on the sum of the OD fit score and the CFU prediction score, and the CFU prediction score itself. The only way I found for the final OD to be lower than the carrying capacity at thirty hours was to add the full dose 3 hours after the start of the experiment. This could be explained by rapid nutrient consumption prior to antibiotic treatment, leading to glucose depletion and insufficiency for full regrowth. This scenario of the final OD of the delayed treatment being lower than the carrying capacity (maximum population density when grown without antibiotics) is supported by experimental data. On Figure 4.6b I show the available experimental data and the results of *in silico* experiments for the optimal treatment, the treatment corresponding to the experimental data and some other possible splits that end up less efficient than the optimal one.

And what about the other strains from Figure 4.3? I tried the same optimisation task for the remaining three isolates. For each of them, from parameter value sets generated through calibration on single and three repeated treatment experiments as presented earlier, I selected a set with the lowest sum of fitting and prediction scores and a minimum prediction score for close total scores. For each strain I selected the highest tested concentrations that allowed regrowth before 30 hours, the time at which we sought to minimise OD. All found solutions are either based on active glucose consumption prior to antibiotic treatment resulting in a lack of nutrients for full regrowth (as in the case of

a Optimizing treatment



b Optimizing treatment through nutrient limitation



c Optimizing treatment for CTX-M-producing clinical isolates

strain	a_0	t_1	a_1	totala	totaltime	finalOD
IB302	39.79	14.60	24.21	64	30	0.13
IB307	0.00	2.01	256.00	256	30	0.17
IB308	0.00	3.12	256.00	256	30	0.30
Nils18	0.00	3.23	64.00	64	30	0.11

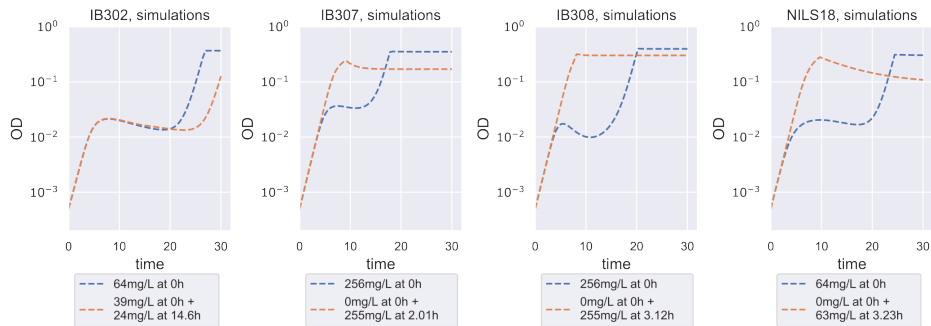


Figure 4.6: **Optimization problem:** Using one of the parameter value sets fitted on single and three repeated treatment experiments, we were looking for treatment optimization: an efficient way to split a given antibiotic concentration into two separate doses, one (a_0) at the beginning and the rest at time t_1 so that OD at 24 hours is minimal. **a.** Left: calibration dataset and fitting results for IB311. Center: surface of the optimization search. Right: Experimental results. Color of lines correspond to specific treatments listed in the table on the left. Position of these treatments on the optimization surface are shown by the points of corresponding color. **b.** Optimal treatment through glucose exhaustion. Left: calibration dataset and fitting results for NILS18. Center: surface of the optimization search. Right: Experimental and *in silico* results. Color of lines correspond to specific treatments listed in the table below. Position of these treatments on the optimization surface are shown by the points of corresponding color. **c.** Top: Summary of the found optimal treatment for the four strains. Bottom: Simulations for each strain: the whole antibiotic concentration administered at the beginning (blue); the optimal treatment for this strain (orange).

NILS18), or do not delay regrowth sufficiently. On Figure 4.6c I presented simulations for putting everything at the beginning and for the optimal treatment. This inability to find the optimal treatment correlates with the observation, that none of the treatments tested for the calibration datasets prevented the regrowth at 30 hours, indicating a high efficiency of their collections of β -lactamases in degrading of cefotaxime.

Interestingly, of the five clinical isolates tested, IB311 is the only one for which we have found a non-trivial optimal treatment. What makes it different from the others? Looking more closely at the temporal evolution of OD in the presence of different concentrations of cefotaxime, we observe some specific characteristics: at low concentrations (up to 8 mg/L) there is no effect of antibiotic treatment on growth dynamics, at a specific concentration from the range tested (16 mg/L) there is the phenomenon of crash, growth arrest and regrowth, at higher concentrations (from 32 mg/L) there is crash and growth arrest but no regrowth. In terms of genotype, this strain expresses three β -lactamases (TEM-1, OXA-181, CMY-2), but does not express a β -lactamase of the CTX-M type, unlike the other four strains tested. The significance of these sets of β -lactamases for the phenotype and the cefotaxime degradation capacity is discussed in more detail in section 3.3.

4.6 Conclusions

The approach presented in this chapter is powerful enough to predict temporal evolution of live cell counts for single treatments, and even some delayed treatments, using only OD data of a range of complex antibiotic treatments. This means that the model allows to use OD - an easily accessible, but notoriously hard to exploit, observable for predicting the CFUs - one that requires long and tedious experimental protocols. This major result might help lighten the experimental load for future susceptibility characterization of clinical isolates by decreasing the number of CFU assays required for the estimate of the killing capacity of antibiotics and the inoculum effect.

The combination of this and the previous chapters demonstrates the importance of the model-based approach. It has allowed us to capture the temporal evolution of both OD and CFU data for a range of clinical isolates subjected to a range of antibiotic treatments, giving us a highly detailed picture of the phenomenon. By adding experiments to characterise the population response to two applications of antibiotics, we were able to learn even more and as a result, predict CFU from OD in a robust and good way and predict optimal treatment where possible. This level of understanding will hopefully help in the fight against recurrent infections.

Chapter 5

Quantifying the impact of growing conditions on cell death

5.1 Introduction

There are many factors that are likely to contribute to the outcome of antibiotic treatment. Some are characteristic of the bacterial strain (resistance genes, resistance mechanisms, adaptive capacity). Some are due to antibiotic properties, some are environmental, such as pH, iron and nutrient availability at the site of infection, host immunity or patient history. Much effort has gone into studying the effects of strain and antibiotic properties, but the role of environmental factors is much less known and understood. However, some studies have already shown that growing conditions play role in the correlation between transcription and gene diversity and that genetic variability increase with gene expression in poor growth conditions [84].

Meanwhile, the course of infection, its severity and the choice of treatment depend to a large extent on the site of infection. Depending on the site of infection, nutritional conditions vary. In the gut, for example, the main source of nutrients comes from the mucus layer, a rich environment that provides a variety of sugars, proteins, lipids and nucleic acids from different sources. The urinary tract is a very different environment. Urine is a very complex medium containing a wide variety of metabolites. The main sources of nutrients in urine are amino acids and carbohydrates. However, urine gen-

erally contains limited amounts of some specific amino acids such as arginine, valine, methionine, uracil, isoleucine and adenine. Iron is also present in limited concentrations. The least abundant carbon source in urine is sugar, especially glucose [85]. As mentioned in chapter 1, urine composition can also be influenced by other medical conditions. It has been shown that trauma, hospitalisation and catheter use play a role in the concentrations of urinary glucose, amino acids, iron, urea and norepinephrine [27]. It has also been shown that patients with type 2 diabetes have a lower pH than healthy volunteers [86]. Some studies also found an increase in urinary glucose concentration in diabetic and hypertensive patients [87].

It is well known that the composition of the medium plays an important role in bacterial growth. It also plays a role in the response to antibiotic treatment. It has been shown that there is a robust correlation between growth rate and β -lactam-mediated lysis rate [57]. In another study, the authors identified an influence of medium composition on both growth rate and hydrogen sulphide production, and subsequently on bacterial tolerance to antibiotics such as ciprofloxacin and chloramphenicol [88]. It was also shown that adaptation to different environments can influence antibiotic resistance and can even be used to sensitise bacteria to some antibiotics [89].

In this chapter, we are interested in exploring the effect of environmental conditions on the response of bacterial populations to antibiotics, and attempting to gain a better understanding of the underlying behavioral differences. To this end, we characterised the response of a collection of clinical isolates to cefotaxime treatments in different media. As a first step, we selected two specific media, taking into account the *in-vitro-in-vivo* gap introduced in chapter 1: Mueller-Hinton (MH) broth, a very rich medium that is the EUCAST standard for antibiotic susceptibility testing medium [33], and pooled urine either from healthy volunteers or purchased from BioIVT, a very complex medium closer to *in vivo* conditions. We made some paradoxical observations that survival in MH was better than in urine for higher concentrations of antibiotic, which goes against the general knowledge that bacteria are more susceptible to β -lactams in richer media. This led us to use a model-based approach to try to explain the observed behaviour. Our approach consisted firstly of measuring both OD and CFU of bacterial population dynamics during antibiotic treatment, and secondly of calibrating the model

[55] to experimental data. Further analysis of the identified model parameter values revealed significant differences between the two media and a possible influence of growth conditions on β -lactamase production and/or activity. Dimensionality reduction results suggest that the influence of the environment is higher than the genetic background of the strain on death and regrowth in presence of cefotaxime.

5.2 Characterization of bacterial population's response to β -lactam treatment in different growing conditions

In chapter 1 I mentioned that there is a well-known gap between *in vitro* tests and *in vivo* conditions at the site of infection. Here we have attempted to tackle this question without adding complexity to the experimental set-up. Our experimental approach is to use a plate reader for incubation, shaking, temperature control and measurement of optical density (OD), and to perform systematic sampling to estimate the number of live cells by performing colony forming unit (CFU) assays. For this study, we selected 5 clinical isolates of different origin ([58, 59], full description in Methods section 7.1), including two strains derived from UTIs: NILS56 and NILS64. All these strains express one or more β -lactamases. Some of them also contain gene mutations that are likely to contribute to antibiotic resistance. These bacteria were exposed to different concentrations of cefotaxime, a third-generation broad-spectrum cephalosporin, while growing in different media. These simple experiments allowed us to make interesting observations (Figure 5.1). For all the strains tested, both the growth rate and the final population size (also known as the carrying capacity) were higher in MH than in urine. This is expected and can be explained by the fact that MH is richer in nutrients.

When subjected to antibiotic treatment, some strains show better survival in urine compared to MH: less decrease in live cell number and earlier regrowth (left side of figure 5.1a). It is well known that cells with a higher growth rate are more susceptible to β -lactam treatment and our observation is in line with this.

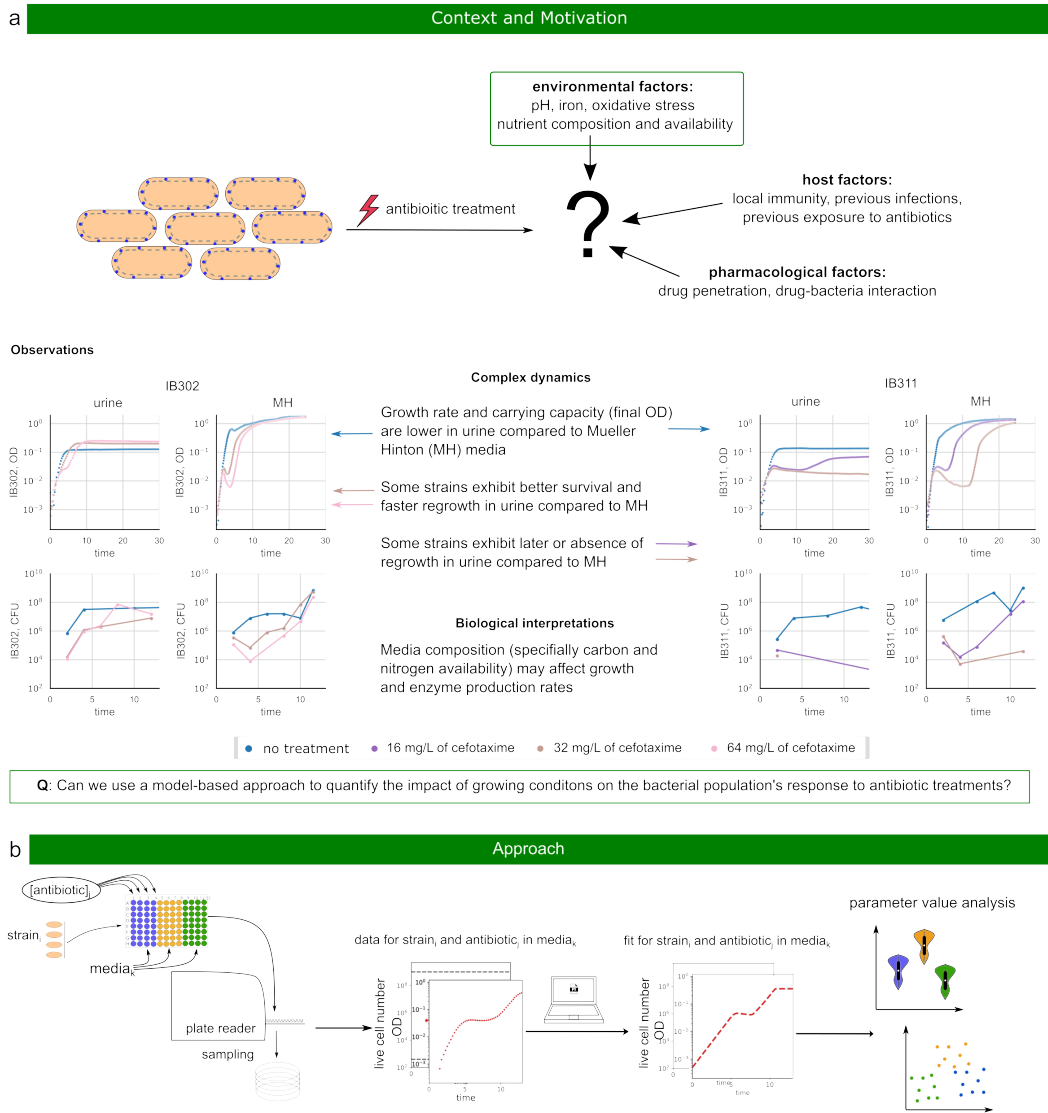


Figure 5.1: Characterisation of bacterial population response to β -lactam treatment in different media. a. *Top:* The outcome of antibiotic treatment of infection is multifactorial. *Bottom:* Description of observed differences between media. For two clinical isolates (IB302 on the left, IB311 on the right), growth kinetic assays were measured together with CFU assays in the absence of antibiotic and in the presence of two concentrations of cefotaxime. These experiments were performed in two different growth conditions: urine (left) and the most commonly used medium for susceptibility testing, Mueller-Hinton (MH) broth (right). b. Approach. For a selection of clinical isolates, growth conditions and antibiotic concentrations, the time course of both OD and CFU was measured. These data were used for model calibration. The resulting model parameter values were further used to quantify the effect of growth conditions on the population response to antibiotics.

Interestingly, however, for some strains, regrowth is faster in MH than in urine (purple line, right-hand side of Fig. 5.1a) or may be present in MH but not in urine (brown line, same plot). A possible explanation could be that although more bacteria are killed by the antibiotic in rich media, there are still more survivors because the total population is larger. Given the richness of the media, more resources may be available for regrowth. These controversial observations lead us to our main question: can we use a model-based approach to quantify the effect of growth conditions on the response of the bacterial population to antibiotic treatment and gain a better understanding of the underlying differences in behaviour between these two media?

The next step in our approach (Fig. 5.1b) is to use experimental OD and CFU data to calibrate the model [55], and to analyse the resulting model parameter values to try to understand the differences between media.

I tested the response of the selected strains to 6-8 concentrations of cefotaxime in both urine and MH (Fig. 5.2). For all strains, growth rate and carrying capacity were higher in MH than in urine. For the majority of strains, bacterial survival is better in urine than in MH at lower antibiotic concentrations: less decrease in live cell number and earlier regrowth. This can be seen for example by comparing the responses to 32 mg/L (brown) and 64 mg/L (pink) for IB302, 8 mg/L (red) and 16 mg/L (purple) for NILS18 and 64 mg/L (pink) for NILS64. However, for higher concentrations of antibiotics for the same strains and for all concentrations (that cause growth changes) for IB311 and NILS56, we observe later growth in urine compared to MH.

Crash time (growth arrest) is earlier in MH than in urine, which is consistent with the common knowledge that faster growing bacteria are killed faster by β -lactams. This may also explain why the decrease in the number of living cells is more important in MH than in urine. As for two contrasted observations on regrowth, this may be related not only to antibiotic killing capacities, but also to β -lactamase activities. At lower concentrations in urine, the enzymes released by lysed cells are sufficient to degrade antibiotics, and since there are fewer losses, the population regrows earlier. At higher concentrations or for strains with weaker β -lactamases, growing in MH means greater population loss, i.e. more β -lactamases in the media, faster degradation of the antibiotic and earlier and faster (due to higher growth rate) regrowth.

Impact of media composition on antibiotic response

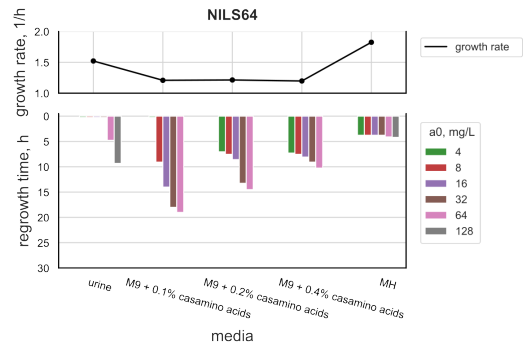
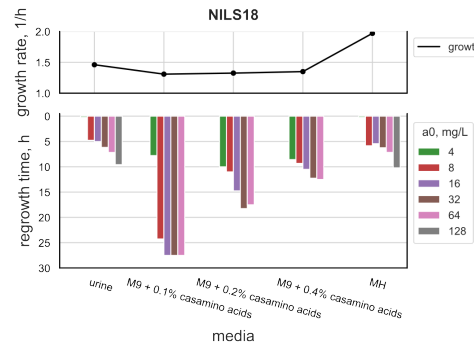
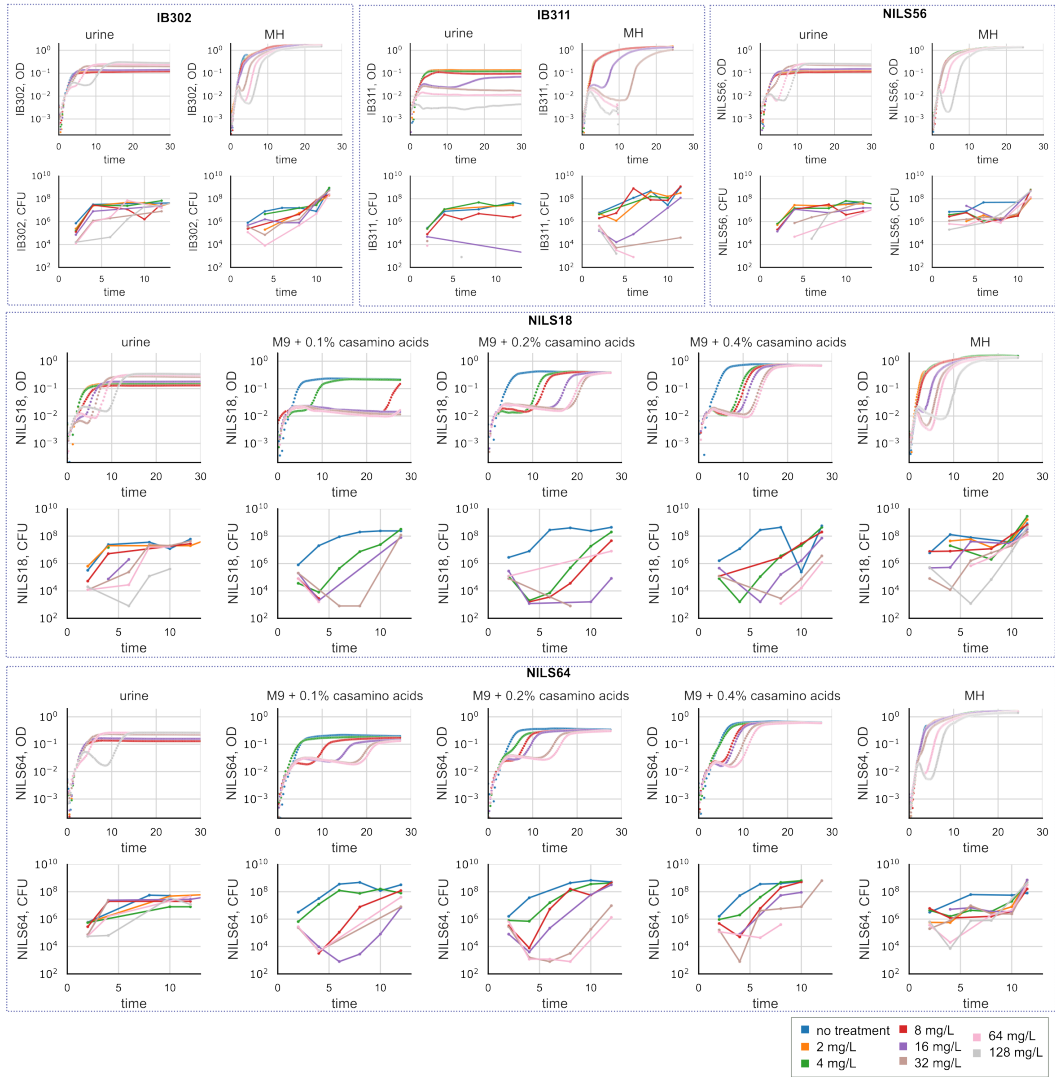


Figure 5.2: **Characterisation of the response of the bacterial population to β -lactam treatment in different media.** *Top:* The response of three clinical isolates (IB302, IB311, NILS56) to cefotaxime treatment was characterised in both urine and MH. Where possible, both OD and CFU data were obtained. *centre:* For two strains (NILS18 and NILS64), experiments were performed in five media: (from left to right) urine, M9 with 0.1% casamino acids, M9 with 0.2% casamino acids, M9 with 0.4% casamino acids and Mueller-Hinton broth (MH). *Bottom:* For the latter two strains (NILS18 on the left, NILS64 on the right) for the five media (x-axis, same order as above) several values were extracted from the data: growth rate (first row of plots, in black), regrowth time for different concentrations of antibiotic (same colour code as above). If there was no regrowth, the regrowth time was set to the end of the experiment (30 hours). If there is no effect of the antibiotic on growth, the regrowth time is set to 0. The y-axis is inverted (fastest regrowth at the top, no regrowth at the bottom).

In urine, amino acids are the main source of nutrients. In MH there are other nutrients, but it contains acid casein hydrolysate, which contains amino acids from the hydrolysis of casein. The main difference between the composition of the two media is the amount of nutrients available. With this in mind, I tested two strains in minimal media containing three different concentrations of casamino acids (amino acids from the hydrolysis of casein). In this way, for the two strains experimental dataset describes the response to cefotaxime treatment in 5 different media: urine, M9 with 0.1% of casamino acids, M9 with 0.2% of casamino acids, M9 with 0.4% of casamino acids and MH. For these two strains for the five media I extracted from the data growth rate and regrowth time for a range of antibiotic concentrations. If there was no effect of the antibiotic on growth dynamics, the time of regrowth was set to 0. If there was no regrowth, this time was set to the duration of the experiment (30 hours). The summary of these metrics is shown in the lower part of Figure 5.2.

The first interesting observation is that the growth rate remains the same in the minimal media with three different concentrations of casamino acids. The main thing that changes is the carrying capacity. We can also observe drastic changes in the regrowth time, which means that growth rate is not the only factor influencing the antibiotic response as the nutrient concentration changes. Interestingly, there is almost no difference

in regrowth time at 4 mg/L (green), but at all higher concentrations there is a significant reduction in regrowth time. In M9 with 0.4% casamino acids there is almost no difference in regrowth time between antibiotic concentrations.

What could cause these effects? Growth rate and crash time remain the same, which means that the killing capacity of the antibiotic does not change significantly. Earlier regrowth could be explained by earlier (more efficient) degradation of the antibiotic, which would mean a higher concentration of β -lactamases released into the media. If the antibiotic kills the same proportion of the population and the growth rate is the same, this would translate into a correlation between amino acid/nutrient availability and the production rate of β -lactamases.

5.3 Model-based approach to identify potential differences between the media

In an attempt to better understand the earlier observations described, I calibrated the model [55] to the data. For each experimental condition (strain-media combination), I tried to use either both OD and CFU data or only OD data (if the first option failed). Fits have been repeated 20 times using stochastic optimization tools. Finally, each parameter value set was evaluated by the corresponding OD score and CFU score, defined as the squared distances between logarithmic values of experimental and simulated data. In Figure 5.3 I show, for each condition, simulations generated with one of the individual model parameter value sets. The simulations obtained are in good agreement with the experimental data, especially considering that the model was designed to mimic the population response to antibiotic in poor media while using sugar as the main nutrient. More importantly, in the majority of cases, the model fits not only the OD data well, but also the CFU data.

As a next step, I used parameter values corresponding to fits with good scores to compare different media and try to identify possible causes for the observed differences. First, I used box plots of the distribution of the parameter values obtained when fitting the model on data from different media (Fig. 5.4).

Can the model capture temporal evolutions of OD and CFU for a range of antibiotic treatments?

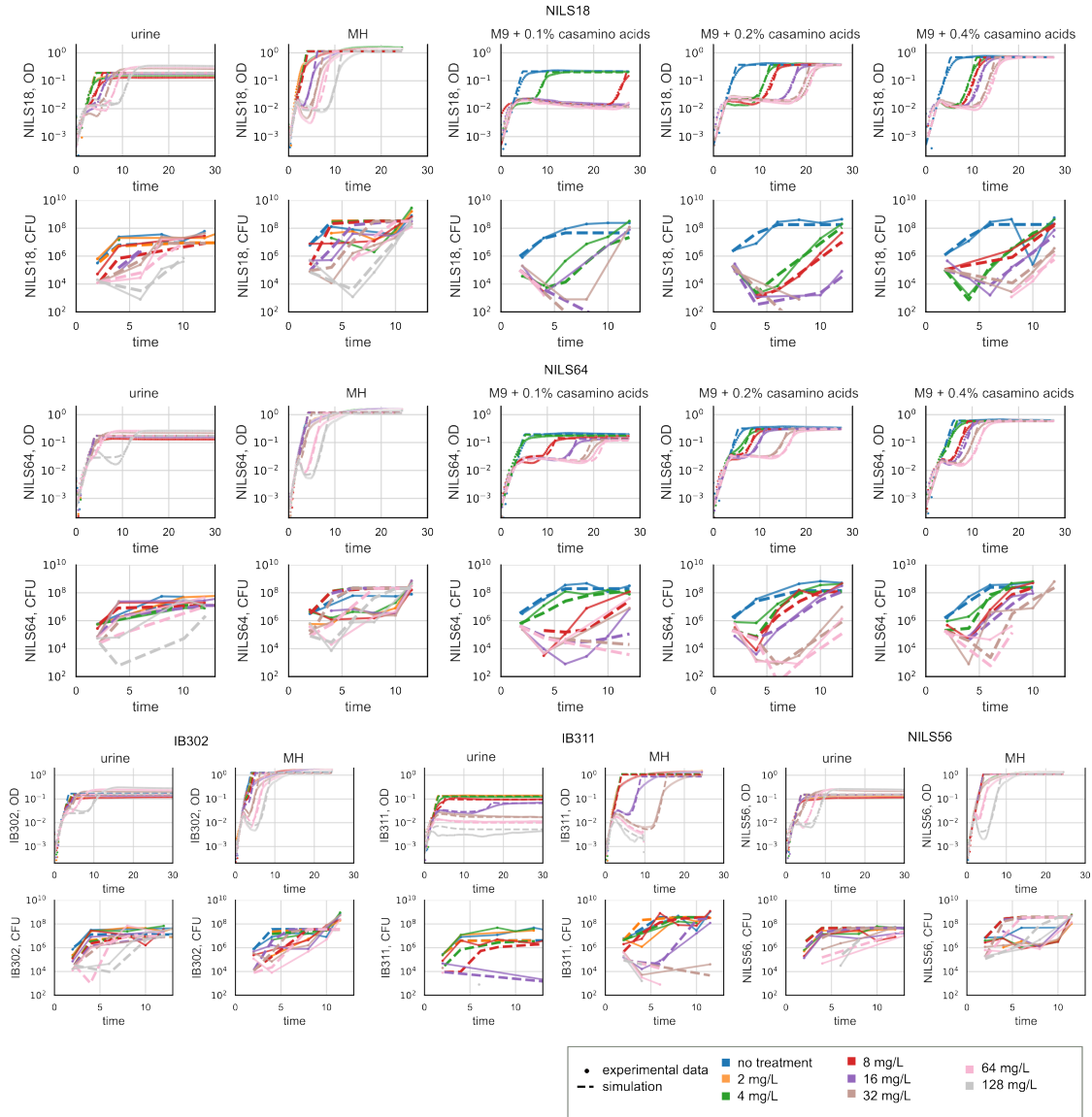


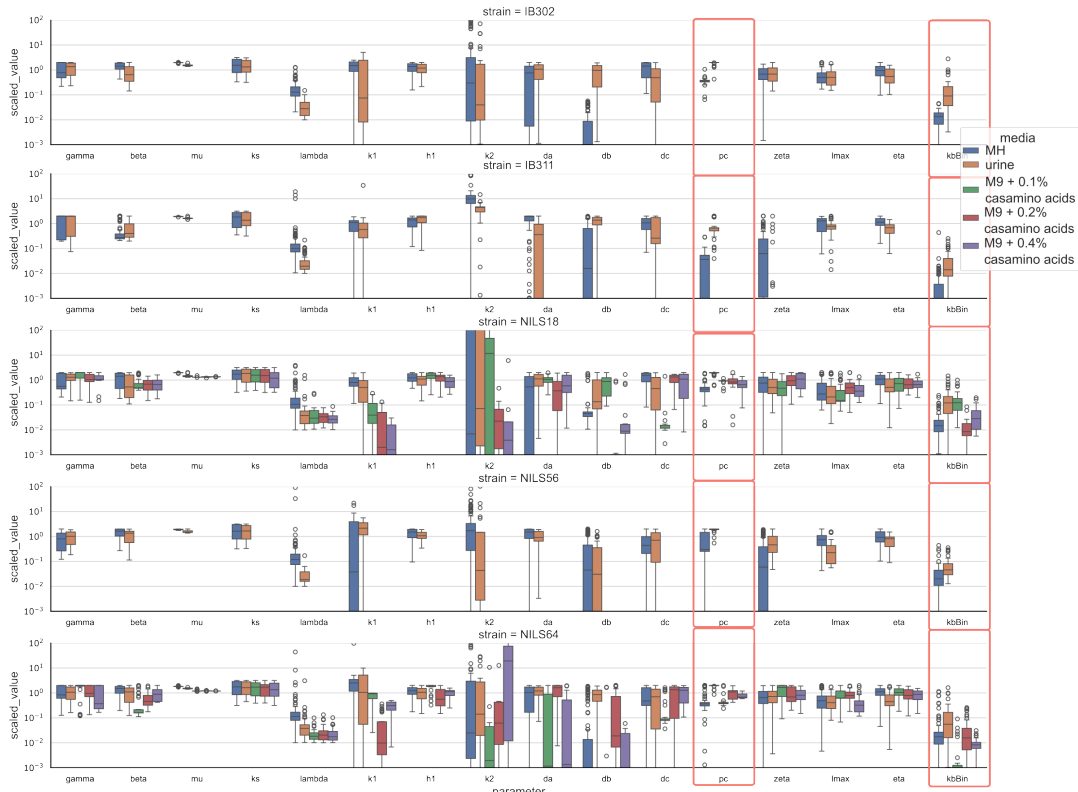
Figure 5.3: Results of model calibration. Comparison of experimental data and the model fit. Five clinical isolates are treated with different concentrations of cefotaxime, and optical density and live cell number are measured as described in Methods section. For two of these strains experiments were performed in five different media (top and center). For the other three experiments were conducted in either urine or MH. We show in points with (CFU) or without (OD) solid lines the experimental data and in dashed lines the output of the model fitted on either just OD data or OD and CFU data simultaneously.

This plot allows not only to compare means, but also to see how identifiable a particular parameter is: some parameters are tightly constrained, such as growth rate, resulting in a very narrow distribution of optimal values. Other parameters are more difficult to identify and are therefore represented by larger distributions with one or sometimes even two modes.

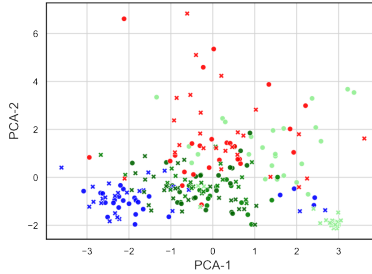
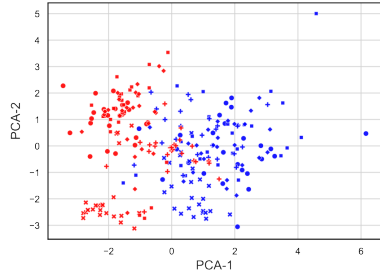
For simplicity's sake, we start the analysis by comparing the median values of the model parameters, which are marked with white dots on the corresponding distribution. This simple test already allowed us to identify some interesting trends. There are two parameters with noticeable differences between urine and MH for all strains: p_c , the proportion of non-degradable dead biomass, and the product of two parameters $k_b * B_{in}$, where k_b is the activity rate of the β -lactamase and B_{in} is the corresponding production rate per unit cell length. The degradable fraction of dead biomass is higher in MH compared to urine, which can be observed as a more pronounced decrease in OD (e.g. grey lines in figure 5.2). This could mean that membrane integrity of dead cells is more degraded in MH, leading to faster degradation of dead biomass. The second observation is that the product $k_b * B_{in}$ is higher in urine compared to MH, meaning that more β -lactamase activity is observed per cell length. This could be due to either a higher production rate and/or a higher activity rate, but we have no way of telling exactly which of the two, as these two parameters suffer from structural unidentifiability and should be analysed together. Another interesting observation is that for the majority of strains (all except NILS56), the minimum antibiotic concentration that stops cell division k_1 is higher in MH compared to urine, meaning that filamentation starts later. We also observe that both k_1 and k_2 (antibiotic concentrations where filamentation and lysis start respectively) can be influenced by changes in casamino acid concentration.

To go further, I performed a dimensionality reduction using Principal Component Analysis (PCA) [90] from 17-dimensional space to 2 (Figure 5.4, middle panel). I selected the 20 best fits for each strain-media combination. For the first PCA (left) I selected fits corresponding to 5 strains in 2 media (urine and MH), for the second (right) I selected fits corresponding to 2 strains (NILS18 and NILS64) in 5 media. Plotting the results using different colours for the fits corresponding to different media revealed two clusters: urine and MH. There was no clear separation of M9 with casamino acids from

Quantifying impact of growing conditions through parameter value analysis



Principal Component Analysis



parameter name	contribution to PCA-1
pc	0.46
beta	0.39
db	0.34
kbBin	0.32

parameter name	contribution to PCA-2
beta	0.39
zeta	0.34
k2	0.24

parameter name	contribution to PCA-1
gamma	0.49
h1	0.43
k1	0.21

parameter name	contribution to PCA-2
kbBin	0.5
db	0.47
pc	0.42

UMAP Visualisation

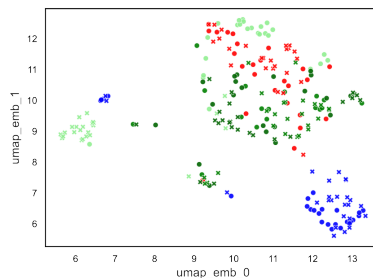
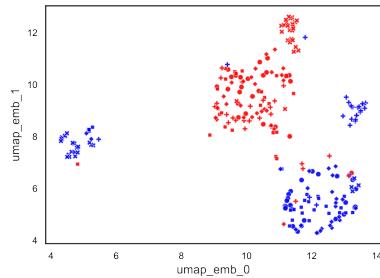


Figure 5.4: **Analysis of model parameter values.** The model was calibrated several times (at least 20 times) on each experimental condition. The obtained sets of parameter values were selected based on the scoring of OD data and CFU data. *Top:* Box plot showing parameter values and corresponding distributions: on the x-axis are different parameters, on the y-axis are relative values (absolute value divided by a reference value for this parameter), colours correspond to media, rows correspond to different strains. *centre:* Dimensionality reduction using Principal Component Analysis (PCA). Points correspond to individual parameter values, colours correspond to media. Tables below show the parameters that contributed most to each component. *bottom:* UMAP [91] visualisation.

the other two media. This clustering was also observed when using other dimensionality reduction mechanisms such as UMAP [91] (Figure 5.4, bottom panel). In each case, the two principal components were able to explain 15 and 12 % of the variance respectively. Interestingly, when looking at the individual contribution of model parameters to each component, p_c and $k_b * B_{in}$ again stood out in both case studies. Another parameter with high contributions is the degradation rate of β -lactamases (d_b).

In addition, the analysis of urine and MH specifically singled out three other parameters: β , ζ and k_2 in terms of high contribution to variance. This means that there could be a correlation between growth conditions and the division rate (β) on the one hand, and antibiotic-induced lysis on the other: k_2 is the antibiotic concentration that induces changes in critical length (beginning of lysis) and ζ is the coefficient of dependence of critical length on antibiotic concentration. The analysis of all media also identified parameters related to antibiotic treatment: the maximum death rate γ and the minimum antibiotic concentration at which cells start filamentation k_1 .

All these results give us food for thought for future experimental design. Interestingly, we were able to classify fits corresponding to different media, but we were not able to separate strains: only IB311 (x symbol) stands out a little. This suggests that the role of the media is more important than the genetic background of the strains in the observed response to the antibiotic. However, this result is biased as all our strains express extended-spectrum β -lactamases.

5.4 Conclusions

In this chapter I described my work on experimental characterisation of clinical isolates in different media including urine and Mueller-Hinton media. Interestingly, impact of growing conditions on antibiotic response varies depending not only on strain but also on antibiotic concentration. I calibrated the model to the experimental data and used PCA analysis to extract possible biological explanations for differences between bacterial behaviour in urine and MH. One of major hypotheses that would be interesting to test experimentally is that β -lactamase activity and/or production rates may depend on growing conditions.

In this work we focused exclusively on nutritional quality of different media, however there are other factors that can affect antibiotic effectiveness. It would be very valuable to extend this study to investigate role of pH, iron concentration, urea presence and anaerobic conditions and to add other strains to the dataset.

Chapter 6

Discussions

6.1 Thesis summary

This thesis started with an introductory overview of antibiotic resistance, treatment failures and recurrent infections. I have also provided a brief summary of the methods commonly used to study the underlying mechanisms of treatment failure. I then presented our approach to in-depth characterisation of population response to antibiotic treatment.

In this manuscript, I have made several methodological and theoretical contributions to the field of antimicrobial resistance. First, in chapter 2 I presented the problem of variability in OD measurements that I had encountered. This problem led to multiple replications of experiments and recurrent model calibration failures. Experimental diagnosis of the underlying problem revealed the presence of biofilms. Here, I proposed a simple solution to address this issue and significantly improve the reproducibility of the observations (addition of Tween 20 to the growth media). The results showed that the proposed approach allowed the generation of high-quality OD data with minimal adjustments and no significant effect on growth rate.

Another optimisation of the experimental protocol (chapter 2, section 2.3) was the development of a new plate-based protocol for CFU assays using a 96-channel pipette to prepare dilutions and spot the whole 96-well plate at once. I also adapted a counting software developed by another team, for which I retrained the machine learning part on

my images and adapted the R code to my project. This approach allowed us to scale up the CFU assays and generate a large dataset, which has been analysed in subsequent chapters.

Other methodological advances are described in annexes. However, their developments have not reached a sufficient maturity given the time frame of the PhD, therefore I did not use them to generate the presented earlier results. One of the methodological advances aimed to test alternative ways to estimate separately live and dead biomass through autofluorescence and propidium iodide staining respectively. Another proposed an enhancement of the plate-reader with a pipetting robot for automated antibiotic administration and automated dilutions. Annex C and D show two set-ups that significantly differ from the one used previously: a bioreactor platform, allowing higher volumes and automated dilutions using peristaltic pumps, and a microfluidic platform, allowing to image cells in monolayer.

This work focused on characterising the response of bacterial populations to different antibiotic treatments in different environmental conditions. In Chapter 3 I presented a filamentation-based model of bacterial population response to β -lactam treatments developed previously. I also showed the extensive dataset I had generated, which included the temporal evolution of both OD and CFU data describing the growth of 11 clinical isolates in the presence of 8 different concentrations of cefotaxime. Calibrating the model to this data allowed us to obtain a detailed picture of collective antibiotic tolerance that reconciled the observed decorrelations between OD and CFU data. By further analysing the model parameter values, we were able to capture differences between strains in terms of β -lactamase type. In this chapter I have also presented the results of similar characterisation for other β -lactam antibiotics.

In Chapter 4, I presented a study of the population response to multiple doses of antibiotics. In the previous chapter, all antibiotics were given at the beginning (also called single treatment). In this chapter, I added experiments where a second dose was given several hours later (repeated treatment). These conceptually simple experiments gave us a lot of valuable information about cell death and β -lactamase activity. They also allowed us to obtain robustly good estimations of live cell counts (very informative, but experimentally demanding) from OD data (easy to generate, hard to use) by model cal-

ibration. This major result was observed for several clinical isolates. In this chapter, we also explored the influence of the composition of the calibration dataset on parameter value constraints, and confirmed high information value of repeated treatment experiments for understanding enzyme-mediated antibiotic escape and for constraining model parameter values. Finally, I have also demonstrated the unique capacities of the model to find optimal treatments.

Finally, in Chapter 5 I compared the bacterial response to antibiotic treatment in different growth conditions, specifically pooled human urine and Mueller-Hinton media (standard media for antibiotic susceptibility testing). We observed several paradoxical effects, for example, for the majority of strains the differences between the two media depended on the antibiotic concentration: better survival in urine at low concentrations, better survival in MH at high concentrations. We were also able to identify interesting trends in parameter values, suggesting that β -lactamase production and activity may differ between the two media. Further analysis revealed a clear distinction between sets of parameter values corresponding to different media. Interestingly, strain identity had less influence than environmental conditions on the results of dimensionality reduction. However, this result may be biased by our strain selection, as all strains tested expressed β -lactamases.

6.2 Discussions and Perspectives

The approach presented in this manuscript is unique in several respects. On the experimental side, following OD curves in a plate reader is one of the most used and simplest experiments for characterisation. Many people working with clinical isolates encounter variability in OD curves and deal with this problem by repeating the experiment many times and using the median as ground truth. However, in a number of cases, using the median is not satisfying, for example, when there are very large differences in re-growth time. There are very few studies that have looked at the underlying problem and tried to address it directly. Ultra low adhesion plates are hard to find and their cost is much higher than standard plates, besides, there are not always efficient. The solution of adding Tween20 to the media was already known and used in larger volumes, but is

overlooked in microplates.

The model we used is also unique. To the best of our knowledge, this is the first model of bacterial population response to β -lactam treatments that is able to simultaneously record live cell counts and optical density of a cell culture subject to filamentation and complex antibiotic treatments. Previous studies [92, 93] have avoided the filamentation problem by focusing on cell count measurements or ignoring the pre-crash part of the OD curve. This way focuses on killing capacity of antibiotic and skips escape mechanisms of bacteria. Many studies also required experiments to include β -lactamase inhibitors to correctly represent the phenomenon [94]. This way ignores all the enzyme-mediated responses and the population resilience. Some studies [54] attempted to address the filamentation problem, but used single cell profiles and microscopy data to predict OD, which is the opposite problem, focusing on biophysics to predict population response not considering resilience mechanisms. One of the drawbacks of the model used in this work is the complexity with which it describes evolution of average cell length and number of live cells. A possible extension of the model would be to use physics-informed machine learning to replace complex ODE approximations of initial PDE model by data-driven approach constrained by biological assumptions. The amount and diversity of data generated for this thesis should allow to train the extended model. When trained, the model might be quicker to use with higher success rate.

Importantly, we have developed an approach that is powerful enough to predict the temporal evolution of live cell counts for single treatments, and even some delayed treatments, using only OD data from a series of complex antibiotic treatments. This means that our approach allows the use of OD - an easily accessible but notoriously difficult observable - to predict CFUs, which requires long and tedious experimental protocols. This important result could help to reduce the experimental burden for future susceptibility characterisation of clinical isolates by reducing the number of CFU assays required to estimate the killing capacity of antibiotics. Moreover, the repeated treatment experiments that allowed us to achieve this result provide us with valuable information on the mechanisms of bacterial response to antibiotics and are simple experimental and conceptually straightforward modifications of the standard protocol.

Another important challenge we have investigated in this manuscript is the gap be-

tween *in vitro* and *in vivo*. Here, we used our model-based approach to characterise the population response to antibiotic treatment in different conditions: pooled human urine (complex media relevant for UTIs) and Mueller-Hinton broth (rich media defined by EUCAST as standard media for MIC measurement). Understanding the differences in bacterial behaviour between these two conditions can shed light on some of the reasons for antibiotic failure. Even in this simple set-up, we were able to observe contradictory responses depending on antibiotic concentration and strain. We were also identify biological processes that could potentially explain the paradoxical observations: β -lactamases activity and/or production rate are influenced by change of media. In addition there might be some environmental effects on filamentation (specifically at which concentration in starts) and on integrity of cells (specifically on how long it takes to degrade dead cells).

There are several possible extensions of this work. In Chapter 3 we used model parameter values to study the effects of bacterial genotype on phenotype and we were able to single out one strain, that has a different set of β -lactamases than the other strains, but it showed a similar level of antibiotic susceptibility. Most of the strains tested express more than one β -lactamase and possess different mutations relevant for β -lactam treatment failure. An interesting experimental extension of this study would be to identify the role of each enzyme and mutation in the population response to antibiotic treatment.

In Chapter 5 we were interested in investigating environmental factors in antibiotic treatment failures. Through careful observation and analysis of model parameter values, we identified possible biological explanations for the observed differences. It would be valuable to test experimentally whether there are differences in the activity or expression level of β -lactamases between the tested media. In this manuscript, we have focused on the nutrient side of the environment, but there are many other factors that could influence the population response, such as the availability of iron or other essential ions, pH, and urea concentration. It would be interesting to use the same approach to characterise the role of these factors on growth rate, filamentation, death and β -lactamase production and activity. It would also be valuable to study the population response to multiple antibiotic applications (as in Chapter 4) in different media (as in Chapter 5). This may shed more light on the biological processes that cause differences between media. This could also

help to predict the outcome of complex antibiotic treatments *in silico*.

To go even further, one could combine the techniques from chapters 4 and 5. Using our model-based approach to study population response to multiple applications of antibiotics in many different media combined with other experimental data such as measures of the beta-lactamase production and activity, quantification of the temporal evolution of the antibiotic concentration and systematic measures of the length of filaments would give an unprecedentedly detailed multi-level picture of the antibiotic escape. This would allow to understand the reason for infection relapses and to develop optimal treatment strategies without using last resort antibiotics or expensive combinations with β -lactamase inhibitors.

Chapter 7

Materials & Methods

7.1 Strains and antibiotics

The strains used in this work have been sequenced as a part of previous studies [[58] for IB strains, [59] for NILS strains], hence, their full genetic information is available, and antibiotic-resistance-related genes and mutations are known. Below, Table 7.1 represents a summary of available information for each strain.

In this table *ftsI* is the gene coding for PBP3. A mutation in this gene can lead to reduced susceptibility of PBP3 to β -lactams. *ompC* and *ompF* respectively code for a precursor of the outer membrane porins C and F. Their mutations can play a role on antibiotic susceptibility because they might prevent the entrance of antibiotic molecules in the cell. Some also contain mutations in *gyrA* and *parC*, that do not confer resistance to β -lactams, but rather to fluoroquinolones.

Cefotaxime was purchased from Sigma-Aldrich and dilutions were made considering the purity specified by the vendor. Cefotaxime, together with ceftriaxone and meropenem, as well as stock solutions were kept at -20°C to limit degradation.

7.2 Growth conditions

Unless specified otherwise, all pre-cultures and cultures were performed in 0.1% glucose M9 liquid medium (1 g/L glucose, 6.78 g/L Na_2HPO_4 , 3 g/L KH_2PO_4 , 1 g/L

strain	origin	sequence type(ST)	β -lactamases	relevant for antibiotic resistance genes	relevant mutations
NILS1	feces	69	TEM-1B	aph6-Id, aph3"-Ib, aadA5, mphA, mdfA, catA1, sul1, sul2, tetB, dfrA17	
NILS11	feces	10	TEM-1B	aph3"-Ib, mdfA, sul2, dfrA5, dfrA1	
NILS12	feces	450	TEM-1B	aph6-Id, aph3"-Ib, aph3'-Ia, aac3-Iid, aadA5, mdfA, mphA, sul1, sul2, tetA, dfrA17	gyrA S83L/D87N, parC S80I
NILS18	blood	69	CTX-M-14, TEM-1B	aph6-Id, aph3"-Ib, mdfA, mphA, sul2, tetB, dfrA14	gyrA S83L, parC S80I
NILS42	urine	38	CTX-M-14B, TEM-1B	aph6-Id, aph3"-Ib, aadA1, mdfA, sul2, dfrA1, dfrA5	
NILS56	urine	405	CTX-M-15	mdfA, tetA, tetB	gyrA S83L/D87N, parE S458A, parC S80I
NILS64	urine	131	CTX-M-15, TEM-1B, OXA-1	aac6'-Ib-cr, aac3-IIa, aadA5, mdfA, mphA, catB3, sul1, tetA, dfrA17	gyrA S83L/D87N, parE I529L, parC S80I/E84V

Table 7.1: Description of clinical isolates - NILS collection

strain	origin	sequence type(ST)	β -lactamases	relevant for antibiotic resistance genes	relevant mutations
IB302	unknown	410	CTX-M-15, TEM-1B, OXA-1	aac(6')Ib-cr; dfrA17; sul2; aadA5; aac(3)-IId; strA; sul1; strB; tet(B); mph(A)	gyrA S83L/D87N, parC S80I
IB307	rectal swap	410	TEM-1B, CTX-M-15, OXA-1, NDM-5, CMY-42	aadA2; dfrA17; aac(6')Ib-cr; tet(A); erm(B); strA; tet(B); sul1; sul2; aadA5; strB; mph(A); qepA; dfrA12	ftsI YRIK, gyrA S83L/D87N, parC S80I/E84
IB308	rectal swap	410	CTX-M-15, OXA-181, CMY-42	QnrS1; sul2; mph(A); tet(A); sul1; aadA5; dfrA17	ftsI YRIK, gyrA S83L/D87N, parC S80I/E84
IB311	rectal swap	410	TEM-1, OXA-181, CMY-2	QnrS1; tet(B); dfrA17; mph(A); sul2; aadA5; aac(3)-IId;	ftsI YRIN 349-532, ompC R195L, ompF -46; C->T (OmpR F3), gyrA S83L/D87N, parC S80I/E84

Table 7.2: Description of clinical isolates - IB collection

NH₄Cl, 0.5 g/L NaCl, 0.24 g/L MgSO₄, 0.01 g/L CaCl₂), and experiments were performed in 0.1% glucose M9 liquid medium with 0.1% Tween 20. The low glucose concentration is meant to create the conditions of a carbon-related growth arrest, a situation that lends itself better to mathematical modelling. The growth arrest happens in this medium between 0.2 and 0.3 OD₆₀₀. For overnights and precultures, cells were incubated at 37°C and at 200 rpm. Other media that were used in this work are: M9 liquid medium with 1, 2 or 4 g/L of casamino acids; urine defrozed, pooled from three healthy volunteers and then passed through 0.22 μm filter; and finally Mueller-Hinton Broth. For each experiment both overnight and morning pre-cultures were done in the same media as the final experiment.

7.3 Growth curves acquisition

Overnight. A single bacterial colony was picked from an agar plate and incubated overnight at 37°C and 200 rpm. **Preculture.** The overnight was vortexed and diluted to 0.05 OD₆₀₀ before a new incubation of 3 hours under the same conditions, aiming to catch the cells in exponential phase for the beginning of the experiment. **Experiment preparation.** Cells from the preculture were vortexed and diluted to 0.01 OD₆₀₀. Each well of a 96-well plate with transparent flat bottoms was filled with 190 μL of antibiotic dilution in M9 media with Tween 20 and 10 μL of the cell suspension. Depending on the plate configuration and the number of replicates, the dilutions were made as much as possible in larger quantities in order to minimize errors related to small-volume pipetting. **Data collection.** 2017 and 2021 Tecan Spark multimode plate readers were used for all OD acquisitions. Thermo Scientific™ Nunc™ Edge 2.0 flat bottom microtiter plates were used. OD measurements were carried out in a loop consisting of measurement and incubation with shaking. The incubation periods are carried out at 37°C and last 300 s. **Repeated treatments.** Stocks of antibiotics were prepared in advance and kept at +4°C. Before application they were warmed up for some time at room temperature, then put into a small container. From there, using an Integra Biosciences Voyager 8-channel electronic pipette antibiotic was administered to a column of the 96 well plate at the same time to limit the time outside of incubation conditions.

7.4 Live cell number estimation.

Live cell number was estimated by the CFU counting method. At every time-point the plate was removed from the plate reader, 5 μl were sampled using an Integra Biosciences MINI 96 electronic pipette with 96 channels into 45 μl of PBS buffer. The experimental plate was put back into the plate reader and the experimental program was resumed. Each dilution step started with washing protocol for pipette tips (3 times in ethanol, dry tips, 3 times in PBS). Next, the dilution was mixed. 5 μl were spotted in a square Petri dish filled with lysogeny broth (LB) agar. 10 μl were transferred into 90 μl of PBS in the next plate. All Petri dishes were kept at room temperature until the last timepoint, when all the plates were put for incubation at 37°C for the night. The next day after 10-12 hours of incubation, plates were photographed on a black background. Colonies were counted with CFU Spot Reader which is a Shiny based application, developed by Vincent Aranzana-Climent and Pharmacology of Antimicrobial Agents and Antibioresistance team in INSERM. This protocol was presented in details in Chapter 2.

7.5 Data analysis

OD blanking. The measured OD of a well is the sum of the OD of the cell culture, and of the OD of the well bottom. For this reason, before an experiment, the OD of a plate filled with media is measured and a constant OD corresponding to an average OD of the plate without bacteria was removed from each well data. **Removal of aberrant timepoints.** Occasionally, an OD reading fails and returns a value much larger than both the previous and the following ones of the same well. As this situation is highly biologically improbable, these outliers were removed.

7.6 Model

Here is a short description of the model used in this project. To describe the temporal evolution of the distribution of cell lengths $n(l, t)$, a growth-fragmentation model was

used. It relies on four main mechanisms: the cells continuously elongate with a rate g , they divide with a rate f and when they divide, regardless of their length, they always split into cells of sizes $\frac{1}{2}$ to 1 (arbitrary unit), meaning that filamented cells might split into more than 2 cells. Finally, they lyse when they reach the critical length L_m . The following PDE describes these phenomena:

$$\frac{\partial n}{\partial t} + gl \frac{\partial n}{\partial l} + gn = \begin{cases} 0 & \text{for } 0 \leq l < \frac{1}{2} \\ f \sum_{i=1}^{\infty} 2^{2i} n(2^i l, t) & \text{for } \frac{1}{2} \leq l < 1 \\ -fn & \text{for } 1 \leq l < L_m \\ -(f + \gamma)n & \text{for } L_m \leq l \end{cases} \quad (7.1)$$

The PDE is initialized with the steady state cell length distribution of an exponentially growing cell population: $n(l, 0) = N(0)y_{\infty, \gamma=0}(l)$ with

$$y_{\infty, \gamma=0}(l) = \begin{cases} \frac{f + g}{f} \frac{l^{f/g} - 2^{-f/g}}{l^{2+f/g}} & \text{for } \frac{1}{2} \leq l < 1 \\ \frac{f + g}{f} \frac{1 - 2^{-f/g}}{l^{2+f/g}} & \text{for } 1 \leq l \end{cases} \quad (7.2)$$

The interaction with the antibiotics is taken into account through the dependency of these rates and threshold with the antibiotics concentration in the culture medium. While the elongation rate is independent on the antibiotic concentration and just follows Monod's law, the division rate f and the critical length L_m are decreasing functions of the antibiotic:

$$g = \mu \frac{s}{K_s + s} \quad f = \frac{\beta}{1 + (\frac{a}{k_1})^{h_1}} \quad L_m = L_{max} * \frac{k_2 + a * \zeta}{k_2 + a} \quad (7.3)$$

Various concentrations are also tracked in the culture medium, such as the nutrients s , the antibiotics a , the β -lactamases b , and the dead biomass c and c_r . Their dynamics are described with the following ODEs:

$$\begin{aligned}
\frac{ds}{dt} &= -\frac{g}{\lambda} \int_0^{\infty} lndl \\
\frac{da}{dt} &= -k_bba - d_aa \\
\frac{db}{dt} &= \gamma B_{in} \int_{L_m}^{\infty} lndl - d_b b \\
\frac{dc}{dt} &= \gamma(1 - p_c) \int_{L_m}^{\infty} lndl - d_c c \\
\frac{dc_r}{dt} &= \gamma p_c \int_{L_m}^{\infty} lndl
\end{aligned}$$

Finally, the optical density is proportional to the sum of the live and dead biomasses:

$$OD(t) = \eta \left(\int_0^{\infty} lndl + c(t) + c_r(t) \right) \quad (7.4)$$

This describes the PDE model. For computational efficiency, for calibration we used an ODE model approximating the PDE model above:

$$\begin{aligned}
\frac{dN}{dt} &= N \left[f \left(\frac{L}{\ln 2} - 1 \right) - \gamma Y_{>} \right] \\
\frac{dL}{dt} &= L \left[g - f \left(\frac{L}{\ln 2} - 1 \right) \right] - \gamma (L_{>} - LY_{>})
\end{aligned}$$

$$\begin{aligned}
\frac{ds}{dt} &= -\frac{g}{\lambda} NL & g &= \mu \frac{s}{K_s + s} & \nu &= \frac{\beta}{g} \\
\frac{da}{dt} &= -k_bba - d_aa & f &= \frac{\beta}{1 + \left(\frac{a}{k_1}\right)^{h_1}} \\
\frac{db}{dt} &= \gamma B_{in} NL_{>} - d_b b & L_m &= L_{max} * \frac{k_2 + a * \zeta}{k_2 + a} \\
\frac{dc}{dt} &= \gamma(1 - p_c) NL_{>} - d_c c & L_0 &= \left(1 + \frac{\mu}{\beta} \ln 2\right) \\
\frac{dc_r}{dt} &= \gamma p_c NL_{>} & OD &= \eta (NL + c(t) + c_r(t))
\end{aligned}$$

$$Y_{>}(x = \frac{L}{L_0 L_m}) = \begin{cases} \frac{x}{v}(x^v - (\frac{x}{2})^v) & \text{for } x \leq 1 \\ x - 1 + \frac{x}{v}(1 - (\frac{x}{2})^v) & \text{for } 1 \leq x \leq 2 \\ 1 & \text{for } 2 \leq x \end{cases}$$

$$L_{>}(x = \frac{L}{L_0 L_m}) = \begin{cases} \frac{x}{v \ln 2}(x^v - (\frac{x}{2})^v) & \text{for } x \leq 1 \\ x \frac{\ln x}{\ln 2} + \frac{x}{v \ln 2}(1 - (\frac{x}{2})^v) & \text{for } 1 \leq x \leq 2 \\ x & \text{for } 2 \leq x \end{cases}$$

The variables and parameters of the model are presented in the following tables (7.3 and 7.4).

Variable	Unit	Comment
t	h	Time
l	1	Cell length [au]
$n(l, t)$	1	Population density
$s(t)$	g/L	Concentration of nutrients
$a(t)$	mg/L	Concentration of antibiotics
$b(t)$	mg/L	Concentration of -lactamase
$c(t)$	1	Dead degradable biomass
$c_r(t)$	1	Dead non-degradable biomass

Table 7.3: Variables of the model

7.7 Model fitting

Each parameter was restricted to a range of biologically plausible values. Depending on the role of the parameter and the size of the range, a change of variable was applied or not, to perform the search of this parameter in the linear space or in a logarithmic space. All 17 search ranges were then brought back to the interval and it is in this space that the parameter search was performed.

Parameter	Unit	Comment
γ	1/h	Death rate
β	1/h	Maximal division rate
μ	1/h	Maximal growth rate
K_s	g/L	Half-velocity constant of nutrients
λ	L/g	Conversion factor from nutrients
k_1	mg/L	Concentration of antibiotics needed to stop cell division
h_1	1	Hill coefficient of this antibiotic action
k_2	mg/L	Concentration of antibiotics needed to stop defect repair
B_{in}	mg/L	Concentration of β -lactamase released by a cell of length 1
k_b	L/mg/h	Activity rate of β -lactamase
d_a	1/h	Degradation rate of antibiotics
d_b	1/h	Degradation rate of β -lactamase
d_c	1/h	Degradation rate of dead biomass
p_c	1	Proportion of non-degradable dead biomass
L_{max}	1	Maximal viable cell length
η	1	Conversion between biomass and OD
ζ	1	Ratio between minimal cell length where lysis can occur and maximal viable cell length

Table 7.4: Parameters of the model

The cost function computes the log-likelihood of the data assuming independent Gaussian measurement noise on each point. This boils down to mean square deviations. Normalizations were made such that each data point has same impact, irrespectively of number of points per time series and of number of time series (e.g. different antibiotic concentrations). Special care was taken when searching on mixed datasets involving both OD measurements and cell counts, to balance the contribution of both data types. The integration of the ODE system was done with the 'diffeqsolve' method of diffrax package [95] with the method 'Tsit5', and absolute and relative tolerances set to 10^{-6} .

Model fitting was performed both with CMAES [96], with an initial , and Latin Hy-

per Cube with 5000 samples and method 'trf', except when a local search was required. This was notably the case for the estimation of parameter uncertainties.

7.8 Crystal violet staining

The protocol was adapted from the one proposed by Hölzl-Armstrong and colleagues [97]. First the experimental plate is emptied and washed several times with PBS. Then it is filled with 35 μl of crystal violet diluted to 0.1% in 10% ethanol and incubated in the dark for 10 minutes. Then the plate is emptied again and washed with water 5 times. After an hour of drying in the dark, the plate is filled with 100 μl of 50% ethanol in each well and left for 10 minutes in the dark. Final step consisted in measured OD at 595 nm.

7.9 eVOLVER experiment

There are several steps to prepare an experiment in eVOLVER platform. The first one is to prepare a Python script specific for the experiment, in which it is specified the mode of experiment (turbidostat, chemostat, batch or something custom), which defines if, when and how dilutions should be done, for which vials and with which pump. Another step is to prepare enough media for potential dilutions. Individual glass vials are filled with 25 mL of appropriate media. Next, pumps are connected to experimental vials and to media bottles. Media in vials are inoculated with bacterial culture in stationary or exponential phase. At this moment the script is launched and the experiment starts. During each experiment OD measurements and pump logs are registered.

7.10 Microscopy experiment using CellASIC ONIX plate

First, the CellASIC plate is emptied because it arrives filled with buffer to avoid drying up of channels. Then every inlet is filled with 300 μL of media. Cell inlets are filled with bacterial culture at exponential phase. When fully filled, the plate is sealed and placed under the microscope. Using CellASIC ONIX software cells are loaded into the

chambers. Then the duration of the flow and the corresponding inlet are defined and the experiment is launched. In [98] there is a detailed protocol of these steps. Image acquisition and positioning is defined with Micro-Manager [99]. The experiment is controlled by MicroMator [100]. Final images were analysed using the open-source segmentation pipeline of DeLTA [101].

Appendix A

Alternatives to CFU assays: auto-fluorescence and propidium iodide staining

As mentioned above, there are two standard ways to characterise population response to antibiotic treatments: growth kinetic assays and CFU assays. The first is done by systematic measurement of optical density, a very simple protocol that allows to measure total biomass (live and dead). The second gives valuable estimates of the number of live cells, but requires the use of time-consuming and laborious protocols.

Here we are interested in exploring other ways to estimate the number of live and dead cells. All bacteria exhibit intrinsic natural fluorescence (hereafter referred to as auto-fluorescence or AF). There are many different structural components and metabolites that contribute to this fluorescence, but flavins and NAD are responsible for most of the cytoplasmic auto-fluorescence. This can be explained by their role in cellular metabolism. Studies have shown that various stresses, including β -lactam treatments, can affect AF levels [102]. This leads us to believe that auto-fluorescence measurements could be a good complement to OD measurement and allow us to see the evolution of live cell numbers. A disadvantage of this method is that flavins are secreted into the environment, and what we are actually measuring is the external fluorescence of these secreted flavins. This means that when cells stop growing and/or start dying, there

is no decrease in fluorescence. Some studies have tried to overcome this problem by analysing the time derivative of AF instead of the absolute values [103].

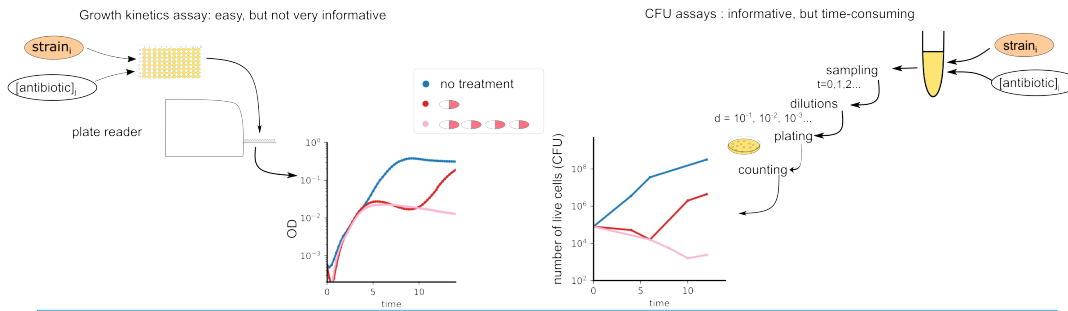
The other well-known technique that could help to separate live and dead biomass measurements is propidium iodide (PI) staining [104, 105]. PI is a small molecule that binds to DNA and therefore increases in fluorescence when the cell membrane is depolarised (otherwise does not enter the cell).

We applied these two techniques to our standard plate reader experiments. Three measurements were taken every 5 minutes: optical density (total biomass), green fluorescence (auto-fluorescence) and red fluorescence (propidium iodide). Below in figure A.1 I show the results for one strain (NLS18) exposed to 6 different concentrations of cefotaxime while growing in two different media (M9 with 0.1% glucose on the left and M9 with 0.1% glucose and 0.2% casamino acids on the right).

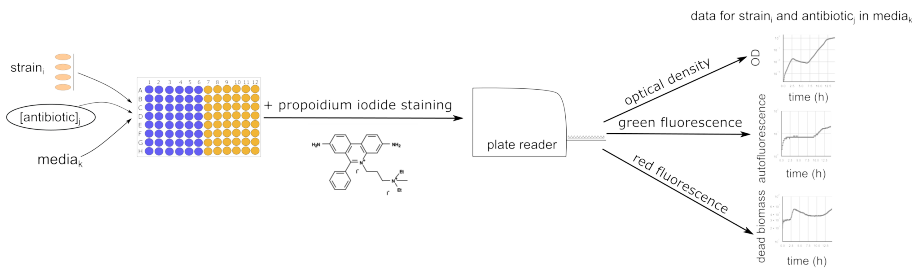
Interestingly, we observe peaks of red fluorescence at the moment of crash (growth arrest) in the OD data. This means that at this moment a significant amount of PI was able to enter the damaged cells and bind to the DNA, i.e. this is the moment when the bacteria start to lyse. At high antibiotic concentrations, especially in M9 with both glucose and casamino acids, this rise in red fluorescence is quite steep, meaning that there are few deaths before the crash moment. This is in line with the assumptions of the model we used for this work: cells filament until they reach a critical length at which they lyse. This peak is even more pronounced on the time derivative plot (e.g. grey line for M9 with glucose and casamino acids). Another interesting observation is that there is a slow increase in red fluorescence during the stationary phase of population growth.

As for the auto-fluorescence, we can observe the regrowth, but the size of the population and the corresponding auto-fluorescence signal are too small to be measurable in our setup. Most of the interesting dynamics are therefore hidden by the detection limit. An interesting observation is that during stationary phase, when OD is increasing very slowly, there is a noticeable increase in both auto-fluorescence and dead biomass. This means that at this stage there is a part of the population that is still growing and a part that is dying.

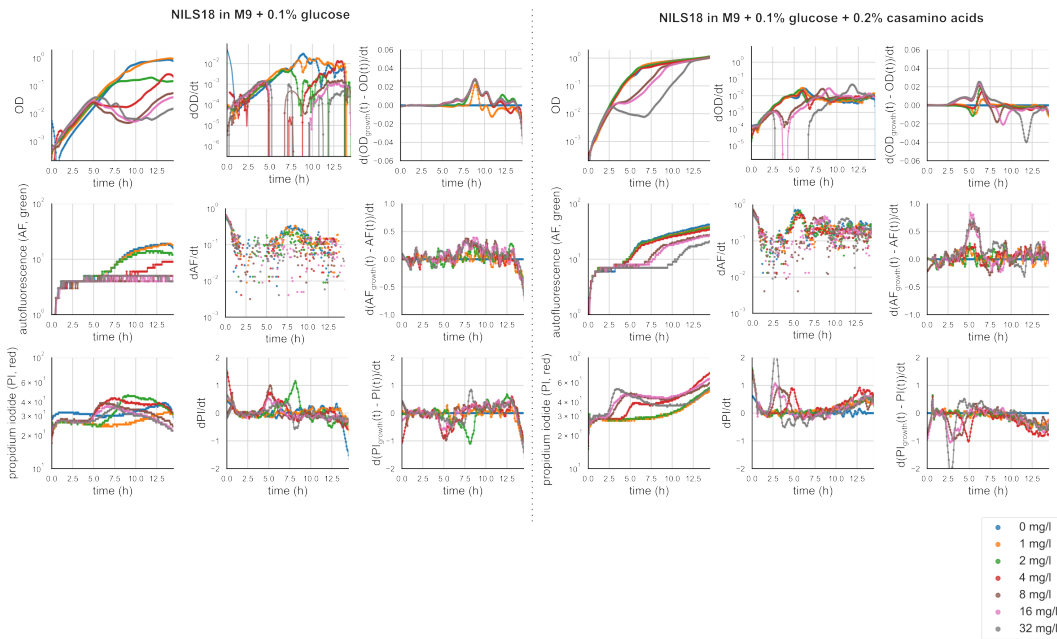
a Standard approaches to quantify antibiotic effectiveness



b Approach



c Complex set of observations



Unfortunately, auto-fluorescence did not give us the insight we were hoping for. We decided to use the same strategy as [103] but for OD. We plotted the time derivative of

Figure A.1: **Exploring alternatives to CFU assays.** **a.** Summary of two standard approaches to quantifying population response to antibiotic treatment: growth kinetics assays (left) and CFU assays (right). **b.** Our approach is to generate three types of readouts: optical density (OD, total biomass), green fluorescence (auto-fluorescence) and red fluorescence (response to propidium iodide staining, dead biomass). **c** Characterisation of the population response to cefotaxime treatments for NLS18 in M9 with 0.1% glucose (left half) and in M9 with 0.1% glucose and 0.2% casamino acids (right half). The first row corresponds to OD, the second to green fluorescence and the third to red fluorescence. For each strain-media combination we show the raw data (first column), the time derivative (second derivative) and the time derivative of the difference between normal growth and growth in the presence of antibiotic.

OD, which allows us to observe the temporal evolution of live biomass. By plotting the time derivative of the difference between normal growth and the response to antibiotic treatment, we can determine the time of the crash (beginning of non-zero values) and the time of the beginning of regrowth (change of sign of this derivative).

Overall, this experiment provided interesting and valuable insights and even confirmed some of the assumptions of the model. However, it does not allow us to easily estimate the number of living cells and cannot replace CFU assays. For example, there is still no way to distinguish a few filamentous cells from many non-filamentous cells.

Appendix B

The automated platform for repeated antibiotic applications

Plate readers offer temperature control, shaking and systematic measurements of OD and fluorescence, which is already very valuable. However, what plate readers often lack is an automated way to change environmental conditions based on OD readings. As part of a large automation project in the team, we added pipetting capabilities to our plate reader (Tecan Spark) by connecting it to a liquid handling robot (Opentrons OT-2) (Figure B.1a, [106]). The pipetting robot was controlled via Flask, a web application framework written in Python. As we did not have access to an API for the plate reader, we used a 'click'-based control provided by the Python library pyautogui, software that implements mouse movement and clicking.

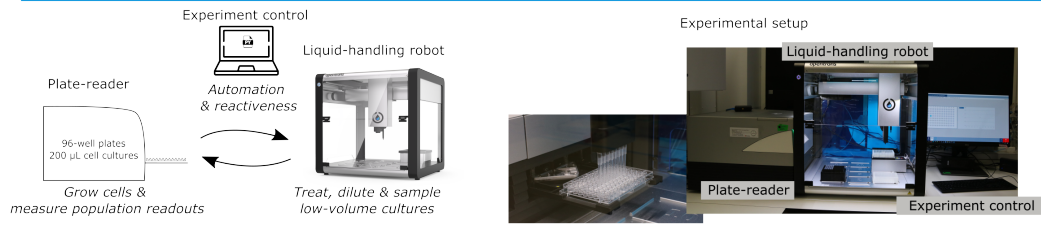
In a first application, we are using the platform to maintain bacterial populations under specific growth conditions for extended periods of time. Bacteria were exposed to a range of sub-lethal concentrations of cefotaxime while growing in M9 media with 0.1% glucose or in M9 with 0.1% glucose and 0.2% casamino acids. When the median of the cell population ODs reached a target value, the bacterial cultures were diluted by a factor of 2, taking into account evaporation, using the same media with the same concentration of antibiotic as the initial conditions (Figure B.1b left). Using this strategy, we were able to keep the median OD close to the chosen target (0.05 or 0.1) for at least 15 generations (Figure B.1b right). Interestingly, we observed better survival in

richer media (containing both glucose and casamino acids) when treated with 1 mg/L cefotaxime (1/2 the MIC for this strain), which is surprising since β -lactams generally have a stronger effect on faster growing cells.

In a second application, we used this setup to test the effect of a second dose of antibiotic on the bacterial population applied at different cell densities (Figure B.1c). The complexity and value of this type of experiment has already been discussed in Chapter 4. The first of the three plots represents the population response to standard treatment when antibiotic alone is applied at the start of the experiment. The other two plots represent the bacterial response to two applications of antibiotic: the first at the beginning, the second when the cell density reaches $2.5 \cdot 10^{-3}$ and $5 \cdot 10^{-3}$ respectively. Interestingly, we observe that the OD at crash (the point at which growth stops) appears to be about 25 times higher than the OD at treatment, and this ratio does not depend on the population density at the time of treatment. This suggests that antibiotic degradation by living cells prior to crash is negligible. This also means that very few cells die before the crash. Another interesting observation is that for the first treatment at 4 mg/L, the time between crash and regrowth is not greatly affected by the second treatment (16 mg/L). This means that the enzymes released into the media by the dead population from the first treatment are sufficiently efficient to degrade both 4 mg/L and 20 mg/L. This suggests that this time lag between crash and regrowth is the time required for the population to regrow to a detectable density.

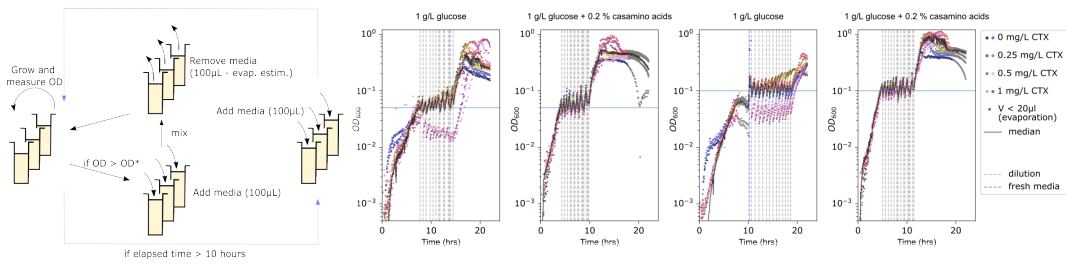
This platform allowed us to perform conceptually simple experiments in an automated manner and provided valuable insights that are not easily observable using only a plate reader without human interaction. A disadvantage of this system is that our pipetting robot is not equipped with a lid lifter, and without a lid liquid cultures tend to evaporate quite rapidly at 37°C. For this reason, we did not use this platform for our repeated treatment experiments in Chapter 4 .

a Enhancing plate-readers with liquid-handling capacities



b Impact of environment and β -lactam treatments on growing cell populations

Maintaining cells in growing conditions by renewing media



c Impact of cell density on β -lactam treatment efficacy

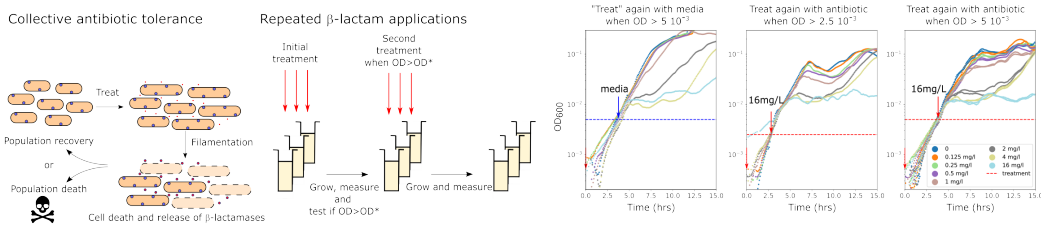


Figure B.1: **ReacSight-based assembly of an automated platform enabling reactive control and characterization of bacterial cultures in low-volumes.** **a.** The platform overview. The platform contains a plate-reader (Tecan Spark) and a liquid-handling robot (Opentrons OT-2). The robot is used to treat cultures in the plate-reader at predefined ODs. The robot is controlled through dedicated Python library, whereas a control API for the plate-reader is created using the 'clicking' Python library pyautogui. **b.** Impact of environment and β -lactam treatments on growing cell populations. Left: bacterial population can be maintained in growing conditions through renewal of the media in either OD- or time-controlled manner. It is important to consider evaporation and compensate if needed. Right: cells in rich media (M9 with glucose and casamino acids vs M9 with glucose alone) grow faster and yet resist better sub-MIC antibiotic concentrations. **c.** Impact of cell density on β -lactam treatment efficacy. Left: There are multiple ways for bacteria to survive antibiotic treatment. For example, when treated with β -lactams, filamentation-based tolerance allows to increase biomass before cell death. Bacteria can also survive higher antibiotic concentrations as a population due to antibiotic degradation by enzymes released upon cell death. The final outcome depends on what arrives first, population eradication or antibiotic degradation. Middle: repeated antibiotic treatment can help understanding the respective roles of cell death and antibiotic degradation. Right: an *E. coli* clinical isolate is treated with different concentrations of cefotaxime (legend) at an initial of OD of $5 \cdot 10^{-4}$, and a second time with either 16 mg/L of CTX (red) or media alone (blue) at a user-defined OD ($2.5 \cdot 10^{-3}$ or $5 \cdot 10^{-3}$). Because of instrument limitations, OD readouts below 10^{-3} are poorly reliable.

Appendix C

Application of bioreactor platform to study antibiotic resistance

In this work we presented a lot of different experiments and a lot of different observations, all obtained in a micro-plate and a plate-reader. In Appendix A we explored alternatives to CFU measures, however, unfortunately there were not sufficient for estimation of number of live cells. In Appendix B we presented an automated platform enhancing plate-reader with pipetting robot, but this set-up had significant evaporation which limited the duration of experiments. Therefore, to get estimates of live cell number, one needs to sample from experimental plate and perform CFU assays on that sample. In a 96-well micro-plate, the maximal usable volume is 200 μL . Due to many different factors including flat bottom shape, surface tensions and mechanism of OD measurement, OD readout of volume less than 50-100 μL are not reliable. This limits our capacity to sample for complementary analysis.

An interesting different set-ups that is more and more used to study antibiotic resistance is a low-volume bioreactor platform [40, 41]. This platform consists in vials for cell culture with temperature and agitation control and *in situ* measurements (OD and in some cases fluorescence) and a set of peristaltic pumps. For this project, we chose commercially available and easily modifiable platform called eVOLVER [107] (Figure C.1a). This system contains 16 bioreactors containing up to 25 mL of bacterial culture and 32 pumps (one set of 16 for influx, the other for efflux) that can be controlled based

on OD and/or time.

In a first application, we used this platform to study the impact of media on bacterial population growth. One clinical isolate (NILS18) was grown in three different media: M9 media with 0.1% casamino acids, 0.2% fructose or 0.4% glucose. Every 8 hours, the population was diluted to OD of 0.01. This allowed us to observe lag, exponential growth and stationary phases in the same experiment with replicates for each experimental condition (Figure C.1b). By fitting the Baranyi deterministic compartment model [108] to this data, we were able to estimate the duration of lag phase and the maximum growth rate. Out of the three tested media, lag time seems to be the longest in the one containing fructose and the highest growth rate was observed in the one containing glucose. Population growing in 0.1% casamino acids does not seem to reach stationary phase in 8 hours, therefore lag time is hard to estimate.

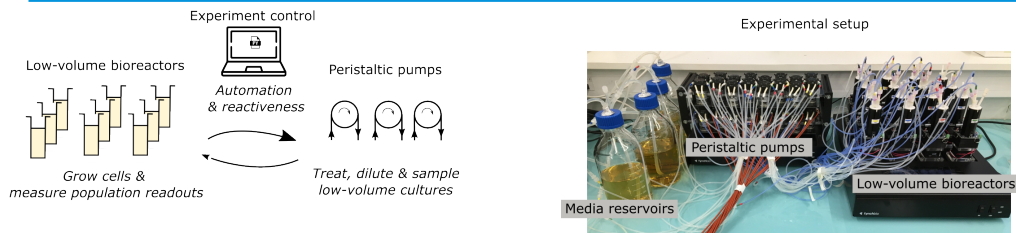
In the second application, we used the platform to characterise bacterial population response to antibiotic (Figure C.1c). We aimed to reproduce experiment that we usually do in plate-reader: subject population at very low OD ($5 \cdot 10^{-4}$) to a concentration of antibiotic and follow the temporal evolution of OD for a long time. We selected two clinical isolates (NILS18 and IB302 and tested them in two media (M9 with 0.4% glucose and M9 with 0.4% fructose). In addition, we varied the time of the antibiotic concentration (at the very beginning, after 1 hour or after 3 hours). This delayed treatment allowed population to grow to higher density before dose administration, therefore, this experiment allowed us to observe the impact of initial population density on survival, i.e. inoculum effect. As expected, when treated at higher OD, population regrowth is shortened. Interestingly, in most cases regrowth was slightly later in media with fructose compared to glucose.

One issue that we encountered is that the starting OD is too low for precise measurements in this set-up. This also means that no OD-based dilutions or other decisions can be made in an automated way until population reached detectable values. For this reason, we decided to test the population response to antibiotic using the low OD detection limit (0.01) as starting OD: for this experiment we either applied antibiotic at the beginning or 1 hour after, or we diluted culture to OD of 0.01 using media with antibiotic. Due to strong inoculum effect for this strain-antibiotic combinations we observed a very

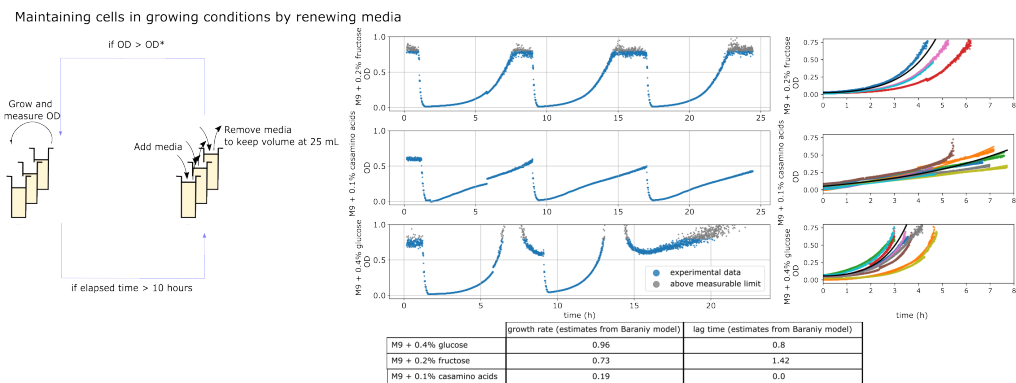
good survival (short regrowth time) for NLS18 and no impact of antibiotic on growth for IB302. We have also tested another antibiotic (meropenem, carbapenem class of antibiotic), and in this case, observed full eradication of the population even when starting at high initial population density.

Using a bioreactor platform allowed us to study lag time and maximum growth rate in different media. It also allowed us to characterise bacterial population response to antibiotics in bigger volume than in micro-plates. We were able to observe inoculum effect. Starting at higher OD we were also able to administer antibiotic at specific time and specific OD. However, this platform has a drawback that is very important for our study: it has high detection limit for low OD. One possible extension of this platform to solve this issue would be to connect this platform to the platform described in Appendix B combining pipetting robot and plate-reader. This way low OD values could be measured through performing systematic sampling and using plate-reader for this samples.

a Low-volume bioreactor platform



b Impact of environment on growing cell populations



c Impact of cell density on β -lactam treatment efficacy

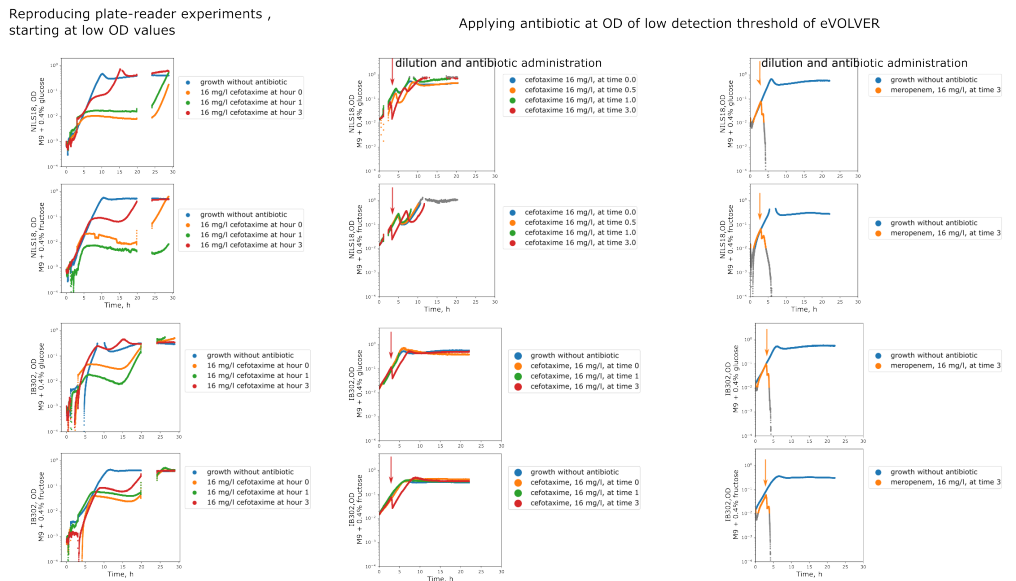


Figure C.1: **Application of bioreactor platform to antibiotic resistance study.** **a.** Overview of the platform. **b.** Impact of media on population growth. Left: An *E.coli* clinical isolate (NILS18) was grown in three different media: M9 with 0.2% fructose, 0.1% casamino acids or 0.4% glucose. Bacterial populations grew for 8 hours, after that they were diluted to OD of 0.01. Right: growth curves in different media. Baranyi model was fitted to this data to obtain estimations of lag time and maximum growth rate (presented in table below). **c.** Impact of initial population density and media on population response to β -lactam treatments. Population response to 16 mg/L of cefotaxime was characterised for two clinical isolates (NILS18, iB302) in M9 with 0.4% glucose or 0.2% fructose. Left: Reproducing plate-reader experiments, starting OD is at $5 \cdot 10^{-4}$, antibiotic applied at different moments (at the beginning, after 1 hour or after 3 hours). Middle: Starting OD is at 0.01 (low detection limit). Antibiotic application at the beginning, at 1 hour or at 3 hours (after diluting culture to OD of 0.01). Right: Characterisation of population response to meropenem (carbapenem class).

Appendix D

Study of filamentation and critical length using microscopy and image segmentation pipelines

In this work, we focused on the population response and different ways to characterise it. This allowed us to study antibiotic escape through the interplay between individual non-susceptibility and resilience at the population level (e.g. collective antibiotic tolerance or inoculum effect). In an attempt to understand individual mechanisms from observed population dynamics, we used a model-based approach. In this chapter we have decided to take a different approach and look at the response of individual cells to β -lactam treatments. The standard way to do this is to use microscopy to follow the evolution of individual bacterial cells.

To improve observability, we decided to use microfluidics, which allows us to keep bacteria in a mono-layer and provide a continuous flow of media with nutrients and, in some cases, antibiotics. In our experiments we used commercially available CellaSIC ONIX plates [98] (Figure D.1a, description of the experimental protocol in Methods 7.10). These plates contain four independent cell chambers, each with traps of six different heights that allow bacteria to be maintained in a mono-layer. For each chamber there are 6 independent inlets for media supply. The presence of multiple independent inlets allows media switching during the experiment. Using this plate together with pressure

pumps, we followed cell dynamics using either bright-field (BF) or phase-contrast microscopy.

To analyse the microscopy images, we used the software pipeline, a U-Net-based package for segmentation and tracking of bacterial cells in mother cells or in monolayers [101]. DeLTA provides segmentation labels for each image. It also allows cells to be tracked from one frame to another and cell division to be identified. It also provides valuable length and fluorescence information for each identified cell.

When treated with β -lactams, and cefotaxime in particular, bacteria can react in different ways. Resistant bacteria continue to divide normally. Some cells cannot divide due to the inhibition of PBP3 by the antibiotics, and they become filamentous. Some cells can neither divide nor repair the cell wall due to the inhibition of PBPs, leading to cell lysis (Figure D.1b left). To observe filamentation and estimate how long filaments can grow before breaking, we grew a clinical isolate (IB302) for several hours before switching to antibiotic-containing media (in bright field (BF) at 63x magnification). Without antibiotics, the cells divided normally. In the presence of cefotaxime, the cells began to form filaments. To see when the antibiotic was added to the media, we stained the second media with propidium iodide (PI), which has a detectable level of fluorescence even before binding to DNA.

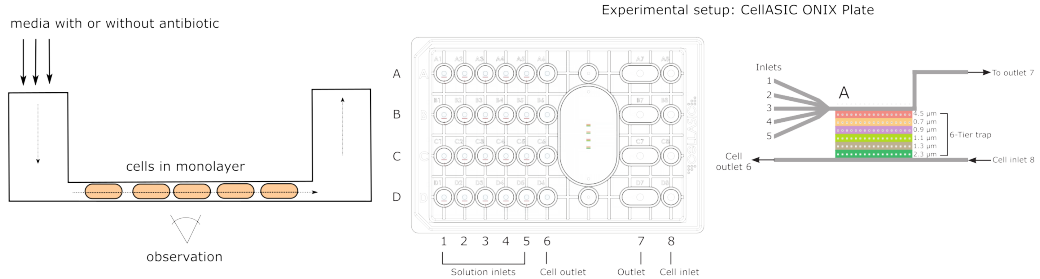
We used DeLTA for segmentation and estimation of cell length (in pixels, Figure D.1b right). On the raw images, we first see this cell dividing into two (frame 25 or about 2 hours), then we start to detect red fluorescence marking antibiotic administration at frame 67 (about 5 hours). From this moment on, the cell filaments without dividing (frame 217 or about 18 hours). Figure D.1b shows the time course of red fluorescence and cell length. We can clearly see the time of first cell division and the time of antibiotic administration. The filaments at the end are about two times longer than at the time of treatment and about six times longer than at the time of division and 'birth' of the second cell. The problem we encountered at this stage is that long cells are difficult to follow because it is not always obvious whether there are several cells or one long filament.

Using a phase-contrast objective with 100x magnification, we followed another clinical isolate (NILS18) exposed to 16 mg/L cefotaxime in three different media: M9 with 0.1% glucose, 20mM/L gluconate and 0.4% casamino acids. We used DeLTA for seg-

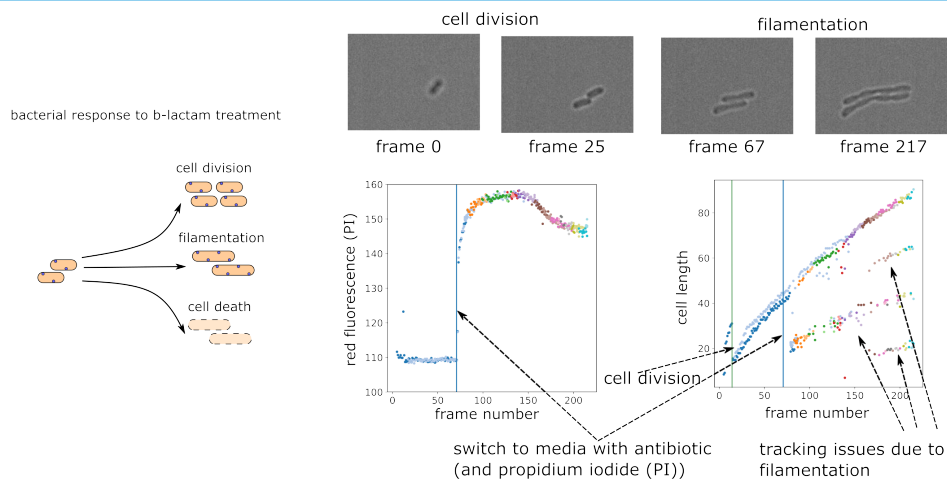
mentation and cell length estimation. The quality of the segmentation was significantly improved by switching to phase contrast, but the problem of tracking filamentous cells was still present. Figure D.1c shows cell length distributions for the three media (different columns) at the beginning of the experiment (first row) and at frame 45 (about 3-4 hours after the start of the experiment, about 2 hours after antibiotic administration). The latter distributions are accompanied by extracts from the corresponding raw images. Interestingly, we observe much longer filaments in M9 with 0.4% casamino acids. There was no significant difference between glucose and gluconate.

In conclusion, CellASIC ONIX plates are a very easy to use and useful tool for observing bacterial behaviour at the single cell level. This setup allowed us to confirm the filamentation response of our clinical isolates when treated with cefotaxime. It also allowed us to observe differences in filamentation levels between media. The DeLTA segmentation pipeline allowed us to extract quantitative information from microscopy images. To obtain good results with DeLTA, it is preferable to use phase contrast microscopy (compared to bright field). Long filamentous cells with possibly weak outer membranes are difficult to track, but this problem can be solved by adding images of filamentous cells to the training and validation datasets and retraining the model. Due to time constraints and the fact that we were more interested in population dynamics, I did not continue this project.

a Microfluidics platform



b Impact of β -lactam treatment on cell morphology



c Impact of environment on β -lactam treatment efficacy

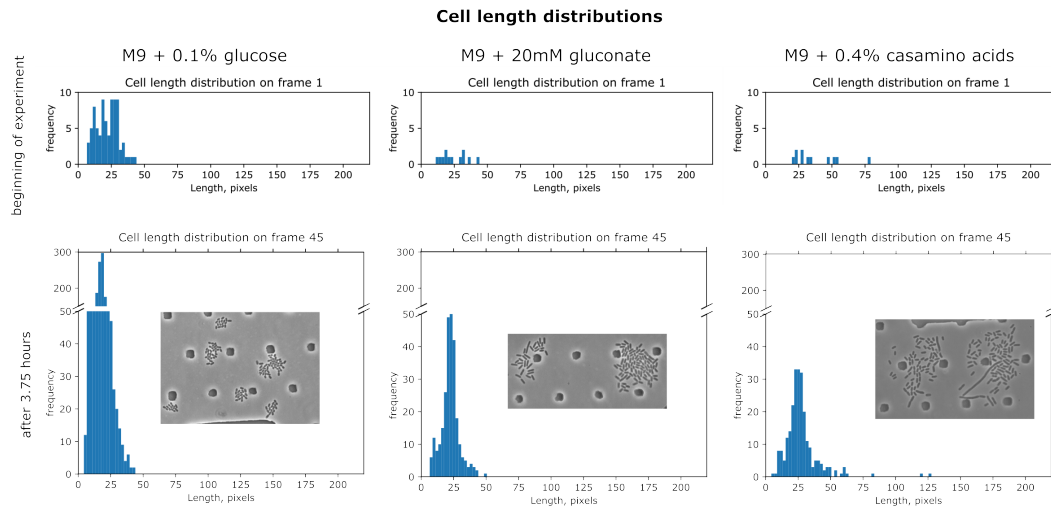


Figure D.1: **Study of filamentation in a microfluidic platform.** **a.** Schematic of the platform, adapted from [98]. Cells are confined in a mono-layer. There is a continuous flow of media providing nutrients and washing out lysed cells. Commercially available CellASIC ONIX plates were chosen for the experiments. *Center:* Scheme of the plate. Having several independent input columns allows switching between different media during the experiment. One plate contains 4 independent chambers. *Right:* Schematic of a single chamber. Media is supplied through a subset of inlets. Bacteria are trapped according to their size (6 sizes available). **b.** A clinical isolate (IB302) was used to produce a mono-layer of cells. Media without antibiotic (M9 with 0.1% glucose) was used for the first 3 hours. The same media was then used, but supplemented with 16 mg/L cefotaxime and propidium iodide. Some images from these experiments are shown in the upper part of the panel. The images were segmented while keeping track of the cell lineages using DeLTA). *Center:* Temporal evolution of the red fluorescence signal. This makes it possible to see the moment of the media change (frame 67). *Right:* The temporal evolution of cell length of segmented bacteria. **c.** Effect of environment on bacterial response to β -lactam treatments. A clinical isolate (NILS18) was exposed to 16 mg/L cefotaxime in 3 different media (M9 with 0.1% glucose on the left, with 20 mM/L gluconate in the middle and with 0.4% casamino acids on the right). Cell length distributions were estimated based on microscopy image segmentation using DeLTA. The top plots correspond to the beginning of the experiment, the bottom plots correspond to the image taken 3.75 hours later. For each medium, a small section of the original image is shown.

Bibliography

1. Organization, W. H. *et al.* *Report of the 6th meeting of the WHO advisory group on integrated surveillance of antimicrobial resistance with AGISAR 5-year strategic framework to support implementation of the global action plan on antimicrobial resistance (2015-2019), 10-12 June 2015, Seoul, Republic of Korea* (World Health Organization, 2015).
2. Cassini, A. *et al.* Attributable deaths and disability-adjusted life-years caused by infections with antibiotic-resistant bacteria in the EU and the European Economic Area in 2015: a population-level modelling analysis. *The Lancet Infectious Diseases* **19**, 56–66 (Jan. 2019).
3. *WHO Bacterial Priority Pathogens List 2024 Bacterial Pathogens of Public Health Importance, to Guide Research, Development, and Strategies to Prevent and Control Antimicrobial Resistance* (World Health Organization, Geneva, 2024).
4. Tenaillon, O., Skurnik, D., Picard, B. & Denamur, E. The population genetics of commensal *Escherichia coli*. *Nature Reviews Microbiology* **8**, 207–217 (Mar. 2010).
5. Denamur, E., Clermont, O., Bonacorsi, S. & Gordon, D. The population genetics of pathogenic *Escherichia coli*. *Nature Reviews Microbiology* **19**, 37–54 (Jan. 2021).
6. King, D. T., Sobhanifar, S. & Strynadka, N. C. J. in *Handbook of Antimicrobial Resistance* (eds Gotte, M., Berghuis, A., Matlashewski, G., Wainberg, M. & Sheppard, D.) 1–22 (Springer New York, New York, NY, 2014). ISBN: 978-1-4939-0667-3.

7. Versporten, A. *et al.* Consumption of cephalosporins in the community, European Union/European Economic Area, 1997–2017. *Journal of Antimicrobial Chemotherapy* **76**, ii22–ii29 (Supplement_2 Aug. 1, 2021).
8. Popham, D. L. & Young, K. D. Role of penicillin-binding proteins in bacterial cell morphogenesis. *Current Opinion in Microbiology* **6** (Dec. 2003).
9. Klein, N. C. & Cunha, B. A. Third-generation cephalosporins. *Medical Clinics of North America* **79** (1995).
10. Alekshun, M. N. & Levy, S. B. Molecular Mechanisms of Antibacterial Multidrug Resistance. *Cell* **128** (Mar. 2007).
11. R.P., A. The structure of beta-lactamases. *Philosophical Transactions of the Royal Society of London. B, Biological Sciences* **289**, 321–331 (May 16, 1980).
12. Bush, K., Jacoby, G. A. & Medeiros, A. A. A functional classification scheme for beta-lactamases and its correlation with molecular structure. *Antimicrobial Agents and Chemotherapy* **39**, 1211–1233 (June 1995).
13. Xiaoliang, W., Huiming, H., Chunlei, C. & Beiwen, Z. Genomic characterisation of a colistin-resistant *Klebsiella pneumoniae* ST11 strain co-producing KPC-2, FloR, CTX-M-55, SHV-12, FosA and RmtB causing a lethal infection. *Journal of Global Antimicrobial Resistance* **19**, 78–80 (Dec. 2019).
14. Balaban, N. Q. *et al.* Definitions and guidelines for research on antibiotic persistence. *Nature Reviews Microbiology* **17**, 441–448 (July 2019).
15. Meredith, H. R. *et al.* Applying ecological resistance and resilience to dissect bacterial antibiotic responses. *Science Advances* **4**, eaau1873 (Dec. 7, 2018).
16. Meredith, H. R., Srimani, J. K., Lee, A. J., Lopatkin, A. J. & You, L. Collective antibiotic tolerance: mechanisms, dynamics and intervention. *Nature Chemical Biology* **11**, 182–188 (Mar. 2015).
17. Rodríguez-Baño, J. & Pascual, A. Clinical significance of extended-spectrum beta-lactamases. *Expert Review of Anti-infective Therapy* **6** (Oct. 2008).

18. Pitout, J. D. Infections with Extended-Spectrum beta-Lactamase-Producing Enterobacteriaceae: Changing Epidemiology and Drug Treatment Choices. *Drugs* **70**, 313–333 (Feb. 2010).
19. Foxman, B. Urinary Tract Infection Syndromes. *Infectious Disease Clinics of North America* **28** (Mar. 2014).
20. Zeng, Z., Zhan, J., Zhang, K., Chen, H. & Cheng, S. Global, regional, and national burden of urinary tract infections from 1990 to 2019: an analysis of the global burden of disease study 2019. *World Journal of Urology* **40**, 755–763 (Mar. 2022).
21. Murray, B. O. *et al.* Recurrent Urinary Tract Infection: A Mystery in Search of Better Model Systems. *Frontiers in Cellular and Infection Microbiology* **11**, 691210 (May 26, 2021).
22. Flores-Mireles, A. L., Walker, J. N., Caparon, M. & Hultgren, S. J. Urinary tract infections: epidemiology, mechanisms of infection and treatment options. *Nature Reviews Microbiology* **13**, 269–284 (May 2015).
23. Lawrenson, R. A. Antibiotic failure in the treatment of urinary tract infections in young women. *Journal of Antimicrobial Chemotherapy* **48** (Dec. 1, 2001).
24. Losada, L. *et al.* Expert Panel Recommendations on Lower Urinary Tract Health of Women Across Their Life Span. *Journal of Women's Health* **25** (Nov. 2016).
25. Colodner, R. *et al.* Risk Factors for the Development of Extended-Spectrum Beta-Lactamase-Producing Bacteria in Nonhospitalized Patients. *European Journal of Clinical Microbiology & Infectious Diseases* **23** (Mar. 1, 2004).
26. Saliba, W., Nitzan, O., Chazan, B. & Elias, M. Urinary tract infections in patients with type 2 diabetes mellitus: review of prevalence, diagnosis, and management. *Diabetes, Metabolic Syndrome and Obesity: Targets and Therapy*, 129 (Feb. 2015).
27. Aubron, C. *et al.* Changes in urine composition after trauma facilitate bacterial growth. *BMC Infectious Diseases* **12** (Dec. 2012).

28. Timsit, J.-F., Ruppé, E., Barbier, F., Tabah, A. & Bassetti, M. Bloodstream infections in critically ill patients: an expert statement. *Intensive Care Medicine* **46**, 266–284 (Feb. 2020).
29. Lazarovits, G. *et al.* Prevalence of Antibiotic Tolerance and Risk for Reinfection Among *Escherichia coli* Bloodstream Isolates: A Prospective Cohort Study. *Clinical Infectious Diseases* **75**, 1706–1713 (Nov. 14, 2022).
30. Vance, M. K. *et al.* Risk Factors for Bloodstream Infections Due to ESBL-Producing *Escherichia coli*, *Klebsiella spp.*, and *Proteus mirabilis*. *Pharmacy* **11** (Apr. 13, 2023).
31. Dheman, N. *et al.* An Analysis of Antibacterial Drug Development Trends in the United States, 1980–2019. *Clinical Infectious Diseases* **73**, e4444–e4450 (Dec. 6, 2021).
32. Rex, J. H. & Outterson, K. Antibacterial R&D at a Crossroads: We’ve Pushed as Hard as We Can . . . Now We Need to Start Pulling! *Clinical Infectious Diseases* **73**, e4451–e4453 (Dec. 6, 2021).
33. Determination of minimum inhibitory concentrations (MICs) of antibacterial agents by broth dilution. *Clinical Microbiology and Infection* **9** (Aug. 2003).
34. Roujansky, A. *et al.* Analysis of Paradoxical Efficacy of Carbapenems against Carbapenemase-Producing *Escherichia coli* in a Murine Model of Lethal Peritonitis. *Antimicrobial Agents and Chemotherapy* **64**, e00853–20 (July 22, 2020).
35. J.S. Cadwell, J. The Hollow Fiber Infection Model for Antimicrobial Pharmacodynamics and Pharmacokinetics. *Advances in Pharmacoeconomics & Drug Safety* **01** (2012).
36. Griffith, D. C., Sabet, M., Tarazi, Z., Lomovskaya, O. & Dudley, M. N. Pharmacokinetics/Pharmacodynamics of Vaborbactam, a Novel Beta-Lactamase Inhibitor, in Combination with Meropenem. *Antimicrobial Agents and Chemotherapy* **63**, e01659–18 (Jan. 2019).

37. Ferran, A. A. *et al.* The Selection of Antibiotic- and Bacteriophage-Resistant *Pseudomonas aeruginosa* Is Prevented by Their Combination. *Microbiology Spectrum* **10** (ed Tyne, D. V.) e02874–22 (Oct. 26, 2022).
38. Auchtung, J. M., Robinson, C. D. & Britton, R. A. Cultivation of stable, reproducible microbial communities from different fecal donors using minibioreactor arrays (MBRAs). *Microbiome* **3** (Dec. 2015).
39. Hobson, C. A. *et al.* MiniBioReactor Array (MBRA) *in vitro* gut model: a reliable system to study microbiota-dependent response to antibiotic treatment. *JAC-Antimicrobial Resistance* **4**, dlac077 (July 4, 2022).
40. Gopalakrishnan, V. *et al.* A low-cost, open-source evolutionary bioreactor and its educational use. *eLife* **11**, e83067 (Nov. 1, 2022).
41. Leyn, S. A. *et al.* Experimental evolution in morbidostat reveals converging genomic trajectories on the path to triclosan resistance. *Microbial Genomics* **7** (May 5, 2021).
42. Lopatkin, A. J. & Collins, J. J. Predictive biology: modelling, understanding and harnessing microbial complexity. *Nature Reviews Microbiology* **18**, 507–520 (Sept. 2020).
43. Zagajewski, A. *et al.* Deep learning and single-cell phenotyping for rapid antimicrobial susceptibility detection in *Escherichia coli*. *Communications Biology* **6**, 1164 (Nov. 14, 2023).
44. Pataki, B. Á. *et al.* Understanding and predicting ciprofloxacin minimum inhibitory concentration in *Escherichia coli* with machine learning. *Scientific Reports* **10**, 15026 (Sept. 14, 2020).
45. Vanstokstraeten, R. *et al.* Genotypic resistance determined by whole genome sequencing versus phenotypic resistance in 234 *Escherichia coli* isolates. *Scientific Reports* **13**, 449 (Jan. 9, 2023).

46. Biggel, M. *et al.* PorinPredict: *In Silico* Identification of OprD Loss from WGS Data for Improved Genotype-Phenotype Predictions of *P. aeruginosa* Carbapenem Resistance. *Microbiology Spectrum* **11** (ed Carvalho-Assef, A. P. D.) e03588–22 (Apr. 13, 2023).
47. Carey, M. E. *et al.* Global diversity and antimicrobial resistance of typhoid fever pathogens: Insights from a meta-analysis of 13,000 *Salmonella* Typhi genomes. *eLife* **12**, e85867 (Sept. 12, 2023).
48. Sherry, N. L. *et al.* An ISO-certified genomics workflow for identification and surveillance of antimicrobial resistance. *Nature Communications* **14**, 60 (Jan. 4, 2023).
49. Kanjilal, S. *et al.* A decision algorithm to promote outpatient antimicrobial stewardship for uncomplicated urinary tract infection. *Science Translational Medicine* **12**, eaay5067 (Nov. 4, 2020).
50. Stracy, M. *et al.* Minimizing treatment-induced emergence of antibiotic resistance in bacterial infections. *Science* **375**, 889–894 (Feb. 25, 2022).
51. Altae-Tran, H., Ramsundar, B., Pappu, A. S. & Pande, V. Low Data Drug Discovery with One-Shot Learning. *ACS Central Science* **3**, 283–293 (Apr. 26, 2017).
52. Chung, H. S. *et al.* Rapid beta-lactam-induced lysis requires successful assembly of the cell division machinery. *Proceedings of the National Academy of Sciences* **106** (Dec. 2009).
53. Wang, Y., Ran, M., Wang, J., Ouyang, Q. & Luo, C. Studies of Antibiotic Resistance of Beta-Lactamase Bacteria under Different Nutrition Limitations at the Single-Cell Level. *PLOS ONE* **10** (ed Webber, M. A.) e0127115 (May 20, 2015).
54. Kim, K. *et al.* Mapping single-cell responses to population-level dynamics during antibiotic treatment. *Molecular Systems Biology* **19**, e11475 (July 11, 2023).
55. Andreani, V., You, L., Glaser, P. & Batt, G. *A model-based approach to characterize enzyme-mediated response to antibiotic treatments: going beyond the SIR classification* preprint (Biophysics, July 17, 2021).

56. Tandar, S. T., Aulin, L. B., Leemkuil, E. M. J., Liakopoulos, A. & Van Hasselt, J. G. C. Semi-mechanistic modeling of resistance development to beta-lactam and beta-lactamase-inhibitor combinations. *Journal of Pharmacokinetics and Pharmacodynamics*. ISSN: 1567-567X, 1573-8744 (Nov. 26, 2023).
57. Lee, A. J. *et al.* Robust, linear correlations between growth rates and beta-lactam-mediated lysis rates. *Proceedings of the National Academy of Sciences* **115** (Apr. 2018).
58. Patiño-Navarrete, R. *et al.* Stepwise evolution and convergent recombination underlie the global dissemination of carbapenemase-producing *Escherichia coli*. *Genome Medicine* **12** (Dec. 2020).
59. Galardini, M. *et al.* Phenotype inference in an *Escherichia coli* strain panel. *eLife* **6**, e31035 (Dec. 27, 2017).
60. Sanchez, C. J. *et al.* Biofilm formation by clinical isolates and the implications in chronic infections. *BMC Infectious Diseases* **13** (Dec. 2013).
61. Mancuso, G. *et al.* Novel Antimicrobial Approaches to Combat Bacterial Biofilms Associated with Urinary Tract Infections. *Antibiotics* **13** (Feb. 4, 2024).
62. Sharma, K. *et al.* Dynamic persistence of UPEC intracellular bacterial communities in a human bladder-chip model of urinary tract infection. *eLife* **10**, e66481 (July 5, 2021).
63. Landini, P. Cross-talk mechanisms in biofilm formation and responses to environmental and physiological stress in *Escherichia coli*. *Research in Microbiology* **160** (May 2009).
64. Wu, C., Lim, J. Y., Fuller, G. G. & Cegelski, L. Disruption of *Escherichia coli* Amyloid-Integrated Biofilm Formation at the Air-Liquid Interface by a Polysorbate Surfactant. *Langmuir* **29**, 920–926 (Jan. 22, 2013).
65. Gutiérrez Mena, J., Kumar, S. & Khammash, M. Dynamic cybergenetic control of bacterial co-culture composition via optogenetic feedback. *Nature Communications* **13**, 4808 (Aug. 16, 2022).
66. Chang, W., Cheng, J., Allaire, J., Xie, Y., McPherson, J., *et al.* Shiny: web application framework for R. *R package version 1*, 2017 (2017).

67. Schindelin, J. *et al.* Fiji: an open-source platform for biological-image analysis. *Nature Methods* **9**, 676–682 (July 2012).
68. Berg, S. *et al.* ilastik: interactive machine learning for (bio)image analysis. *Nature Methods* (Sept. 2019).
69. Andreani, V. *Modelling and efficient characterization of enzyme-mediated response to antibiotic treatments* PhD thesis (Dec. 2020).
70. Zahir, T. *et al.* Image-based dynamic phenotyping reveals genetic determinants of filamentation-mediated beta-lactam tolerance. *Frontiers in Microbiology* **11** (2020).
71. Wehrens, M. *et al.* Size laws and division ring dynamics in filamentous *Escherichia coli* cells. *Current Biology* **28** (Mar. 2018).
72. Spratt, B. G. Distinct penicillin binding proteins involved in the division, elongation, and shape of *Escherichia coli* k12. *Proceedings of the National Academy of Sciences* **72** (Aug. 1975).
73. Botta, G. A. & Park, J. T. Evidence for involvement of penicillin-binding protein 3 in murein synthesis during septation but not during cell elongation. *Journal of Bacteriology* **145** (1981).
74. Rolinson, G. N. Effect of beta-lactam antibiotics on bacterial cell growth rate. *Journal of General Microbiology* **120** (Oct. 1980).
75. Boman, H. G. & Eriksson, K. G. Penicillin induced lysis in *Escherichia coli*. *Journal of General Microbiology* **31** (June 1963).
76. Vigouroux, A. *et al.* Class-A penicillin binding proteins do not contribute to cell shape but repair cell-wall defects. *eLife* **9** (eds Akhmanova, A., Xiao, J., Xiao, J. & Dörr, T.) (Jan. 2020).
77. Livermore, D. M. beta-lactamases: quantity and resistance. *Clinical Microbiology and Infection* **3** (Jan. 1997).
78. Spratt, B. G. The mechanism of action of mecillinam. *Journal of Antimicrobial Chemotherapy* **3**, 13–19 (suppl B Jan. 1, 1977).

79. Tängdén, T. Combination antibiotic therapy for multidrug-resistant Gram-negative bacteria. *Uppsala Journal of Medical Sciences* **119**, 149–153 (May 2014).
80. Thompson, C. A. Ceftazidime with beta-lactamase inhibitor approved for complicated infections. *American Journal of Health-System Pharmacy* **72**, 511–511 (Apr. 1, 2015).
81. Giacobbe, D. R. *et al.* Ceftolozane/tazobactam: place in therapy. *Expert Review of Anti-infective Therapy* **16**, 307–320 (Apr. 3, 2018).
82. Blee, J. A., Goroehowski, T. E. & Hauert, S. Optimization of periodic treatment strategies for bacterial biofilms using an agent-based *in silico* approach. *Journal of The Royal Society Interface* **21** (Apr. 2024).
83. Tan, C. *et al.* The inoculum effect and band-pass bacterial response to periodic antibiotic treatment. *Molecular Systems Biology* **8**, 617 (Jan. 2012).
84. Feugeas, J.-P. *et al.* Links between Transcription, Environmental Adaptation and Gene Variability in *Escherichia coli* : Correlations between Gene Expression and Gene Variability Reflect Growth Efficiencies. *Molecular Biology and Evolution* **33**, 2515–2529 (Oct. 2016).
85. Mann, R., Mediati, D. G., Duggin, I. G., Harry, E. J. & Bottomley, A. L. Metabolic Adaptations of Uropathogenic *E. coli* in the Urinary Tract. *Frontiers in Cellular and Infection Microbiology* **7** (June 8, 2017).
86. Cameron, M. A., Maalouf, N. M., Adams-Huet, B., Moe, O. W. & Sakhaee, K. Urine Composition in Type 2 Diabetes: Predisposition to Uric Acid Nephrolithiasis. *Journal of the American Society of Nephrology* **17**, 1422–1428 (May 2006).
87. De Sousa Vieira, E. E. *et al.* Biochemical Analysis of Urine Samples from Diabetic and Hypertensive Patients without Renal Dysfunction Using Spectrophotometry and Raman Spectroscopy Techniques Aiming Classification and Diagnosis. *Bioengineering* **9** (Sept. 24, 2022).
88. Smirnova, G. *et al.* Influence of Growth Medium Composition on Physiological Responses of *Escherichia coli* to the Action of Chloramphenicol and Ciprofloxacin. *BioTech* **12** (June 1, 2023).

89. Maltas, J., Krasnick, B. & Wood, K. B. Using Selection by Nonantibiotic Stressors to Sensitize Bacteria to Antibiotics. *Molecular Biology and Evolution* **37** (ed Barlow, M.) 1394–1406 (May 1, 2020).
90. Wold, S., Esbensen, K. & Geladi, P. Principal component analysis. *Chemometrics and Intelligent Laboratory Systems* **2** (Aug. 1987).
91. UMAP: Uniform Manifold Approximation and Projection for Dimension Reduction. Publisher: [object Object] Version Number: 3 (2018).
92. Nikolaou, M. & Tam, V. H. A new modeling approach to the effect of antimicrobial agents on heterogeneous microbial populations. *Journal of Mathematical Biology* **52**, 154–182 (Feb. 2006).
93. Clarelli, F. *et al.* Drug-target binding quantitatively predicts optimal antibiotic dose levels in quinolones. *PLOS Computational Biology* **16**, e1008106 (Aug. 2020).
94. Baig, Y., Ma, H. R., Xu, H. & You, L. Autoencoder neural networks enable low dimensional structure analyses of microbial growth dynamics. *Nature Communications* **14**, 7937 (Dec. 1, 2023).
95. On Neural Differential Equations. Publisher: [object Object] Version Number: 1 (2022).
96. *The CMA evolution strategy: a comparing review* (2006).
97. Hölzl-Armstrong *et al.* Characterising Mutational Spectra of Carcinogens in the Tumour Suppressor Gene TP53 Using Human TP53 Knock-in (Hupki) Mouse Embryo Fibroblasts. *Methods and Protocols* **2**, 85 (Nov. 13, 2019).
98. Merck. *CellASIC ONIX plate for bacteria cells* [https://www.merckmillipore.com/FR/fr/product/CellASIC-ONIX-plate-for-bacteria-cells-4-chamber , MM_NF - B04A - 03 - 5PK?ReferrerURL=https%3A%2F%2Fwww . google . com%2F#anchor_UG](https://www.merckmillipore.com/FR/fr/product/CellASIC-ONIX-plate-for-bacteria-cells-4-chamber%2C-MM_NF-B04A-03-5PK?ReferrerURL=https%3A%2F%2Fwww.google.com%2F#anchor_UG).
99. Edelstein, A., Amodaj, N., Hoover, K., Vale, R. & Stuurman, N. Computer Control of Microscopes Using μ Manager. *Current Protocols in Molecular Biology* **92** (Oct. 2010).

100. Fox, Z. R. *et al.* Enabling reactive microscopy with MicroMator. *Nature Communications* **13**, 2199 (Apr. 22, 2022).
101. O'Connor, O. M., Alnahhas, R. N., Lugagne, J.-B. & Dunlop, M. J. DeLTA 2.0: A deep learning pipeline for quantifying single-cell spatial and temporal dynamics. *PLOS Computational Biology* **18** (ed Coelho, L. P.) (Jan. 18, 2022).
102. Surre, J. *et al.* Strong increase in the autofluorescence of cells signals struggle for survival. *Scientific Reports* **8**, 12088 (Aug. 14, 2018).
103. Mihalcescu, I., Van-Melle Gateau, M., Chelli, B., Pinel, C. & Ravanat, J.-L. Green autofluorescence, a double edged monitoring tool for bacterial growth and activity in micro-plates. *Physical Biology* **12**, 066016 (Dec. 10, 2015).
104. Rossi, N. A., El Meouche, I. & Dunlop, M. J. Forecasting cell fate during antibiotic exposure using stochastic gene expression. *Communications Biology* **2**, 259 (July 11, 2019).
105. Ueckert, J. *et al.* Flow cytometry applications in physiological study and detection of foodborne microorganisms. *International Journal of Food Microbiology* **28**, 317–326 (Dec. 1995).
106. Bertaux, F. *et al.* Enhancing bioreactor arrays for automated measurements and reactive control with ReacSight. *Nature Communications* **13**, 3363 (June 11, 2022).
107. Wong, B. G., Mancuso, C. P., Kiriakov, S., Bashor, C. J. & Khalil, A. S. Precise, automated control of conditions for high-throughput growth of yeast and bacteria with eVOLVER. *Nature Biotechnology* **36**, 614–623 (Aug. 2018).
108. Baranyi, J. Comparison of Stochastic and Deterministic Concepts of Bacterial Lag. *Journal of Theoretical Biology* **192**, 403–408 (June 1998).